2006

# Fatigue life investigation for cams with translating roller-follower and translating flat-face follower systems

Mwafak Mohammed Shakoor
*Iowa State University*

# Fatigue life investigation for cams with translating roller – follower and translating flat – face follower systems

by

Mwafak Mohammed Shakoor

A dissertation submitted to the graduate faculty

in partial fulfillment of the requirements for the degree of

DOCTOR OF PHILOSOPHY

Major: Mechanical Engineering

Program of Study Committee
Donald Flugrad, Co – major Professor
Abir Qamhiyah, Co – major Professor
Loren Zachary
Carolyn Heising
Gloria Starns

Iowa State University
Ames, Iowa
2006

Graduate College
Iowa State University

This is to certify that the doctoral dissertation of

Mwafak Mohammed Shakoor

has met the dissertation requirements of Iowa State University

Signature was redacted for privacy.

Co – major Professor

Signature was redacted for privacy.

Co – major Professor

Signature was redacted for privacy.

For the Major Program

DEDICATION

Dedicated to the memory of my father **Mohammed A. Shakoor**

All I know and all I have

Is by the making of his hand

To the memory of my sister **Feryal**

To my Mother for her loving guidance and sacrifice

and

To my Family for their endless love and support

# TABLE OF CONTENTS

## LIST OF FIGURES

## LIST OF TABLES

## ACKNOWLEDGEMENTS

My utmost thanks should go to ALLAH (swt) for His guidance and love for me throughout my life. I am indebted to many individuals for their care and support given to me during my doctoral studies. First of all, I would like to express my deep appreciation, respect and gratitude to Professor Donald Flugrad. As my advisor, he has provided me constant encouragement, insightful comments, and invaluable suggestions that benefited me not only on the completion of this thesis, but also my career in a long time to come. Professor Flugrad who was not only a mentor of mine, but his friendship has been of greatest value.

This work would not have been completed without the support and encouragement of many people. Special acknowledgement goes to my co – mentor Dr. Abir Qamhiyah whose continues guidance and tireless assistance made this project a success. I am indebted to my committee members, Dr. Carolyn Heising, Dr. Loren Zachary, and Dr. Gloria Starns who provided extensive personal and professional guidance and taught me a great deal about both scientific research and life in general. Also, I would like extend my gratitude to the staff members of Mechanical Engineering Department and Graduate College for providing me the facilities and resources during the research.

I would like to take this opportunity to express my thanks to Muhammad Ali for all his help in Matlab coding. Ali's taught me much in Matlab programming and his advice, feedback, and friendship have made my Ph.D. experience both more educational and fun. Ali's sincerity and vision always inspired me.

In the last but not least I acknowledge my gratefulness to my family, my brothers, and my sisters who endured this long process with me, always offering sheer support and love. I am very lucky to have such wonderful family members. I am indebted to my parents for everything they have given to me. They taught me the value of knowledge, the joy of love, and the importance of family. They have stood by me in everything I have done, providing constant support, encouragement, and love. They are an inspiration to me in all that they do. My special thanks should go to my mother since she always have loved me, believed in me, and encouraged me to succeed in life.

## ABSTRACT

The cam fatigue life of the translating roller- follower and translating flat – faced follower system has been investigated for polynomial and cycloidal displacement functions. Ioannides and Harris (IH) life prediction model are used to estimate the cam fatigue life. Computer program codes are written to calculate and simulate the different types of loads that act on the cam, the contact stresses in the cam and the followers and the 'volume under risk'. Ioannides – Harris theory is applied to the 'volume under risk' and expected fatigue life is calculated. The effects of cam base circle radius, cam angular velocity, roller – follower radius of curvature, cam thickness, follower eccentricity (offset), total lift (rise or fall), and second dwell angle on the fatigue life are studied for the translating roller – follower and flat – faced follower. In the cam translating roller – follower systems, it is found that the main design parameter governing the cam fatigue life is the cam base circle radius. In this system, the fatigue life curve shows an improvement in the fatigue life up to a critical cam base circle radius value. Any further increase in the cam base circle radius appears as a decrease in the fatigue life. While in the cam translating flat – faced follower systems, the fatigue life curve shows an improvement in the fatigue life up to a cam base circle radius value where the fatigue life was infinite. Also it is found that the cam radius of curvature plays the major rule in controlling the cam fatigue life in the flat – face follower systems.

# CHAPTER 1. Introduction

A cam is a mechanical part of a machine used to transmit a rotary motion into a translating or oscillating motion through a follower using a prescribed motion program by direct contact. Generally speaking, cam mechanisms consist of three elements: the cam, the follower and the frame. Cam – follower systems are widely used in industry and different types of follower systems used to transmit the cam rotary motion through a follower into a translating or oscillating motion. The use of cam – followers are very common and they can be found in different types of machines. Cam – follower mechanisms are found in almost all mechanical devices and machines like the timer knob of the dishwasher or washing machine. Many sewing machines use cams to obtain patterned stitching. In fitness centers, there are many training machines that include one type of cam used to actuate these machines. Cam – follower mechanisms can be found in textile machines, printing presses, and food processing machines. "Automated production machinery, such as a screw machines, spring winders, and assembly machines, all rely heavily on cam – follower systems for their operation. The cam – follower is an extremely useful mechanical device, without which the machine designer's tasks would be much more difficult to accomplish" [1]. But the most popular application for cams is the valve actuation in internal combustion engines. The cam opens and closes the valves through the valve – train by rotation of the camshaft (see figure 1.1).

As mentioned above, there are different types of follower systems used in the industry and two of these follower systems are the flat – face follower system and the roller follower system that is widely used and very popular in the industry (figure 1.2).

Roller follower systems are the most widely used in industrial machinery. In roller follower systems, the cam rotates in contact with a cylindrical roller follower. When the cam rotates, the roller follower is pushed by the cam to translate or oscillate. The roller follower has the advantage of lower friction. Figure 1.2 shows a flat face follower where the contact surface is a flat plane. Flat – faced followers may give high surface stresses due to friction when the flat – faced follower slides on the cam in addition to the applied loads on the follower.

Cams fail like any other machine parts and cams failure has been defined and documented. Cams failure can be categorized into three different types of failure. Those different types of failure in cam follower systems are pitting, scuffing, and polish wear [2, 3, 4]. The mechanism, which defines a particular type of failure, is complex [5]. Failure by pitting is caused by the repeated cyclic stresses that caused by time varying loads. The time varying loads in cams are due to inertia force that varies over the time, radius of curvature and the spring force. Pitting occurs as a direct consequence of the repeated cyclic stresses where the crack initiates beneath the surface and propagates to the surface as a function of time ending with a surface fatigue. For design purposes, the ability to accurately predict the number of loading cycles to develop pitting failure under a given load, speed and other different design parameters is essential.

Major efforts are currently underway in industry and academia to better understand the fatigue life of machinery parts and the factors that influence the performance and life of cams and try to predict when the parts will fail in order to prevent catastrophic accidents and high cost. Fatigue performance is of particular interest because of its sensitivity to a host of

processing variables. Increased understanding and control of these variables could lead to more optimized service performance.

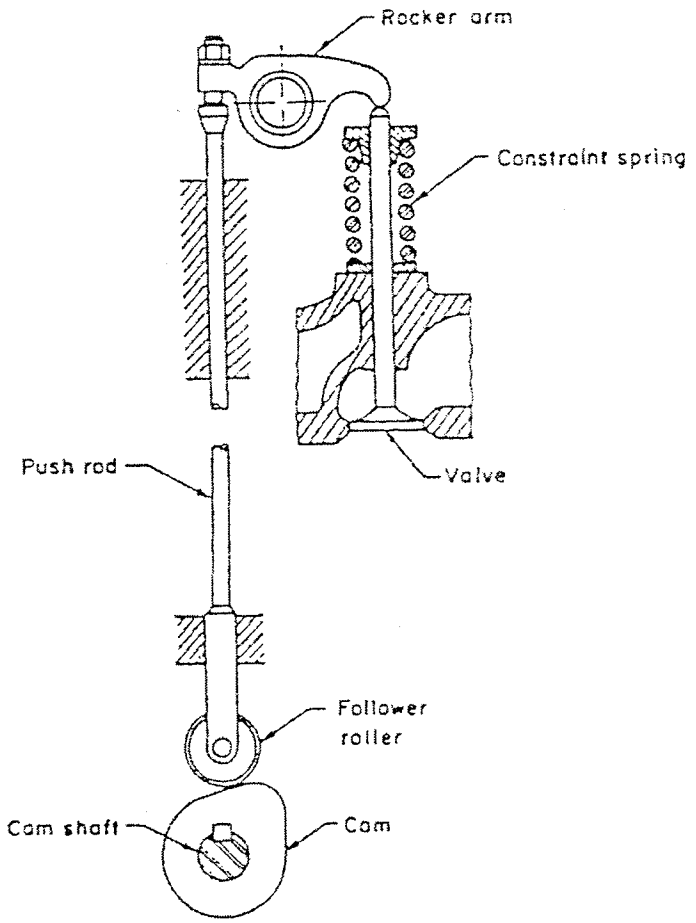


Figure 1.1: Valve train model

The work presented here will be focused on cams in general. The cam may be in contact with a flat – faced follower or a roller follower. The flat – faced follower entails friction loads, while the roller follower, because of rolling contact with the cam, generates

only normal loads. In either case, the cam is subject to a fatigue failure due to the cyclic stresses induced by each revolution of the shaft.

Most failures in machinery are due to time – varying loads rather than to static loads. These failures typically occur at stress levels significantly lower than the yield strengths of the materials. So when the cam rotates, it is subjected to a time – varying or dynamic load. These dynamic loads will reduce the cam life. Therefore, researchers are interested in understanding the effect of these dynamic loads on the cam fatigue life. By finding a model to determine the cam fatigue life, designers will be able to estimate the useful life of the cam and the optimum size of the cam. Researchers have devoted a lot of their efforts and time to estimate fatigue life and to reach the optimum design that will lead to economic benefits. Fatigue failure constitutes a significant cost to the economy [6]. Dowling suggests, based on data in U.S. Government report by Reed et al., [7] that:

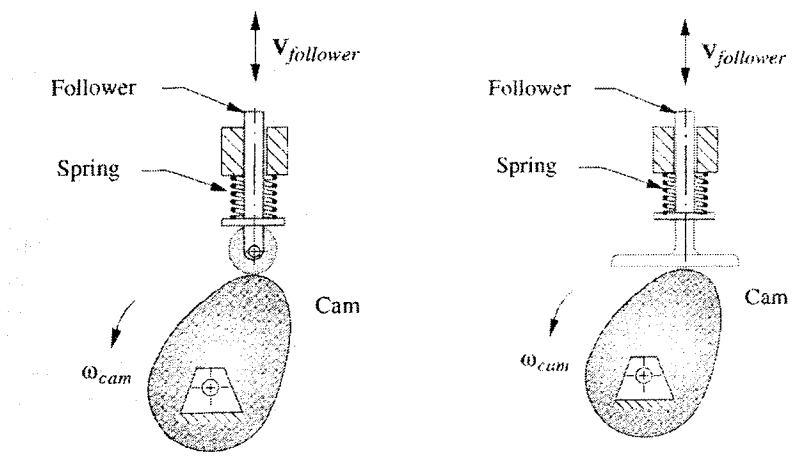


(a) Roller Follower (b) Flat – Faced Follower

Figure 1.2: Common types of cam followers

"The annual cost of fatigue of materials to the U.S. economy in 1982 dollars is around $100 billion, corresponding to about 3% of the gross national product (GNP). These costs arise from the occurrence or prevention of fatigue failure for ground vehicles, rail vehicles, aircraft of all types, bridges, cranes, power plant equipment, offshore oil well structures, and a wide variety of miscellaneous machinery and equipment including everyday household items, toys and sport equipment" [8]. The cost can also involve human life. Fatigue failure gives no warning! It's sudden and total, and hence dangerous.

From the above discussion, it's apparent that finding a way to calculate fatigue life in cams is essential in design. Also, calculating the optimum size of the cam will save a lot of money.

The goal of this study was to predict fatigue life in cams and to determine the optimum design. The individual tasks are performed as follows:

- Modeling of the cyclic stresses in the cam
- Development of an appropriate fatigue model for cams
- Determination of the cam optimum size
- Investigation the effect of other cam parameters on fatigue life

# CHAPTER 2. Literature Review

This literature review deals with three general areas of study –contact stresses, crack initiation and fatigue life, and cams. Each one of these three areas has a vast number of work done that be enough to publish books in each area. The aim of this chapter is to provide apart of the work that have been done in the past in these areas with a concentration on the stresses and fatigue life

## 2.1 Contact Stresses:

The contact problem between two elastic bodies has had the attention of many researchers in the last century. In 1881, Hertz [9] investigated the contact of elastic bodies under normal loading for the first time. Hertz conducted experiments and computed the load distribution over the contact area and then solved for stresses in the body. In 1913, S. Fuchs [10] performed a laborious arithmetical integration to obtain the stresses. Morton, W. B. and Close, L. J. [11] used zonal harmonics to calculate the stresses in a half space on which a spherical ball is pressed by a normal load. Coker and Ahmed [12] conducted experimental analysis and analytical work to study the plane – stress problem when the part of the boundary of a half plane was loaded with normal pressure.

Thomas, H. R. and Hoersch, V. A. [13], in 1930, discovered that the shearing stress on the axis of symmetry is a maximum at a distance somewhere beneath the surface under the center of the contact area. Thomas and Hoersch calculations for the stresses agreed with the experimental results. In 1936, Foeppl, L. [14] calculated the stress for the case of a cylinder and a spherical ball pressed on a flat plate. Foeppl verified his findings

experimentally by a photo – elastic technique. Lundberg, G. [14], in 1939, was the first one who considered the effect of the tangential load on the stresses. Lundberg developed a general theory of elastic contact between two semi – infinite bodies where he introduced three potential functions that correspond to three components of the load along three axes of a Cartesian coordinate. Lundberg considered the components of the load tangent to the contact area as the frictional forces between the contact surfaces. Lundberg didn't calculate the stresses due to the frictional forces in addition to the normal loads.

In 1949, Mindlin, R. D [15], investigated the stress distribution due to the tangential load when one elastic body slides over the other across the contact area. Mindlin found that the stress on the bounding curve of the contact area due to the tangential load is infinite and consequently a state of impending slipping prevails. Corresponding to this condition the intensity of tangential force at a point in the contact area cannot usually exceed the product of the coefficient of friction between the sliding surfaces and the normal pressure at the same point. In this paper, a value of 1/3 is used for the coefficient of friction, in order to show the stress distributions due to the tangential load superimposed on the normal load acting over the same contact area. Poritsky, H. [16], in December 1949, investigated the same problem by two different methods and his results agreed for both methods. Poritsky used a coefficient of friction of 0.3 in his study. In this paper, Poritsky extended the results of the solution to include an interpretation of the significance of these stresses in causing failure by inelastic yielding and by fatigue. In 1949, M'Ewen [17] evaluated the contact between two cylinders and calculated the stress field, taking into account the tangential load due to the friction on the contact area. His study was the first to include the friction force on the model.

In 1953, Smith and Liu [10] studied the contact between elastic bodies with and without creep. Their model could be applied only to rectangular contact areas. They deducted the equations to calculate the normal and shear stresses analytically, both in the contact surface and inside the bodies. They used the maximum value for the tangential force, as described by Coulomb's Law. Their studies represented a big step in contact stress evaluation because they calculated the stresses under the surface, instead of only on it, like Hertz did.

**2.2 Crack Initiation and Fatigue Life:**

Cracks may lead to component failure and then it could damage the adjacent components and in worse scenarios can endanger human life. Cracks could be found in the parts as a small flows or contamination during the material manufacturing stage or it could be introduced during the fabrication process or could be there due to cyclic stresses when the component in service then it's a well know fact that cracks cannot be eliminated.

Griffith [18] was the first one who investigated fracture phenomenon about eighty years ago. He conducted experiments on brittle materials (glass). In his experiments, Griffith introduced different sizes of cracks into different glass rods as flaws to imitate the crack size growth under the action of external loads. After that he measured the strengths of the glass rods and provided a relationship between fracture strength and defect size. Griffith's work showed that the last cycle of fatigue is a brittle fracture that caused by the fatigue crack growth to an unstable length. Nothing quantitative was done on the crack propagation problem until forty years later by Paris. Paris proposed methods for predicting the rate of growth of individual fatigue cracks in the face of initial scepticism and popular defence of Miner's phenomenological approach.

In 1946, Sneddon [19] analyzed a penny shaped crack in an infinite solid. Sneddon found that the stress behavior in this case is closely similar to the behavior of the stress field near the crack tip. He showed that the controlling parameter for the two-dimensional crack is differed from Westergaard's [20] one-dimensional crack by a simple multiplicative factor. Irwin [21] and Orowan [22] independently pointed out that for less brittle materials Griffith's energy balance must be between the stored strain energy and the surface energy plus the work done in plastic deformation. Irwin also recognized that for relatively ductile materials the energy required to form new crack surfaces is generally insignificant compared to the work done in plastic deformation. Another important contribution by Irwin [23] was that he recognized the universality of the crack – tip stress field.

Fatigue is the progressive, localized, and permanent structural damage that occurs when a material is subjected to cyclic or fluctuating strains at nominal stresses that have maximum values less than the static yield strength of the material. The resulting stress may be below the ultimate tensile stress, or even the yield stress of the material, yet still cause catastrophic failure. It has been known for very long time that machine components subjected to time varying loads may fail abruptly without any permanent deformation. The cause of this mysterious type of failure caught the attention of researchers since the very beginning of the use of metals in machines and structures.

Fatigue of metals has been studied for over 150 years. Fatigue failure phenomenon was first noticed in the 1800s when railroad – car axles began failing after only limited time in service. The railroad – car axles were manufactured from ductile steel but when they failed, their failure was like a brittle material failure. Therefore, during the period from about 1850 to 1875, researchers were interested to know the reasons behind the railroad axels

failure. They conducted experiments to establish a safe alternating stress below which failure wouldn't occur.

In 1829, Wilhem Albert [24, 25]. A German mining administrator was the first person who recorded observations of metal fatigue. He subjected mine – hoist chains to time varying loading for the first time before they were put into service. The loading frequency was about 10 times per minute, and the number of loading was in some cases as much as 100,000. Albert published the first article on fatigue. Albert findings and report was the first record account of metal fatigue.

In 1839, Jean-Victor Ponceleta [6] a French mathematician and engineer was the first one who used the fatigue term described metals as being tired in his lectures at the military school, *école d'application*, at Metz, France. He coined the term *fatigue* to describe the failure of materials under repeated stress.The brittle appearance of the surface failure in the ductile material made Poncelet to think that failure happened because the ductile material became tired and embrittled from load oscillations. After that the fatigue failure term stuck to describe this phenomenon and it is still in use to describe the failure due to time – varying loads.

In the early of 1843, a British engineer Rankine [6, 26] defined the danger of machine parts and structures that contains sharp angles. He published a paper on the Causes of Unexpected Breakage of Journals of Railway Axels, in which he postulated that the material had crystallized and become brittle due to the fluctuating stress. Axles were designed with the engineering knowledge available at that time based on statically loaded structures. Dynamic loads were then a new phenomenon resulting from the introduction of steam – powered machinery. These axels were fixed to the wheels and turned with them. Thus the

bending stress at any point on the surface of the Axel varied cyclically from positive to negative.

Hodgkinson [27] in 1849 was commissioned by the British Government to study the question of the use of wrought iron and cast iron on railways, particularly in the construction of bridges. Hodgkinson tested beams by subjected it to repeated bending loads by means of a rotating cam which deflected them at their mid – points. Hodgkinson found that the beams didn't fail after 100,000 repetitions if the deflection equal to one – third of that corresponding to static failure while he noticed that the beams failed when the deflection was half the static corresponding failure. Hodgkinson test showed that the beams failed in the second case by fracture after about 900 repetitions.

Breakages of rails and axles in railways brought attention to study this phenomenon so in the period between 1852 and 1869, August Wohler [28] a German engineer who was the chief locomotive engineer of the Royal Lower Silesian Railways conducted a numerous tests on axles to define the reason of failure in these axles at that time. August Wohler considered being the first scientist who conducted a scientific investigation about fatigue failure. Wohler also constructed the first testing machines for repeated loading and tested axels in laboratory under fully reversed loading and he published his findings in 1870, which identified the number of cycles of time – varying stress as the culprit and found the existence of an endurance limit for steel. The S – N or Wohler diagram became the standard way to characterize the behavior of materials under completely reversed loading. Wohler [6] also investigated the broken axle – halves and he found out that the broken material was still as strong and ductile in tensile tests as was the original material.

Fairbairn [29], in 1864, carried out time varying bending tests on iron beams that supported at the ends and deflected at the middle of the beams by means of the system of levers actuated by a hydraulic wheel.

Bauschinger [30], in 1884, confirmed the accuracy of several of the points that Wohler had established. Bauschinger studied the relationship between small inelastic strains and the safe stress in fatigue. He believed in a natural elastic limit below which fatigue wouldn't occur.

About 1900, Ewing [31], Rosenhain [32] and Humfrey [33] studied the mechanism of fatigue with the aid of the metallurgical microscope. They showed the formation of slip – bands and fatigue cracks in iron crystals that had been subjected to repeated stresses. Ewing and Humfrey motivated by the work of Wohler and Bauschinger and published their paper entitled "The Fracture of Metals under Repeated Alternations of Stress". They tested flat high quality Swedish iron specimens in annealed condition and optical microscopy used to examine the same area of the specimen at various stages of the fatigue life. They stated " The course of the breakdown was as follows: The first examination, made after a few reversals of stress, showed slip – lines on some of the crystals, the slip – lines were quite similar in appearance to those which are seen when a simple tensile stress exceeding the elastic limit is applied. After many reversals they changed into comparatively wide bands with rather hazily defined edges. As the number of reversals increased this process of broadening continued, and some parts of the surface became almost covered with dark markings. When this stage was reached it was found that some of the crystals had cracked. The cracks occurred along broadened slip bands. In some instances they were first seen on a single crystal, but soon they

joined up from crystal to crystal, until finally a long continuous crack was developed across the surface of the specimen".

Also about 1900, Gilchrist [34] expanded the work of Wohler and published a hypothesis that fatigue crack began as a result of localized stresses that exceeded the breaking strength of the metal. Guillet [35], in 1909, showed that the internal damping varied with the period over which the repeated stresses had been applied. He suggested that measurement of this internal damping might play a part in the study of the elastic properties of metals and especially in the study of fatigue.

Bairstow [36], in 1910, while studying vibration in metals, demonstrated the existence of 'hysteresis of elastic deformation' and showed its connection with fatigue. At the congress of the International Association for Testing Materials held at Copenhagen in 1910, Le Chatelier [37] estimated that the number of fatigue tests undertaken up to that time was insufficient to allow designers of machinery fully to appreciate the pertinent properties of the metals they used.

But since that time, the development and ever – increasing demands of engineering practice have given rise to numerous researches on fatigue, notably in Britain, by Stanton, Gough, Haigh and Hanson, and in the United States where research committees have been formed, subsidized by interested sections of industry (railways, electrical machinery, automobile, shipbuilding, aircraft, etc.). The Engineering Experiment Station of the University of Illinois under the direction of H. F. Moore, the Naval Engineering Experimental Station under D. J. McAdam and the laboratory of the McCook Aviation Field, Dayton, Ohio, under R. R. Moore, have made important documentary contributions in the course of these last few years.

Many researchers published interesting books in fatigue. In 1926, a British scientist named Gough [38] published a book under the name "*The Fatigue of Metals*" in which he presented the research results of the Engineering Division of the National Physical Laboratory. In 1927, two American scientists named H. F. Moore and J. B. Kommers [39] also published a book in fatigue field under the name "*The Fatigue of Metals*" in which they talked about the important contribution that they achieved in this area. This book and the work of Moore and his associates had a large effect on fatigue design and testing in the United States. Moore worked for many years on a number of practical fatigue problems, especially those relating to the railroad industry. Moore was responsible for organizing an ASTM; the Society for Experimental Stress Analysis in 1942. In 1941, Battelle Memorial Institute with cooperation of a committee of individuals interested and experienced in fatigue field in United States prepared a manual on the *Prevention of the Failure of Metals Under repeated stress* [40]. This manual summarized most of the information concerning the materials fatigue properties available at that time and it contained 914 bibliographical references. In 1960, three American scientists named H. J. Grover, S. A. Gordon and L. R. Jackson [41] prepared a book under the name *Fatigue of Metals and Structures* for the Battelle Memorial Institute that commissioned by the Navy Bureau of Aeronautics. This book provided additional help to the designers with some knowledge in fatigue problems.

A French scientist called Fermont [42] published a paper to the Academie des Sciences entitled "The Premature Failure of Steel Machine Parts under Repeated Stresses". He concluded that the machine part subjected to alternating stresses will run for infinite period as long as the elastic limit doesn't exceeded.

In 1954, Coffin and Mason [43] began their work on fatigue problems and came up with mathematical relationships between the plastic strain and fatigue life. They explained fatigue crack-growth in terms of plastic strain in the tip of cracks. Coffin and Mason investigated problems of fatigue of metals at high temperatures where inelastic strain cannot be ignored. During the period of 1960's, many researchers have provided significant contributions into fatigue life field. Many researchers pioneered the development of fracture mechanics as a practical engineering tool.

Different other scientists from different countries had significant contributions in fatigue field. Otto Graf [44], Lehr, Mailander [45] Thum, Oschatz and Fischer in Germany, Ludwik [46] in Austria, Prever and Locarti [47] in Italy and Ros [48] in Switzerland.

Fatigue life predictions in bearings are based on the work performed by Lundberg and Palmgren [49, 50] that was conducted during the late 1930's and early 1940's. The Lundberg – Palmgren work was a substantial step forward in the development of rolling bearing technology. They established a mathematical model for the prediction of fatigue failure of rolling bearings.

The Lundberg – Palmgren fatigue theory assumes that a fatigue crack is initiated somewhere beneath the contact surface where the magnitude of the orthogonal shear stress is the largest and a weak point in the material and propagates to the surface, forming crack or spall. Such weak points are assumed to be stochastically distributed throughout the material.

The Lundberg – Palmgren theory states that the fatigue life of a bearing ring subjected to a number of cycles, N, of repeated concentrated stress is proportional to the different parameters such as the volume under risk, the maximum orthogonal shear stress, the depth at which the maximum orthogonal shear stress occurs and a survival probability. The

LP theory doesn't account for the presence of a stress threshold value, below which the stressed volume element will not fail by fatigue. When Lundberg – Palmgren examined failed bearings, they noticed that subsurface cracks run parallel to the Hertz stressed surface so they concluded that the maximum orthogonal shear stress was the failure causing stress. The LP theory became, and remains; the basis for all bearing capacity and fatigue life rating standards and a similar theory was developed for roller bearings [51].

Harris and Wei [51] investigated the Lundberg – Palmgren theory and the distribution of stresses in that theory. They demonstrated that the subsurface volume with a potential for fatigue cracking is substantially different from that used by Lundberg and Palmgren. This difference in volume, particularly in the presence of surface shear stresses, can have a profound effect on the method and prediction of bearing fatigue lives.

Harries and Wei demonstrated the limitations of the Lundberg – Palmgren theory. The Lundberg – Palmgren theory was first published in Sweden in 1947. So at that time digital computers and numerical integration techniques were unknown. Therefore Lundberg – Palmgren were forced to assume that failure was associated with a single stress $\tau_o$ rather than the subsurface stress distribution from which it was obtained. Lundberg – Palmgren didn't consider the influence on the subsurface stress distribution of surface shear stresses and also they didn't consider the effectiveness of lubrication. Furthermore, the influence of ring hoop stresses as influenced by press fitting, ring rotation, heat treatment, and surface finishing techniques was not included

Harris and Wei [51] investigated the stress distribution used by LP and demonstrated that the maximum value of the subsurface orthogonal shear stress distribution used in the LP mathematical formula doesn't give an accurate prediction of the fatigue life. They

demonstrated that the selection of the maximum orthogonal shear stress $\tau_o$ as the failure – initiating stress was not appropriate.

Harris and McCool [52] showed that the octahedral shear stress $\tau_{oct}$ might be used as the fatigue – causing stress, yielding more accurate fatigue life prediction than does the LP – based theory. Harris and Barnsby [53] indicated that the surface shear (frictional) stress has a significant effect – in many modern high-speed bearing applications – on the bearings life.

In conclusion, Harries and Wei concluded that surface shear stresses can cause significantly reduced fatigue lives and since their effects can be included in the octahedral shear stress and Von Mises stress, there is a substantial reason to use the octahedral shear stress or Von Mises stress, as the failure – fatigue stress in fatigue life prediction analyses.

In 1985, Ioannides and Harris [54] presented a novel mathematical model for the prediction of fatigue life in ball bearings. Ioannides and Harris work was an extension of Lundberg – Palmgren theory that conducted during the late 1930's and early 1940's. Ioannides and Harris tackled the deficiencies, flaws and omissions in Lundberg – Palmgren theory. They considered the effect on subsurface stresses of surface shear stress, in addition to the normal stress, that been ignored by LP. Also IH defined a fatigue limit below, which the stressed volume element that known as the volume under risk will not fail by fatigue. In IH fatigue prediction model, any choice of fatigue criterion is permitted as long as that criterion can be calculated from the local stress tensor components instead of the maximum orthogonal shear stress that been used by LP which ignore the stresses that caused by the tangential loads due to friction. IH used the Weibull weakest link theory that been used by LP too.

For verification purposes, Ioannides and Harris calculated the fatigue life for rotating beams, beams in torsion and flat beams in reversed bending by applying their model at these cases. When Ioannides and Harris compared the calculated fatigue lives by applying their model on these cases with the experimental data, a good agreement have been reached.

**2.3 Cams:**

Cams are being used since long time and the origin of cams goes back deep into the history. It argues that the begging of cams was with the start of civilization. Angeles and Lopez – Cajun [55] claims that the origin of the cam mechanisms was in the ancient time in the *wedge,* one of the simple mechanisms in that time. Muller [56] claimed that the origin of the cam mechanisms goes back to the Paleolithic age about 10,000 years ago.

Kormas [57] presented graphs to calculate the maximum pressure angle and the minimum radius of curvature for a radial cam with a roller follower. Also Koumans provided graphs to calculate the maximum pressure angle and the minimum radius of curvature for a barrel cam with a roller follower. Both graphs have been made for sinusoidal acceleration. The above-mentioned graphs can be used for cams with an offset follower.

Cam design and size optimization has had the attention of many researchers in the last sixty years. Researchers have devoted a lot of their time and effort studying cam size optimization. Researchers followed different paths and approaches trying to optimize the cam size and achieve this goal. Researchers tried to optimize the cam size on the basis of the radius of the cam base circle, the width of the cam, the follower roller radius and its offset and so on. Chicurel [58] (1962) studied the effect of offsetting (eccentricity) on the cam size and published a paper where he showed that cam size could be reduced by introducing an

offsetting in the cam design. Chicurel showed in his paper that follower offset effects the pressure angle and then the cam size and he introduced a method that the follower optimum offset can be defined.

Suchora et al [59] (1994) plotted the maximum pressure angle values for simple harmonic, cycloidal and modified harmonic motion on nomograms for both full rise and full return motions. By using nomograms, they were able to compare several tentative designs to arrive at an optimum design quickly and easily. Chan and Sim [60] (1996) presented computer – aided design software, OPTICAM, which can be used to design and optimize the radial cams with different follower configurations. Their method based on an exploratory search method known as the Monte Carlo method, in which random points are generated over the range of all the variables.

# CHAPTER 3. Cam – Follower Systems and Follower Displacement Functions

Cam design and manufacture has changed dramatically in the second half of the last century. Until about the late 1960's cam design was very simple. Cams were designed and manufactured by manual graphical layout techniques and then manufactured in low quantities. At that time, cam design was closer to an art than to engineering science. The machinist used to lay the cam out with bluing using circle arcs and straight lines, cut it out on the band saw, sand it smooth with the belt sander and stick it on the machine [6]. Cams designed and manufactured in this way will not work for high speeds and also will not be precise. Nowadays, with the development of computers, cam design and manufacture have greatly improved and have moved from the art stage to an engineering science stage.

## 3.1 Cam – Follower Systems Classification:

In industry, there are many different types of cam – follower systems. Cam – follower systems can be classified in several ways:

- **Type of follower motion**: this classification refers to the type of follower motion. There are different types of motion like translating and oscillating motions. Translating roller follower and oscillating flat – face follower are considered in this study.
- **Type of joint closure**: this refers to the force-closed cam joint to keep the follower in contact with the cam all the time. In this study there was a spring to keep the follower in contact with the cam.

- **Type of follower**: there are many types of followers in industry. The most widely used type of followers in industrial machinery has a cam that rotates in contact with a cylindrical roller follower. The investigation was limited to the roller followers and flat – faced followers in this study.
- **Type of cam**: different types of cams are available in industry. Radial or axial cam are investigated in this study.
- **Type of motion constraints**: there are two general categories of motion constraint, critical extreme position and critical path motion. Critical extreme position refers to a category where the design specifications define only the start and end positions of the follower while there are no constraints on the follower path in between. Critical path motion is more constrained and there is a constraint on the motion path or one of its derivatives. Critical extreme position was investigated in this study.
- **Type of motion program**: this classification refers to the rise portion of the cam, the fall portion of the cam, and the number of dwells present in the full cycle of motion. Cams have different motion programs like rise – fall (RF), rise – fall – dwell (RFD), and rise – dwell – fall – dwell (RDFD) [61]. Dwells produce no output motion for a specified period of input motion. To make the study more general, the rise – dwell – fall – dwell (RDFD) motion are investigated in the study – figure 3.1.

Once the type of motion program has been specified, the first step for a designer is to select the mathematical functions to be used to define the motion of the followers. When choosing the mathematical displacement functions, the fundamental law of cam design requires that the cam – follower function must be continuous through the first and the second derivatives of displacement (i.e. velocity and acceleration) across the entire cycle [6]. Also,

the jerk function must be finite across the entire interval. The chosen mathematical displacement functions should be dynamically acceptable. Two different types of functions will be investigated in this study, the 3 – 4 – 5 polynomial and cycloidal displacement functions for double dwell cams.

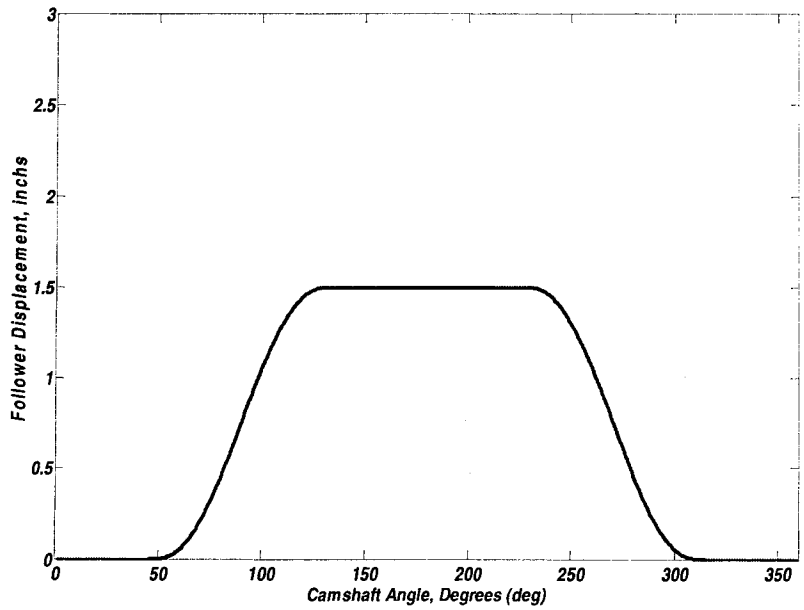


Figure 3.1 Follower displacement diagram

### 3.2 Cam and Follower Types:

As mentioned earlier, there are different types of cam – follower systems in the industry. In this study, two types of the cam – follower system are investigated for fatigue life which are radial cam with translating roller follower and radial cam with translating flat – face follower.

### 3.2.1 Radial Cam with Translating Roller Follower:

Figure 1.2a shows a radial cam with a roller follower. The smallest circle that can be drawn tangent to the cam surface is the base circle. The prime circle in the cam is the smallest circle that can be drawn tangent to the locus of the centerline of roller follower. Both the cam base circle and the prime circle have the same center line which the center of the cam rotation as shown in figure 3.2.

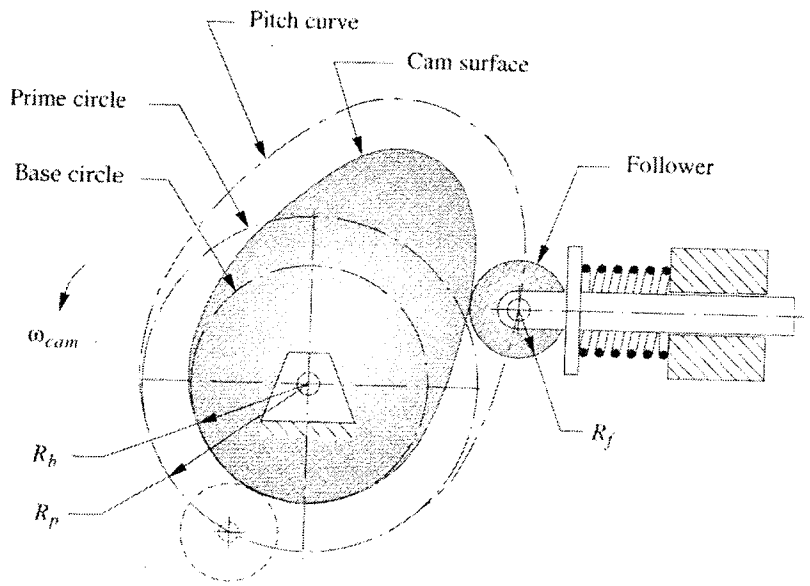


Figure 3.2 Base circle and prime circle of a radial cam with roller follower [1]

Two major factors in cam design, which determine the cam size, are the pressure angle and the radius of curvature. The pressure angle is the angle between the direction of the follower path and the normal to the pitch curve through the center of the cam follower [62] as shown in figure 3.3. Pressure angle is given by equation (3 – 1):

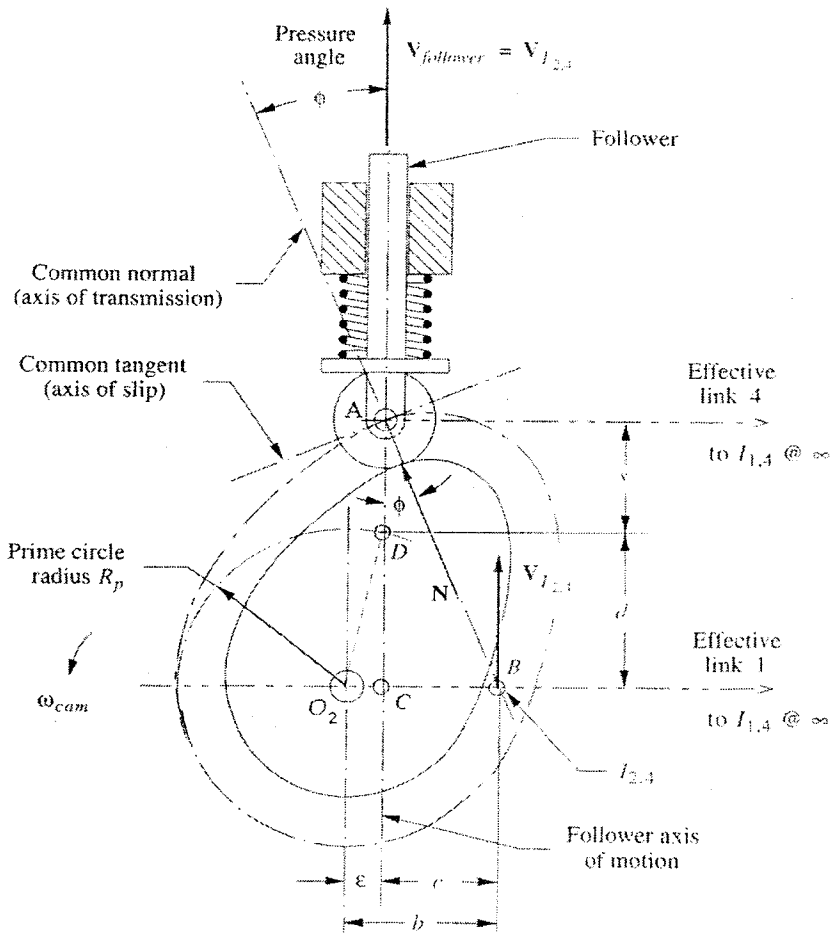


Figure 3.3 Geometry for radial cam with offset translating roller follower [1]

$$\phi = \arctan \frac{v - \varepsilon}{s + \sqrt{R_p^2 + \varepsilon^2}} \qquad (3-1)$$

Where $\phi$ = The pressure angle

$R_p$ = The prime circle radius

s = Follower displacement, in inches

$\varepsilon$ = Offset or eccentricity

$v = \frac{ds}{d\theta}$ = Follower velocity, in inches/rad (translating follower) or rad/rad

From the above equation, the pressure angle is a function of the prime circle radius, eccentricity, follower velocity and displacement. Therefore, pressure angle varies during the cycle due to the variation in the prime circle radius, follower velocity and displacement during the cycle. The pressure angle should be between zero and $\pm 30^{o}$. When the pressure angle exceeds these values, it will produce an appreciable lateral force exerted on the stem of the follower, which in the presence of friction, to undesirable limits that tend to bind the translating follower in its guides.

The radius of curvature at a point of the cam profile is the radius of a circle tangent at that point to the cam profile. The radius of curvature could be positive or negative values. In the rise or fall potion of the cam, the cam radius of curvature changes simultaneously. While in the first or second dwell, the radius of curvature has a constant value because those dwell portions are simply circular parts. For the radial with translating roller follower, the radius of curvature can be calculated using the following equation:

$$\rho = \frac{\left[\left(R_p + s\right)^2 + v^2\right]^{3/2}}{\left(R_p + s\right)^2 + 2v^2 - a\left(R_p + s\right)} \qquad (3-2)$$

Where $\rho$ = Radius of curvature of cam pitch curve, in inches

$R_p$ = The prime circle radius, in inches

s = Follower displacement, in inches

$a$ = Follower acceleration, in rad/sec$^2$

$v = \frac{ds}{d\theta}$ = Follower velocity, in inches/rad (translating follower) or rad/rad

The rule of thumb is to keep the absolute value of the minimum radius of curvature, $\rho_{min}$, of the cam pitch curve preferably at least 1.5 to 3 times as large as the radius of the roller follower, $R_f$ [6].

### 3.2.2 Radial Cam with Translating Flat – Face Follower:

Figure 1.2b shows a radial cam with a translating flat - face follower. In translating roller follower cam system, the pressure angle is zero for all positions of cam and follower. The radius of curvature for the translating flat – face follower can be defined by the following formula:

$$\rho = R_b + s + a \qquad (3-3)$$

$$a = \frac{dx}{d\theta} = \frac{dv}{d\theta} \qquad (3-4)$$

Where $R_b$ = Cam base circle radius

$s$ = Follower displacement

$a$ = Follower acceleration

From the above equation, the radius of curvature is a function of the base circle radius, follower displacement and follower acceleration.

### 3.3 Follower Displacement Functions:

A wide variety of follower displacement functions are available for moving the follower. Selection the mathematical function that be used to define the motion of the follower is very important in cam design. In this study, two types of follower displacement functions will be investigated; the 3 – 4 – 5 polynomial function and the cycloidal function.

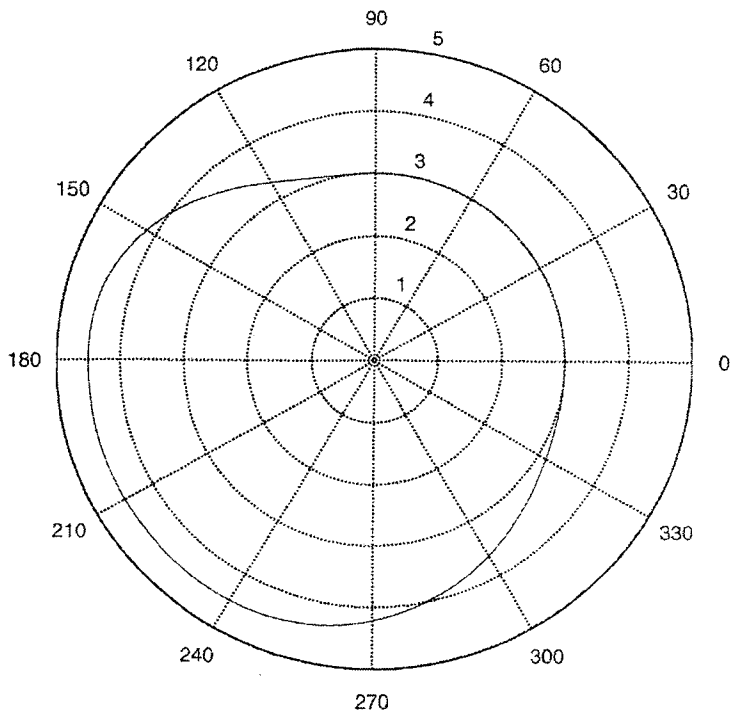


Figure 3.4 Cam profile using the 3 – 4 – 5 polynomial displacement function

#### 3.3.1 Polynomial (3 – 4 – 5) Displacement Function Analysis:

Polynomial displacement functions are among the most versatile for cam design. They are not limited to either single or double dwell applications and can be tailored to many design specifications. The 3 – 4 – 5 polynomial displacement function is used to represent the

follower displacement. This polynomial function is used to draw the cam profile (See figure 3.4). The general form of a polynomial function is:

$$s = C_o + C_1 x + C_2 x^2 + C_3 x^3 + C_4 x^4 + C_5 x^5 + C_6 x^6 + .... + C_n x^n \qquad (3-5)$$

The 3 – 4 – 5 polynomial displacement function is a special case of the polynomial general form family. The 3 – 4 – 5 polynomial displacement function, and the velocity, acceleration and jerk functions for the rise portion are given by the following:

The displacement function:

$$s = h\left[10\left(\frac{\theta}{\beta}\right)^3 - 15\left(\frac{\theta}{\beta}\right)^4 + 6\left(\frac{\theta}{\beta}\right)^5\right] \qquad (3-6)$$

Where s = Follower displacement, in inches

h = Total lift (rise or fall) of any one segment, in inches

$\beta$ = Total angle of any segment, rise, fall, or dwell, in degrees

$\theta$ = Angular displacement, in degrees

Differentiating the above equation with respect to $\theta$ gives the expression for velocity:

$$v = \frac{h}{\beta}\left[30\left(\frac{\theta}{\beta}\right)^2 - 60\left(\frac{\theta}{\beta}\right)^3 + 30\left(\frac{\theta}{\beta}\right)^4\right] \qquad (3-7)$$

Differentiating once again with respect to $\theta$ gives the expression for acceleration:

$$a = \frac{h}{\beta^2}\left[60\left(\frac{\theta}{\beta}\right) - 180\left(\frac{\theta}{\beta}\right)^2 + 120\left(\frac{\theta}{\beta}\right)^3\right] \qquad (3-8)$$

And differentiating a final time with respect to $\theta$ gives the expression for jerk:

$$j = \frac{h}{\beta^3}\left[60 - 360\left(\frac{\theta}{\beta}\right) + 360\left(\frac{\theta}{\beta}\right)^2\right] \qquad (3-9)$$

The 3 – 4 – 5 polynomial displacement function, the velocity, acceleration and jerk functions for the fall portion are given by the following:

The displacement function:

$$s = h\left[1 - 10\left(\frac{\theta}{\beta}\right)^3 + 15\left(\frac{\theta}{\beta}\right)^4 - 6\left(\frac{\theta}{\beta}\right)^5\right] \qquad (3-10)$$

$$v = \frac{h}{\beta}\left[-30\left(\frac{\theta}{\beta}\right)^2 + 60\left(\frac{\theta}{\beta}\right)^3 - 30\left(\frac{\theta}{\beta}\right)^4\right] \qquad (3-11)$$

$$a = \frac{h}{\beta^2}\left[-60\left(\frac{\theta}{\beta}\right) + 180\left(\frac{\theta}{\beta}\right)^2 - 120\left(\frac{\theta}{\beta}\right)^3\right] \qquad (3-12)$$

$$j = \frac{h}{\beta^3}\left[-60 + 360\left(\frac{\theta}{\beta}\right) - 360\left(\frac{\theta}{\beta}\right)^2\right] \qquad (3-13)$$

### 3.3.2 Cycloidal Displacement Function for Double Dwells:

The cycloidal displacement function is generated from a cycloid and has a sine acceleration curve. A cycloidal is the locus of a point on a circle that is rolled along a straight line. The circumference of the circle is equal to the follower rise $h$. In cycloidal functions; the jerk is finite which makes the cycloidal profile a good choice for high – speed applications. The cycloidal displacement functions, the velocity, acceleration and jerk functions for the rise portion are given by the following:

$$s = h\left[\frac{\theta}{\beta} - \frac{1}{2\pi}\sin\left(2\pi\frac{\theta}{\beta}\right)\right] \qquad (3-14)$$

$$v = \frac{h}{\beta}\left[1 - \cos\left(2\pi\frac{\theta}{\beta}\right)\right] \qquad (3-15)$$

$$a = 2\pi\frac{h}{\beta^2}\sin\left(2\pi\frac{\theta}{\beta}\right) \qquad (3-16)$$

$$j = 4\pi^2 \frac{h}{\beta^3} \cos\left(2\pi \frac{\theta}{\beta}\right) \qquad (3-17)$$

The cycloidal displacement function, the velocity, acceleration and jerk functions for the fall portion are given by the following:

$$s = h\left[1 - \frac{\theta}{\beta} + \frac{1}{2\pi} \sin\left(2\pi \frac{\theta}{\beta}\right)\right] \qquad (3-18)$$

Differentiating the above equation with respect to $\theta$ gives the expression for velocity:

$$v = \frac{h}{\beta}\left[\cos\left(2\pi \frac{\theta}{\beta}\right) - 1\right] \qquad (3-19)$$

Differentiating the above equation with respect to $\theta$ gives the expression for acceleration:

$$a = -2\pi \frac{h}{\beta^2} \sin\left(2\pi \frac{\theta}{\beta}\right) \qquad (3-20)$$

And differentiating the above equation with respect to $\theta$ gives the expression for jerk:

$$j = -4\pi^2 \frac{h}{\beta^3} \cos\left(2\pi \frac{\theta}{\beta}\right) \qquad (3-21)$$

The study has been divided into two parts: a radial cam with a translating roller follower and a radial cam with a translating flat – faced follower. So in this study, the roller follower and flat – faced follower has been investigated for fatigue life using the 3 – 4 – 5 polynomial displacement function and the cycloidal displacement function and the cam size and other parameters has been optimized. Program codes has been written for this purpose to calculate the spring constant needed to keep the follower in contact with the cam, the resultant force on the cam, the stress distributions on the cam surface and beneath the surface, the depth for these stresses distribution, the cam radius of curvature and the volume under risk (VUR). Once all of these variables are determined, the Ioannides – Harris (IH) approach will be applied to predict fatigue life.

# CHAPTER 4. Force and Contact Stress Analysis

## 4.1 Force Analysis

There are forces associated with the motion of the cam and the follower. Different types of forces act on cams during their rotational movement. In design process, the magnitude, direction and line of forces action should be defined and evaluated so that the stress distribution can be defined and the dimensions of the cam can chosen to provide sufficient strength and rigidity, given the appropriate choice of materials. Generally cams and follower system are subjected to different types of forces. The type of forces that act on the cam depends on the cam application, which means that not every cam should be subjected to the same type of forces. In general, the forces acting on the cam and follower system are the inertia forces, spring forces, vibratory forces, frictional forces between the cam and the follower and other external forces.

### 4.1.1 Inertia Forces:

The inertia forces in most cam – follower systems are among the most important of all the forces analyzed, especially at high speeds. Inertia forces are caused by the necessity of moving the follower masses linearly or rotationally. The inertial force on a linearly moving follower is a product of the follower mass and the acceleration of the follower

$$F = mA \qquad (4-1)$$

Where $A$ = Acceleration, in $in/\sec^2$

m = Follower mass, $lb$

F = Force, in $lb$

The inertia force, passing through the center of gravity of the body, has a direction opposite to that of the acceleration.

**4.1.2 Spring Force:**

The main functions of the spring force are to counteract the inertia forces of the follower and to keep the follower in contact with cam all the time throughout the motion cycle. The spring rate is the product of the follower mass and the follower displacement. Therefore, the rate is proportional to the follower displacement. The spring force should be adequate to keep the follower in contact with the follower. High spring force will increase the resultant or normal load on the cam and therefore will increase the stress distribution and will lead to excessive wear and reduce the cam fatigue life. Conversely, low spring force will let the follower jump off the cam surface. The required spring stiffness is determined at the point where the follower inertia force is a maximum and tends to eliminate contact between cam and the follower. The inertia force is a maximum at the point where the acceleration has a maximum negative value. Therefore, jump will occur if the inertia force exceeds the spring force at this point.

The spring force, $F_s$, on the roller follower can be calculated using Hooke's law as follows:

$$F_s = K(\delta + x) \qquad (4-2)$$

Where $K$ = Spring rate, lb/in

$\delta$ = Spring initial deflection (inch)

$x$ = Spring compression (inch) that can be calculated using the cam displacement function

### 4.1.3 Vibratory Forces:

Forces due to vibration are a result of the sudden changes in the elastic deformations. These vibration forces which are superimposed on the follower inertia forces increases the stress distribution in the cam. In this study, it's assumed that there are no forces due to vibration or sudden movement so forces due to vibrations are ignored.

### 4.1.4 Friction Forces:

Friction is inherent between contacting parts in relative motion. In the case of a cam – roller follower mechanisms, the contact is approximated by a contact between two cylinders. The contact is assumed to be a pure rolling contact therefore; the frictional forces are very small so they can be neglected, while in the case of a flat – face follower, the frictional forces are considered in the analysis.

### 4.1.5 External Forces:

External forces may fall into anyone of these categories: impact forces (mechanical shock), gradually applied forces or suddenly applied forces. In this study, it is assumed that there no external forces applied at the cam or follower.

Finally the normal force (the resultant force) between the cam follower can be calculated as follows:

$$F_n = (\frac{1}{\cos\phi})(F_{Inertia} + F_{Spring} + F_{ext}) \qquad (4-3)$$

Where $\phi$ = The pressure angle

$F_{ext}$ = External forces

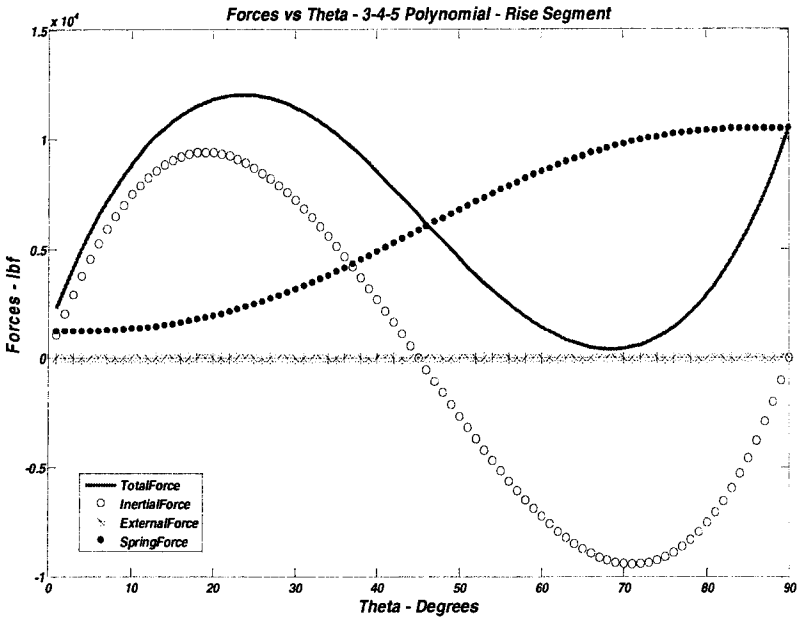


Figure 4.1: Forces applied on the cam

In the cam roller – follower mechanism, an important assumption has been made in this study. The assumption is that the rolling is pure rolling, and the vibration in the system has been neglected. Therefore, the forces due to friction and vibration are ignored in the cam roller – follower mechanism case. The only forces in this system will be the inertia forces, the spring force and the normal force between the follower and the cam. These forces have been calculated and simulated using a program code written in Matlab and the required spring constant has been determined.

In this study, the follower mass was $0.5\,lb$, the follower radius $R_f$ was 0.5 inch and the cam angular speed was 700 $rev/\min$. From figure 4.1, its evident the inertia forces on the follower becomes negative which means that the follower will tend to fly off the cam. To keep the follower in contact with the cam, a positive force should be applied. This force can

be provided by a spring. The spring force is proportional to the follower mass and the angular velocity of the cam due to equation 4.1:

$$F = mA$$

From the above equation, it's clear that the stresses due to inertia force on the cam will be less when the angular velocity is low. While the stresses will be much higher when cam angular speeds are at higher levels.

In the cam flat – face follower mechanism, the forces due to friction between the cam and the flat – face follower are considered in the analysis and the stresses due to these tangential forces are calculated.

### 4.2 Contact Stress Analysis

The contact stresses studied herein pertain to stresses developed at the contact surface between the follower and the cam due to tangential and normal loads. The problem of the cam and follower is simplified by assuming two parallel cylinders in contact, as shown in figure 4.2, for the Hertzian stress analysis. This way, the problem is easier to deal with, but still close to reality, and all the results are applicable to the case of the cam and roller follower. This assumption is valid for the roller follower, which is a short cylinder. However, for the cam lobe that has a general shape, different cylinder radii are considered depending on the location: that is, the second dwell, the base circle, the rise and the fall segments.

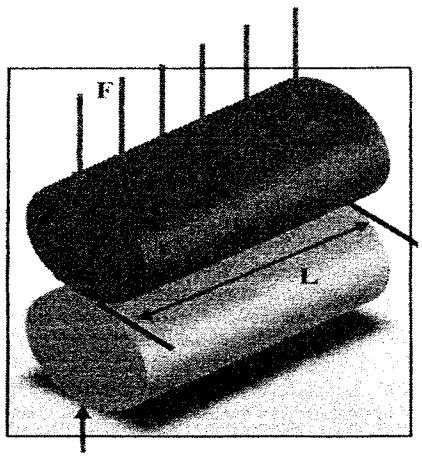


Figure 4.2 Two cylinders in contact

According to Hertzian theory [63], the shape of the contact surface between the roller follower and the cam is a rectangular of width 2a and length L, and the pressure distribution $P$ is characterized by a semi – ellipse as illustrated by figure 4.3

Calculating the contact stresses requires knowledge of the pressure distribution, $P$, and the maximum pressure $P_{max}$. All these data are obtained by knowing the load on these cylinders and the geometric and material properties, such as Young's modulus, Poisson ratio, the radius of each cylinder, etc.

The applied load F on the contact patch is equal to the volume of the half – prism [6]:

$$F = \tfrac{1}{2}\pi a L P_{max} \qquad (4-4)$$

Where F = the total applied load

L = the length of contact along the cylinder axis.

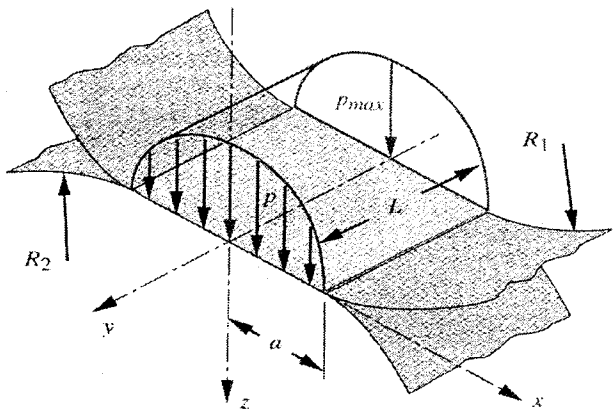


Figure 4.3 Ellipsoidal – prism pressure distribution in cylindrical contact

This can be solved for the maximum pressure:

$$P_{\max} = \frac{2F}{\pi aL} \qquad (4-5)$$

The average pressure is the applied force divided by the contact – patch area:

$$P_{avg} = \frac{F}{Area} = \frac{F}{2aL} \qquad (4-6)$$

Now we define a cylinder geometry constant that depends on the radii $R_1$ and $R_2$ of the two cylinders:

$$B = \frac{1}{2}\left(\frac{1}{R1} + \frac{1}{R2}\right) \qquad (4-7)$$

To account for a flat face follower, $R_2$ becomes infinite, making $\frac{1}{R_2}$ zero. The contact – patch half – width $a$ is then found from:

$$a = \sqrt{\frac{2}{\pi}\frac{m_1+m_2}{B}\frac{F}{L}} \qquad (4-8)$$

Where $m_1$ and $m_2$ are material constants as defined by the following equations:

$$m_1 = \frac{1-\nu_1^2}{E_1} \text{ and } m_2 = \frac{1-\nu_2^2}{E_2} \qquad (4-9)$$

Where $E_1$, $E_2$ and $\nu_1$, $\nu_2$ are the Young's moduli and Poisson's ratios for the materials of cylinder 1 and cylinder 2, respectively.

Then the pressure at any point in the contact area can be defined simply by using x, since the pressure distribution here has a constant value along the $x-axis$ :

$$P = P_{\max}\sqrt{(1-\frac{x^2}{a^2})} \qquad (4-10)$$

Which is an ellipse as shown in figure 4.3.

### 4.2.1 Stress Analysis in Cam Roller – Follower Mechanisms:

As mentioned earlier in this study, the cam roller – follower mechanism is considered to be of two cylinders in pure rolling contact. Therefore, the tangential sliding forces due to

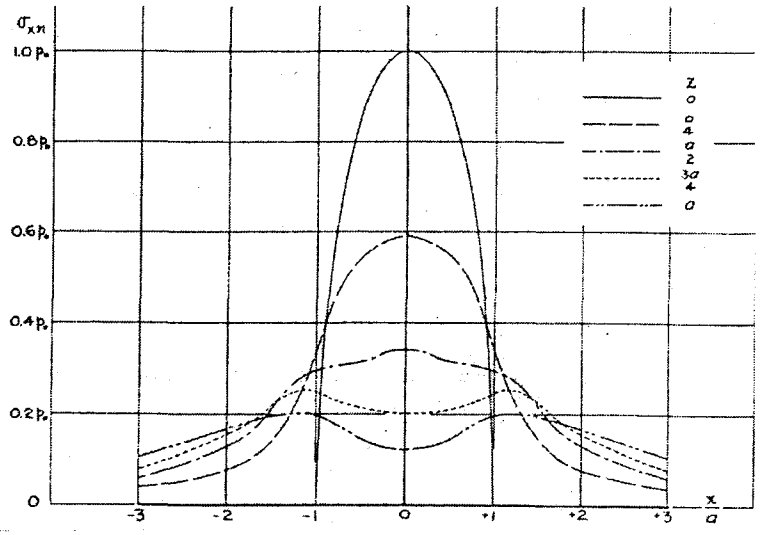


(a): Curves showing values of stress $\sigma_{xn}$ for various values of x, at surface and at various depths below surface

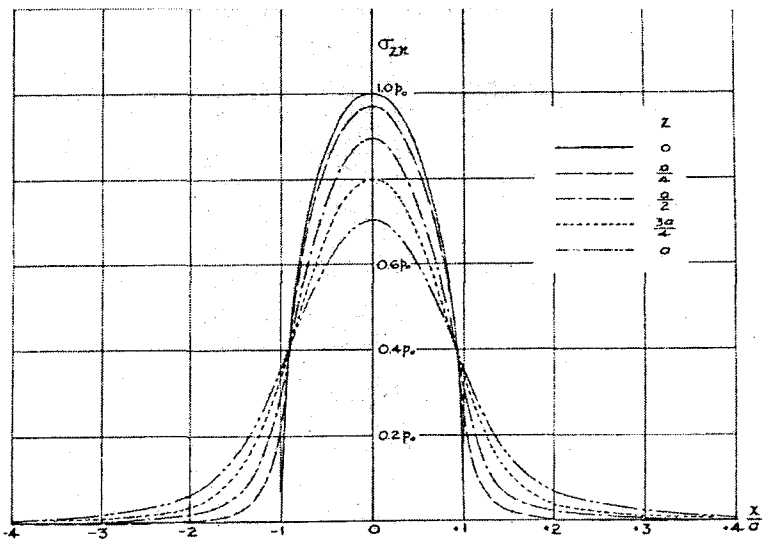


(b): Curves showing values of stress $\sigma_{zn}$ for various values of x, at surface and at various depths below surface

Figure 4.4 Normal plane stresses ($\sigma_x$ and $\sigma_z$) at various points within the contact zone [7]

friction has been ignored. Hertzian stress analysis is for static loading but is also applied to pure rolling contact. Figure 4.4 shows normal plane stresses ($\sigma_x$ and $\sigma_z$) at various points within the contact zone for the case of two parallel cylinders normally loaded. The normal plane stress values are given in terms of $P_{max}$ and the distance along the $x-axis$ is expressed in terms of $a$. From figure 4.4, it's clear that the applied stresses have their maximum value on the load axis $(x=0)$ and as we depart from the load axis $(x=0)$, the applied stresses start decreasing. Stresses have been studied at the centerline of contact $(x=0)$ and figure 4.5 shows the principle stresses, maximum shear stresses and von Mises stress distributions across the patch width at the surface and along the z-axis for two cylinders in pure contact. From figure 4.5, it is clear that the principle stresses are a maximum at the surface and they diminish rapidly with depth. The Von Mises stress distribution has the maximum value somewhere below the surface.

With reference to figure 4.5, on the surface (z=0) at the load axis (x=0), the applied and principle stresses are:

$$\sigma_x = \sigma_z = -p_{max}$$

$$\sigma_y = -2\upsilon p_{max} \qquad (4-11)$$

$$\sigma_1 = \sigma_x,\ \sigma_2 = \sigma_y \text{ and } \sigma_3 = \sigma_z$$

The normal and shear plane stresses can be calculated adopting the method of Smith and Liu [7] assuming no sliding between the cam and the follower in the case of the roller cam follower. At the surface, the plane stresses can be calculated using equations (4 – 11).

The subsurface stress field can be calculated using the following equations:

$$\sigma_{x_n} = -\frac{z}{\pi}\left[\frac{a^2+2x^2+2z^2}{a}\beta - \frac{2\pi}{a} - 3x\alpha\right]p_{\max}$$

$$\sigma_{z_n} = -\frac{z}{\pi}[a\beta - x\alpha]p_{\max} \qquad (4-12a)$$

$$\tau_{xz_n} = -\frac{1}{\pi}z^2\alpha p_{\max}$$

Where $\alpha$ and $\beta$ are defined by the following equations:

$$\alpha = \frac{\pi}{k_1}\frac{1-\sqrt{\frac{k_2}{k_1}}}{\sqrt{\frac{k_2}{k_1}}\sqrt{2\sqrt{\frac{k_2}{k_1}}+\left(\frac{k_1+k_2-4a^2}{k_1}\right)}} \qquad (4-12\text{ b})$$

$$\beta = \frac{\pi}{k_1}\frac{1+\sqrt{\frac{k_2}{k_1}}}{\sqrt{\frac{k_2}{k_1}}\sqrt{2\sqrt{\frac{k_2}{k_1}}+\left(\frac{k_1+k_2-4a^2}{k_1}\right)}} \qquad (4-12\text{ c})$$

And $k_1$ and $k_2$ are given by:

$$k_1 = (a+x)^2 + z^2 \text{ and } k_2 = (a-x)^2 + z^2 \qquad (4-12\text{d})$$

Equations (4 – 12) define the behavior of the stress functions below the surface, but when z=0, the factors $\alpha$ and $\beta$ become infinite and these equations fail. Other forms are needed to account for the stresses on the surface of the contact patch [6].

When z =0

$$\text{If } |x| \le a \text{ then } \sigma_{x_n} = -p_{\max}\sqrt{1-\frac{x^2}{a^2}} \text{ else } \sigma_{x_n} = 0$$

$$\sigma_{z_n} = \sigma_{x_n} \qquad (4-13a)$$

$$\tau_{xz_n} = 0$$

$$\text{If } x \ge a \text{ then } \sigma_{x_t} = -2f_{\max}\left(\frac{x}{a} - \sqrt{\frac{x^2}{a^2}-1}\right)$$

$$\text{If } x \le -a \text{ then } \sigma_{x_t} = -2f_{\max}\left(\frac{x}{a} + \sqrt{\frac{x^2}{a^2}-1}\right) \qquad (4-13b)$$

$$\text{If } |x| \le a \text{ then } \sigma_{x_t} = -2f_{\max}\frac{x}{a}$$

$$\sigma_{z_t} = 0 \qquad (4-13c)$$

$$\text{If } |x| \le a \text{ then } \tau_{xz_t} = -f_{\max}\sqrt{1-\frac{x^2}{a^2}} \text{ else } \tau_{xz_t} = 0$$

The total stress on each Cartesian plane is found by superposing the components due to the normal and tangential loads:

$$\sigma_x = \sigma_{x_n} + \sigma_{x_t}$$

$$\sigma_z = \sigma_{z_n} + \sigma_{z_t} \qquad (4-14a)$$

$$\tau_{xz} = \tau_{xz_n} + \tau_{xz_t}$$

The total stress on each Cartesian plane is found by superposing the components due to the normal and tangential loads:

$$\sigma_x = \sigma_{x_n} + \sigma_{x_t}$$

$$\sigma_z = \sigma_{z_n} + \sigma_{z_t} \qquad (4-14b)$$

$$\tau_{xz} = \tau_{xz_n} + \tau_{xz_t}$$

Since the tangential sliding forces due to friction have been ignored according to the assumption of pure rolling contact between the cam and the roller follower, the tangential stress distribution components ($\sigma_{x_t}$, $\sigma_{z_t}$, $\tau_{x_t}$) are deleted from the above equations in the stress analysis for the roller – follower when the program codes were written.

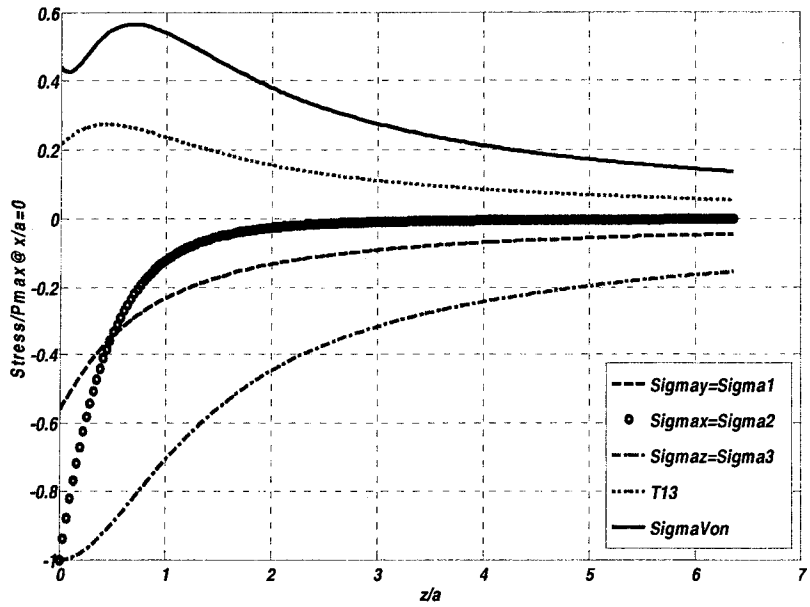


Figure 4.5 Applied, principle and Von Mises stresses with depth @ x/a =0

The stress distribution has been studied with the angular displacement of the cam using the code written in Matlab. By using the program codes, the applied stresses; principal stresses and Von Mises stress distribution in the cam has been calculated as shown in figure 4.5 and figure 4.6. Figure 4.6 shows that the Von Mises stress distribution has the maximum value at $\frac{x}{a}=0$. Figure 4.7 shows the Von Mises stress distribution in the cam at different rotation angles and at different depths below the cam contact surface. Also the graph shows the endurance limit that appears as a straight horizontal line. The program code calculates the stresses distributions for all the cam segments – the rise portion, the fall portion and the dwell portions. Figure 4.7 shows the Von Mises stress distribution in just the rise portion of the cam.

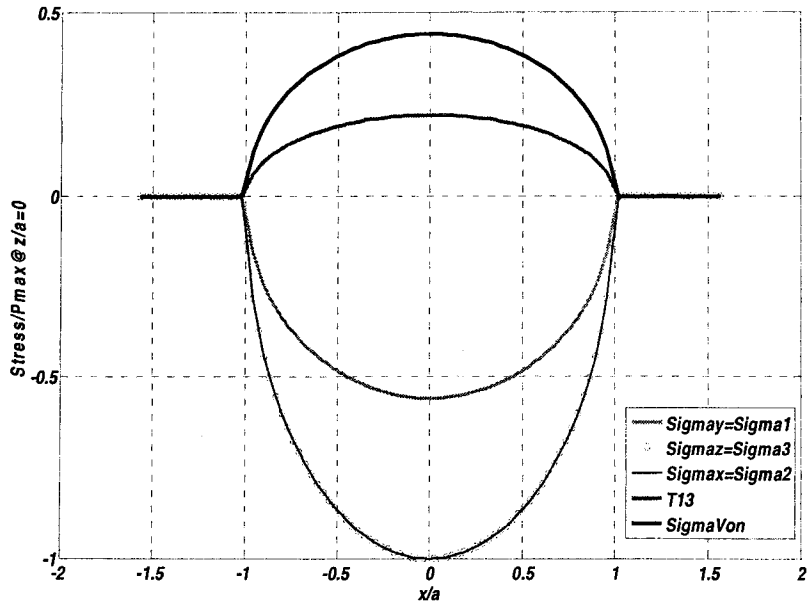


Figure 4.6 Applied, principle and Von Mises stresses with x – axis @ z/a =0

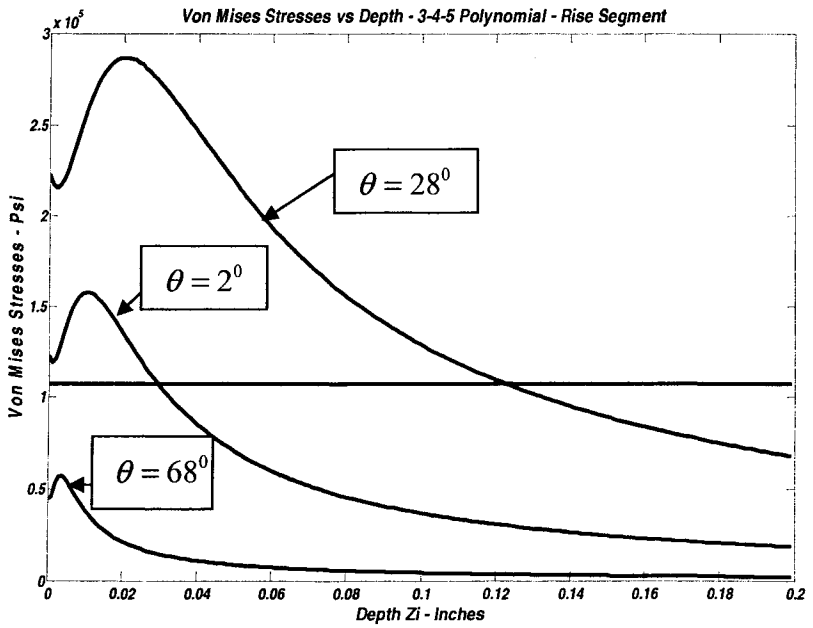


Figure 4.7 Von Mises stress distribution in the cam rise segment ( $90 \geq \theta \geq 0$ )

### 4.2.2 Stress Analysis in Cam Flat – Face Follower Mechanisms:

The cam flat – face follower mechanism is considered to be of two cylinders in contact. The radius of curvature $R_2$ of the second cylinder which is the flat face – follower is infinite, making $\frac{1}{R_2}$ zero in equation (4 – 15)

$$B = \tfrac{1}{2}(\tfrac{1}{R1} + \tfrac{1}{R2}) \qquad (4-15)$$

The tangential sliding forces due to friction in the flat – face follower are introduced in the analysis. The presence of the tangential sliding forces has a significant effect on the stresses compared to pure rolling. The stresses distribution due to the frictional loading are calculated using the following equations:

$$\sigma_{x_t} = -\frac{1}{\pi}[(2x^2 - 2a^2 - 3z^2)\alpha + 2\pi\frac{x}{a} + 2(a^2 - x^2 - z^2)\frac{x}{a}\beta]f_{\max}$$

$$\sigma_{z_t} = -\frac{1}{\pi}z^2\alpha f_{\max} \qquad (4-16)$$

$$\tau_{xz_t} = -\frac{1}{\pi}[(a^2 + 2x^2 + 2z^2)\frac{z}{a}\beta - 2\pi\frac{z}{a} - 3xz\alpha]f_{\max}$$

The stress distribution due to the normal loading between the cam and the flat – face follower is calculated using the same equations that used for the roller follower. The total stress on each Cartesian plane is found by superposing the components due to the normal and tangential loads:

$$\sigma_x = \sigma_{x_n} + \sigma_{x_t}$$

$$\sigma_z = \sigma_{z_n} + \sigma_{z_t} \qquad (4-14b)$$

$$\tau_{xz} = \tau_{xz_n} + \tau_{xz_t}$$

The maximum shear stress that the material experiences depends on depth and location around the cam. Differentiating between plane stress and plane strain conditions is important because the maximum shear stress is different in each case. Plane stress is assumed to occur at points of the material close to the edge. The normal and shear stresses in the axial direction at this location are zero. Plane strain is assumed to occur at points in the middle of the body in the axial direction (y – axis) – figure 4.3. In this case, the normal and shear strains in the axial direction are neglected. In the case of plane strain, the stress in the y direction will be:

$$\sigma_y = \upsilon(\sigma_x + \sigma_z) \qquad (4-17)$$

The tangential unit force $f_{\max}$ is found from the normal load and a coefficient of friction $\mu$

$$f_{\max} = \mu p_{\max} \qquad (4-18)$$

After defining the equations for calculating both normal and tangential stresses, the next logical step would be to get the equations to find the principal stresses. The principal stresses can be calculated using the following equations:

$$\sigma^3 - (\sigma_x + \sigma_y + \sigma_z)\sigma^2 + (\sigma_x\sigma_y + \sigma_x\sigma_z + \sigma_y\sigma_z - \tau_{xy}^2 - \tau_{yz}^2 - \tau_{zx}^2)\sigma$$
$$-(\sigma_x\sigma_y\sigma_z + 2\tau_{xy}\tau_{yz}\tau_{zx} - \sigma_x\tau_{yz}^2 - \sigma_y\tau_{zx}^2 - \sigma_z\tau_{xy}^2) = 0$$

$$a_1 = -(\sigma_x + \sigma_y + \sigma_z) \qquad (4-19)$$

$$a_2 = (\sigma_x\sigma_y + \sigma_x\sigma_z + \sigma_y\sigma_z - \tau_{xy}^2 - \tau_{yz}^2 - \tau_{zx}^2)$$

$$a_3 = -(\sigma_x\sigma_y\sigma_z + 2\tau_{xy}\tau_{yz}\tau_{zx} - \sigma_x\tau_{yz}^2 - \sigma_y\tau_{zx}^2 - \sigma_z\tau_{xy}^2)$$

$$x^3 + a_1x^2 + a_2x + a_3 = 0$$

Where $\sigma_x, \sigma_y, \sigma_z, \tau_{xy}, \tau_{yz}$, and $\tau_{xz}$ are the six components of the stress tensor.

Now after calculating all of the three principal stresses, the Von Mises stress is determined using the following equation:

$$\sigma' = \sqrt{\frac{(\sigma_1 - \sigma_2)^2 + (\sigma_2 - \sigma_3)^2 + (\sigma_1 - \sigma_3)^2}{2}} \qquad (4-20)$$

Harries and Wei [51] concluded that the surface shear stresses can significantly reduced fatigue lives and since their effects can be included in the Von Mises stress, there is a substantial reason to use the Von Mises stress, as the failure – causing stress in fatigue life

prediction analyses. Since Von Mises can be calculated from the components of the local stress tensor, so the Von Mises stress distribution will be the criterion that will be used in the cam – follower systems fatigue life prediction analysis.

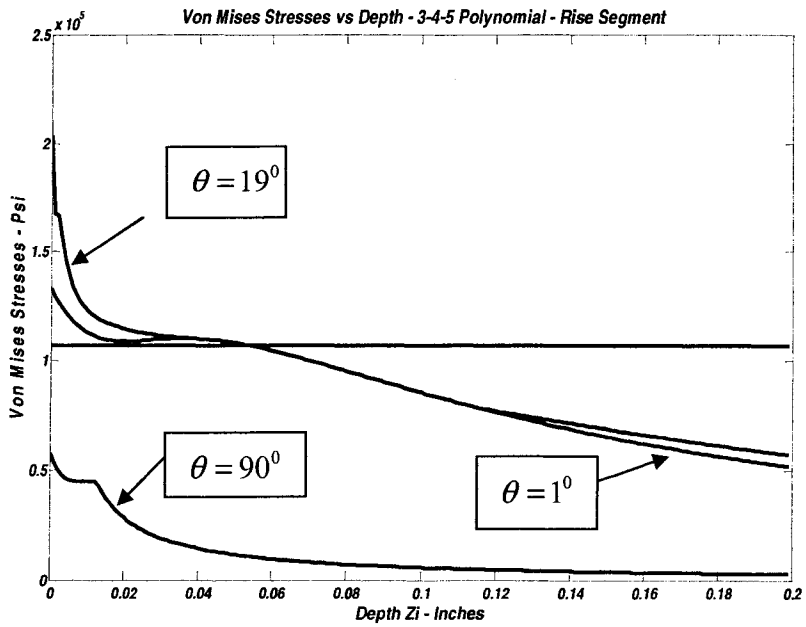


Figure 4.8 Von Mises stress distribution in the cam flat face follower – rise segment

$$(90 \geq \theta \geq 0)$$

The stress distribution in the cam flat – face follower mechanism has been simulated using the program codes written in Matlab. Figure 4.9 shows the Von Mises stress distribution with depth. The Von Mises stress distribution is a maximum at the contact surface and then diminish rapidly with the depth. Comparing the Von Mises stress distribution in flat – face follower with that in the roller follower shows that the Von Mises

stress distribution in the roller follower had its maximum value somewhere beneath the surface while in the flat – face follower, the maximum value of the Von Mises stress distribution is at the surface. Also it is found that the Von Mises stress distribution in the case of the roller follower is much higher than the Von Mises stress distribution in the flat – face follower case. These differences are due to the inclusion of the tangential stresses due to sliding frictional forces in the flat – face follower and due to the influence of the infinite radius of curvature of the flat follower.

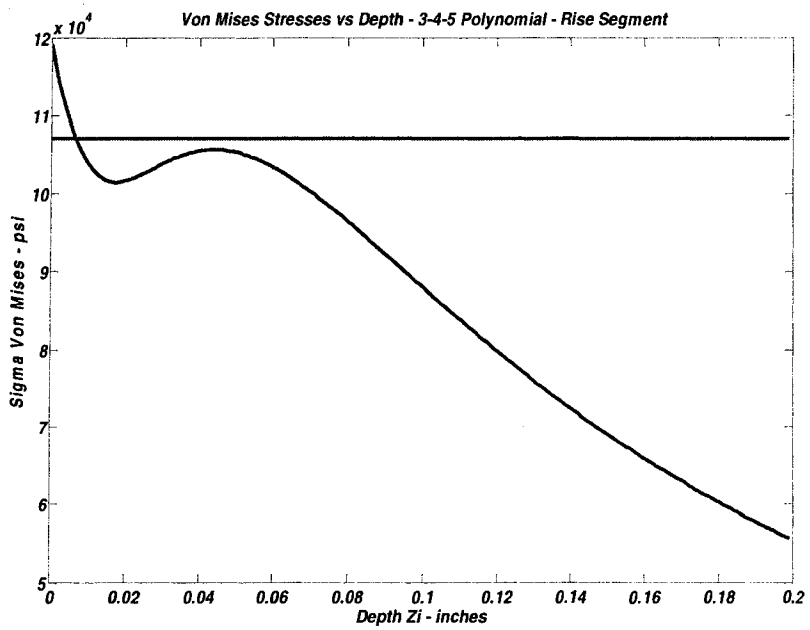


Figure 4.9 Von Mises stress distribution in the cam flat face follower at a specific angle – rise segment

The principal stresses and Von Mises stress distribution in the cam has been calculated as shown in figure 4.10 and figure 4.11 respectively. Figure 4.11 shows that the Von Mises stress distribution is a maximum at $\frac{x}{a} = 0.4$ when $\mu = 0.33$.

The Von Mises stress distribution in the cam flat – face follower system has been studied at different angular displacement of the cam. Figure 4.8 shows the Von Mises stress distribution in the cam at different rotation angles and at different depths below the cam contact surface. Also the graph shows the endurance limit that appears as a straight horizontal line. From figure 4.8, its clear that only small areas in the cam have a Von Mises stress distribution higher than the endurance limits compared with the roller follower case. This is due to the effect of the infinite radius of curvature of the flat – face follower. As it mentioned earlier, the radius of curvature of the flat follower is infinite which cancel the term $\frac{1}{R_2}$ from equation (4 – 15) due to the fact that $\frac{1}{R_2}$ is zero when the radius of curvature is infinite. The cancellation of the term $\frac{1}{R_2}$ from equation (4 – 15) will reduce the cylinder geometry constant $B$. The reduction in $B$ will increase patch half – width $a$ in equation (4 – 8). This increase in $a$ will increase the contact area between the flat follower and the cam due to the improvement in the degree of conformity between the flat follower and the cam and therefore the Hertzian stresses will drop in the cam flat – face follower.

The program code calculates the stresses distributions for all the cam segments – the rise portion, the fall portion and the dwell portions. Figure 4.8 shows the Von Mises stress distribution in just the rise portion of the cam.

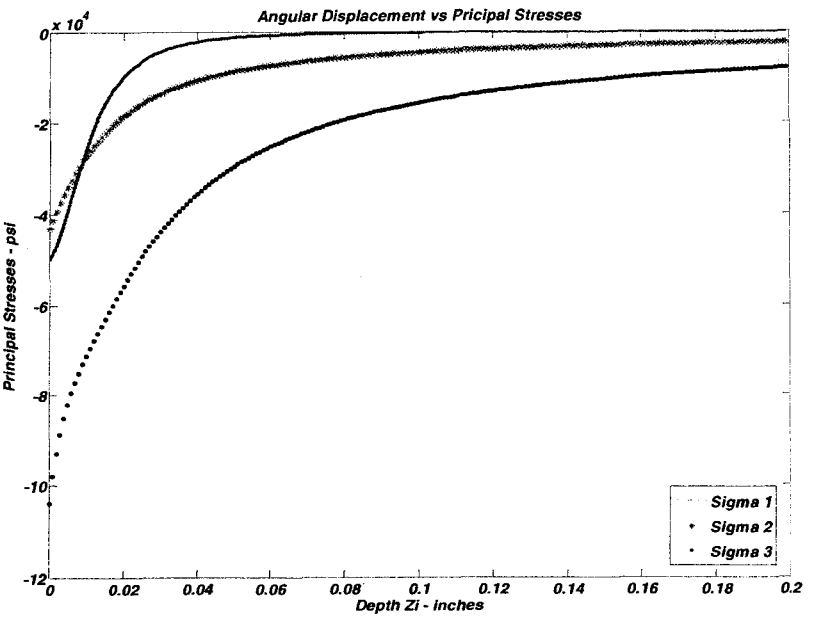


Figure 4.10 Principal stresses in flat face follower

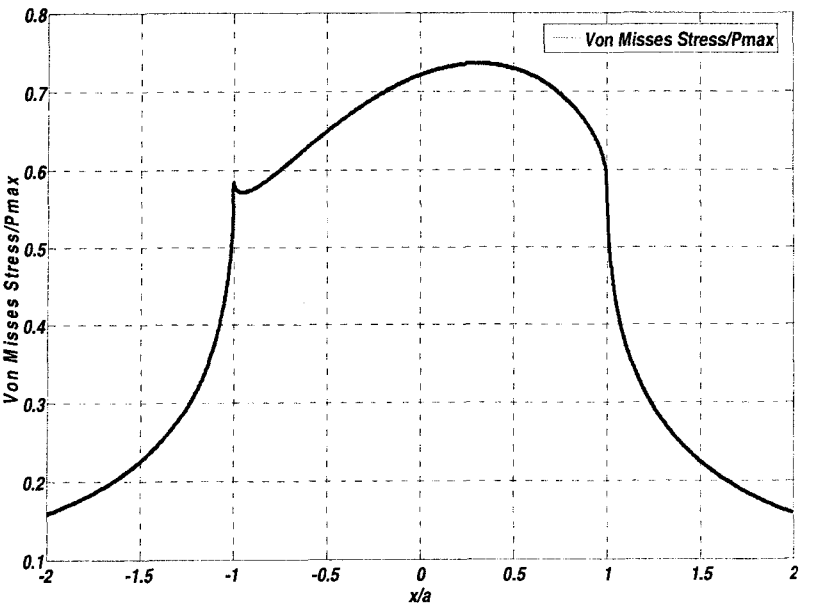


Figure 4.11 Normalized Von Mises stress distribution in flat face follower

**4.3 Ioannides – Harris (IH) Model for the Prediction of Fatigue Life:**

By using the program codes written in Matlab, the numerical simulation provided the stress distributions through out the cam's body. After that, a fatigue life model is required to estimate the fatigue life of the cam. As it mentioned earlier in the literature review, in 1985, Ioannides and Harris [54] propound a life model based on spalling process arising at defects or beneath the contact surface. Their model was a modification of the Lundberg-Palmgren (LP) life theory. The IH theory is based on the statistical relationship between the probability of survival, the fatigue life and the stress level above the endurance limit in a certain region of the cam, called the risk volume. The basic IH equation is:

$$\ln\frac{1}{\Delta S_i} = F(N, \sigma_i - \sigma_{ui})\Delta V_i \qquad (4-21)$$

Where:

$\Delta S_i$ : The probability of survival

$\Delta V_i$ : Volume element where the stress is higher than the endurance limit

$N$ : Fatigue life

$\sigma_i$ : Stress – related fatigue criterion (e.g. Von Mises Stress Distribution)

$\sigma_{ui}$ : Fatigue limit (e.g. Endurance limit)

In IH theory, the choice of the critical stress is left open for any fatigue criterion as long as that criterion can be calculated from the local stress tensor components instead of the maximum orthogonal shear stress that been used by LP theory which ignore the stresses that

caused by the tangential loads due to friction. In this analysis, the failure – causing stress has been assumed to be the Von Mises stress.

The final IH mathematical formulation for calculating fatigue life is as follows:

$$\ln\frac{1}{S} = AN^{e}\int_{V_R}\frac{(\sigma' - \sigma_u)^c}{z'^h}dV \qquad (4-22)$$

Where A = Constant of proportionality

c = Stress criterion exponent

$\sigma_u$ = Fatigue limit which is the endurance limit *Se* in this study

$\sigma'$ = Von Mises stress distribution defined by equation (4 – 20)

N = Fatigue Life

e = Life exponent

S = Probability of survival

h = Depth exponent

z' = Stress weighted average depth

From equation (3 – 22), the fatigue life formula can be expressed as follows:

$$N = \left[\frac{\ln(1/S)}{A.\int_V \frac{(\sigma - \sigma_u)^c}{z'^h}.dV}\right]^{1/e} \qquad (4-23)$$

Calculating the cam fatigue life will require the determination of the constant A experimentally. However, since the concern in this study is to investigate the cam fatigue life

and the effect of the cam base circle radius and the other cam design parameters on the fatigue life, then the concern will be in the relative fatigue life other than the absolute life. The relative life $L_{rel}$ will be the life L divided by a reference life. The reference life in this study will be the fatigue life at the minimum acceptable cam base circle radius. As it mentioned earlier, the minimum acceptable cam base circle radius is the radius where the absolute value of the minimum radius of curvature $\rho_{\min}$ of the cam pitch curve preferably at least 1.5 to 3 times as large as the radius of the roller – follower $R_f$ and the pressure angle to be between zero and $\pm 30^0$.

For this purpose; to calculate the relative fatigue life; Nikas formula [64] (equation (4 – 24)) will be adopted in this study:

$$L_{(ref)} = \left[ \int_{V_{ref}} (\sigma - \sigma_u)^c .dV \Big/ \int_{V_\sigma} (\sigma - \sigma_u)^c .dV \right]^{1/e} \qquad (4-24)$$

# CHAPTER 5. Results and Discussion

Fatigue life has been investigated in this study for both the 3 – 4 – 5 polynomial displacement function and the cycloidal displacement function. The study conducted under the following conditions: the cam angular velocity was 700 rev/min, the total lift (rise or fall) $h$ was 1.5 inches, eccentricity or offset was zero and the follower mass was 0.5 lb and the follower and cam material were steel 4140.

## 5.1 Cam Roller – Follower Systems Results:

The results and discussion of the cam roller – follower mechanism for the 3 – 4 – 5 polynomial and cycloidal displacement functions will be presented in this part of the study.

### 5.1.1 Polynomial (3 – 4 – 5) Displacement Function Results:

In the previous chapter of this study, the stress distribution in the contact zone in the cam has been determined and simulated using the program codes that been written in Matlab. After that the volume under risk; where the stress distribution in this volume is higher than the endurance limit; has been studied and calculated. The endurance limit is defined as "The stress level below which a specimen will withstand cyclic stress indefinitely without exhibiting fatigue failure. Rigid, elastic, low damping materials such as thermosetting plastics and some crystalline thermoplastics do not exhibit an endurance limit" [65]. Endurance limit can be calculated using the following equation [66]:

$$S_e^{'} = \begin{cases} 0.504 S_{ut} & S_{ut} \le 212 kpsi (1460 Mpa) \\ 107 kpsi & S_{ut} > 212 kpsi \\ 740 Mpa & S_{ut} > 1460 Mpa \end{cases} \qquad (5-1)$$

The volume under risk plays a major rule in fatigue life determination. Figure 5.1 shows the volume under risk (VUR) in the cam at different angular displacement angles (Theta) for the rise portion. The volume under risk in the cam has been calculated for the rise, fall and second dwell segments.

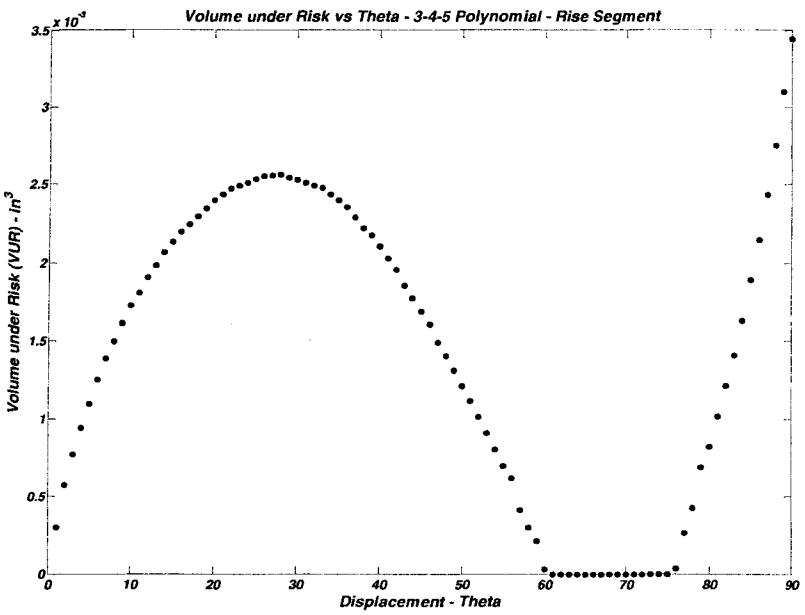


Figure 5.1 Volume under risk in the cam – rise portion

Once the stress distribution, the volume under risk and the stress weighted average depth has been calculated and determined, Ioannides – Harris mathematical fatigue life model was applied to calculate the fatigue life and the Nikas model was applied to calculate the relative fatigue life. Relative fatigue life has been investigated and calculated for the 3 – 4

– 5 polynomial function at different base circle radii. Also other cam parameters such as the eccentricity, second dwell angles, follower mass and diameter, total lift $h$, and angular velocity $\omega$ has been investigated and the results will be presented in the following sections.

#### 5.1.1.1 Cam Base Circle Radius:

Starting at a very small cam base circle radius, the cam fatigue life improves with increasing the cam base circle radius. The cam fatigue life kept improving with increasing the cam base circle till a critical cam base circle was reached were the cam fatigue life is a maximum as shown in figure 5.2. Any further increase in the cam base circle resulted in a decrease in the cam fatigue life.

From figure 5.3 it is evident that increasing the cam base circle radius resulted in a significant drop in the Hertzian stresses and the Von Mises stresses in the contact zone when the cam base circle radius was less than one inch. After that when the cam base circle radius exceeded one inch the drop in the Von Mises stress distribution in the contact zone was insignificant. Figure 5.3 shows that increasing the cam base circle radius beyond two inches didn't affect the Mises stresses substantially. It is clear that the Von Mises stress curve becomes a horizontal line no matter how large the cam base circle radius.

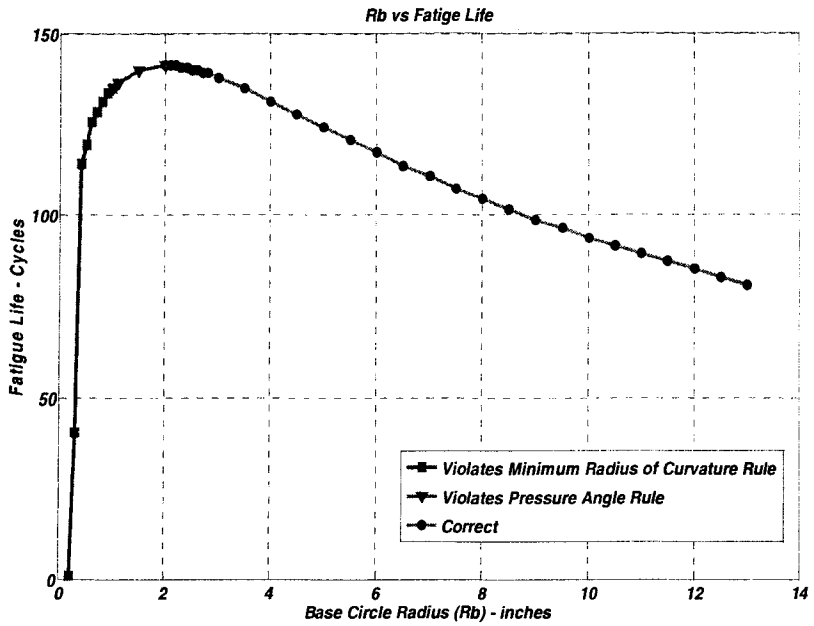


Figure 5.2 Cam fatigue life at different cam base circle radii

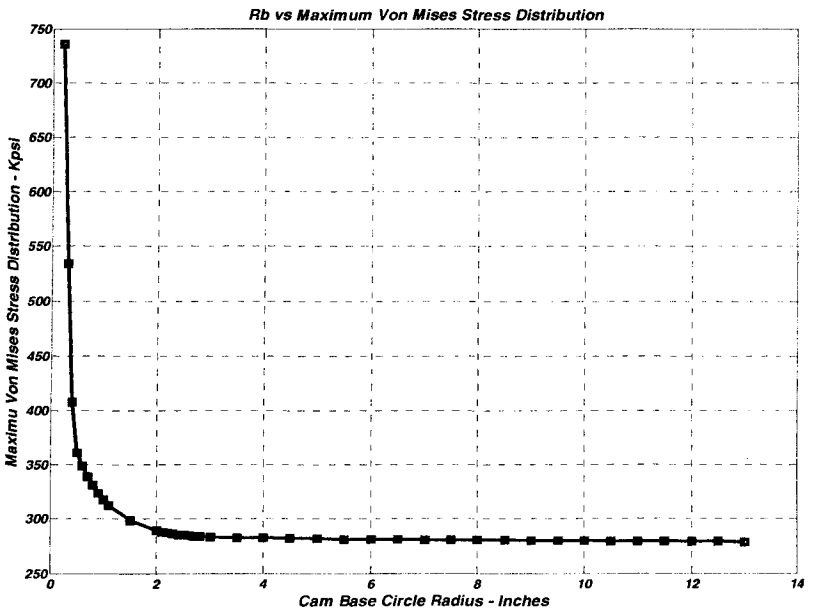


Figure 5.3 Von Mises stresses at different cam base circle radii

Increasing the cam base circle radius increases the cam volume. Furthermore, increasing the cam base circle radius increases the volume under risk in the rise, fall and second dwell segments in the cam as shown in figure 5.4. It is found that a linear relationship between the cam base circle radius and the volume under risk in the rise, fall, second dwell duration and the total volume under risk in the cam exists as shown in figures 5.4 and 5.5.

Consequently, the volume under risk keeps increasing linearly with the cam base circle radius. In contrast, the Von Mises stress distribution drops sharply with the increase in cam base circle radius however, the rate of change of stresses with respect to cam base circle radius is almost zero for the values of the radius higher than two inches.

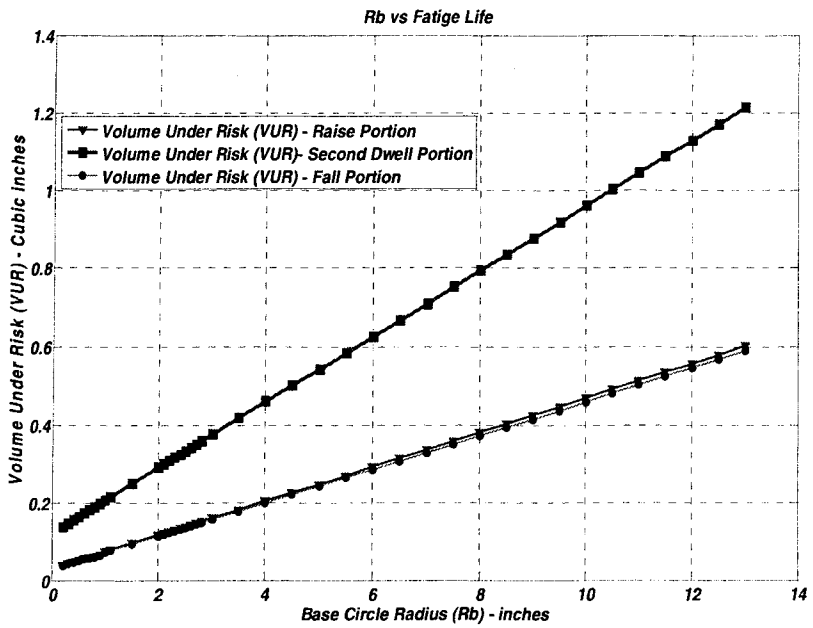


Figure 5.4 Volume under risk in rise, fall and second dwell at different cam base circle radii

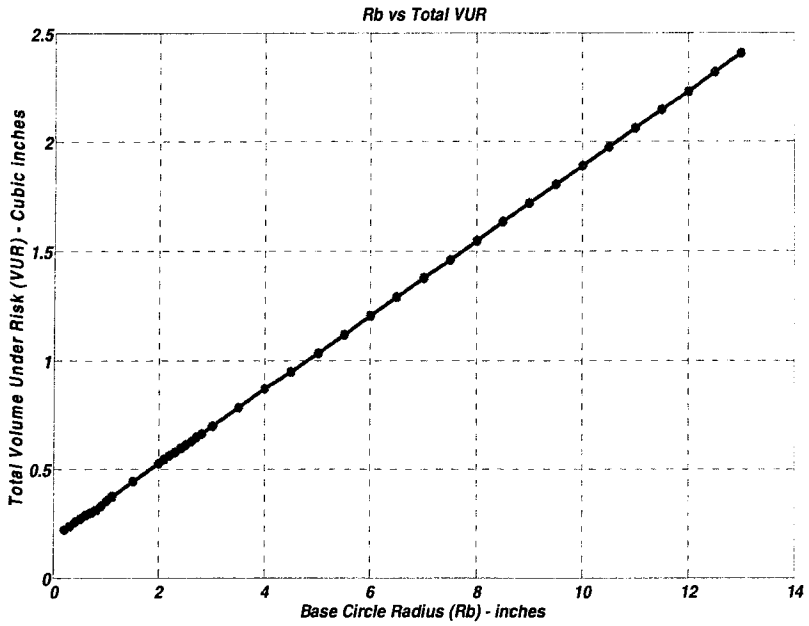


Figure 5.5 Total volume under risk at different cam base circle radii

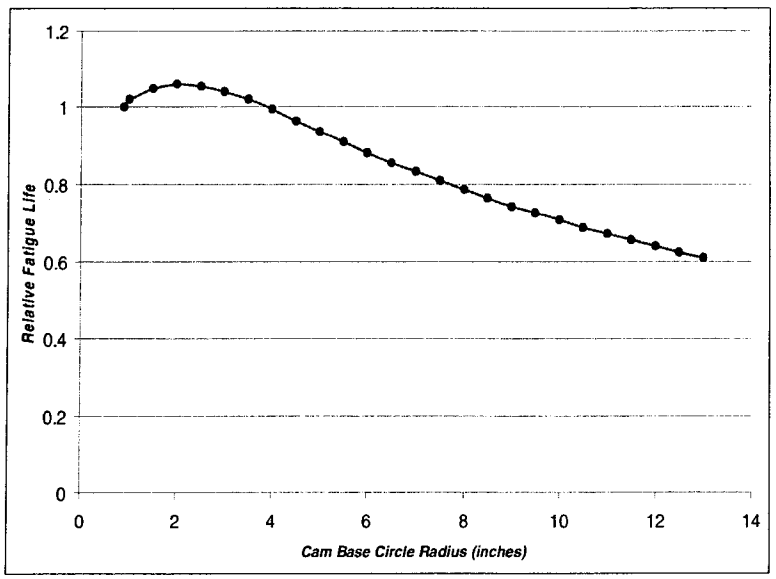


Figure 5.6 Cam relative fatigue life at different base circle radii using 3 – 4 – 5 polynomial displacement function

From the above discussion, it is clear that increasing the cam base circle radius has an effect on the Von Mises stress distribution and the volume under risk in the cam. Hence, the effect of cam base circle radius and therefore the effect of the Von Mises Stress distribution and the volume under risk controls the cam fatigue life to behave in the shape shown in figure 5.2.

There are two major factors that affect the cam size, the pressure angle and the radius of curvature. As a rule of thump [1], the pressure angle for the translating roller – follower should be between zero and about $\pm 30$ because as mentioned earlier when the pressure angle exceeds these values, it will produce an appreciable lateral force exerted on the stem of the follower, which in the presence of friction, to undesirable limits that tend to bind the translating follower in its guides. For the cam radius of curvature, there will be a problem when the roller – follower $R_f$ is larger than the smallest cam local radius of curvature. This problem is called undercutting. To avoid this problem, as a rule of thump, the absolute value of the minimum radius of curvature of the cam pitch curve should be at least 1.5 to 3 times as large as the radius of the roller – follower $R_f$ [1]. Therefore, according to the above rules, some of the cam base circle radii in figure 5.2 are out of range which means that the cam base circle radius is not acceptable at that range. It is found that when the cam base circle radius is less than 0.9 inches, the pressure angle or the radius of curvature violates the above rules which means that any cam design with a cam base circle radius less than 0.9 inches is not acceptable. Figure 5.6 shows the relative fatigue life curve of the cam where the cam base circle satisfies the design constraints. Relative fatigue life calculated in figure 5.6 with

respect to the fatigue life at the minimum acceptable cam base circle radius (0.9 inches) where the cam base circle radius at that point doesn't violate the previous mentioned rules.

| *Rb* | Relative Fatigue life | Percentage |
|---|---|---|
| 0.9 | 1 | 0 |
| 1 | 1.02 | 2 |
| 1.5 | 1.05 | 5 |
| 2 | 1.06 | 6 |
| 2.5 | 1.05 | 5 |
| 3 | 1.04 | 4 |
| 3.5 | 1.02 | 2 |
| 4 | 0.995 | -0.5 |
| 4.5 | 0.962 | -3.8 |
| 5 | 0.935 | -6.5 |
| 5.5 | 0.909 | -9.1 |
| 6 | 0.882 | -11.8 |
| 6.5 | 0.855 | -14.5 |
| 7 | 0.833 | -16.7 |
| 7.5 | 0.812 | -18.8 |
| 8 | 0.785 | -21.5 |
| 8.5 | 0.763 | -23.7 |
| 9 | 0.742 | -25.8 |
| 9.5 | 0.726 | -27.4 |
| 10 | 0.71 | -29 |
| 10.5 | 0.688 | -31.2 |
| 11 | 0.672 | -32.8 |
| 11.5 | 0.656 | -34.4 |
| 12 | 0.639 | -36.1 |
| 12.5 | 0.624 | -37.6 |
| 13 | 0.61 | -39 |

Table 5.1 Relative Fatigue Life at different Base Circle Radii

Figure 5.6 shows that the cam fatigue life increased with increasing the cam base circle radius till it reached a maximum value, after that any further increase in the cam base circle radius resulted in a decrease in the cam fatigue life. Designing and sizing the cam at that cam base circle radius will provide a cam with an optimum fatigue life. Table 5.1 shows the cam relative fatigue life and the percentage of increase or decrease in the came fatigue life at different cam base circle radii. After determining the cam optimum size, other parameters that affect the volume under risk, Von Mises stress distribution and fatigue life in cams have been investigated at the optimum size. The parameters that have been investigated are angular velocity $\omega$, total lift h (rise or fall), eccentricity, second dwell duration, follower radius of curvature and cam width.

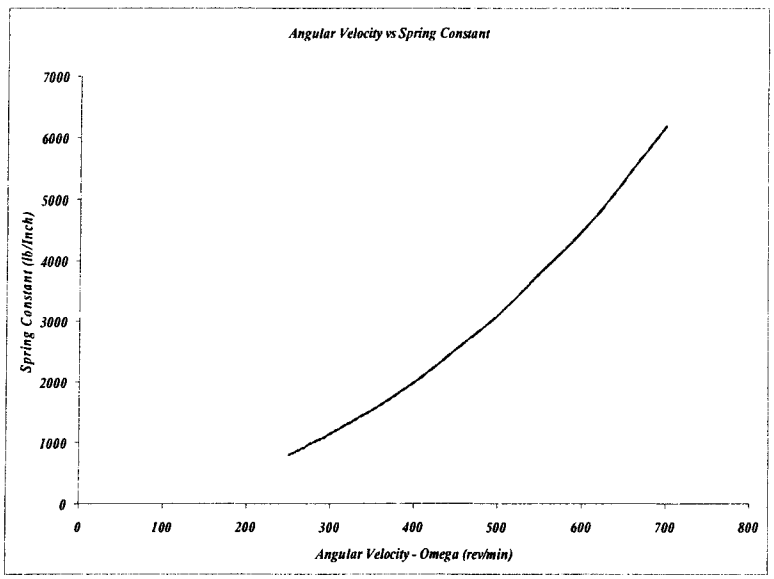


Figure 5.7 Spring constant required to keep the follower in contact with the cam

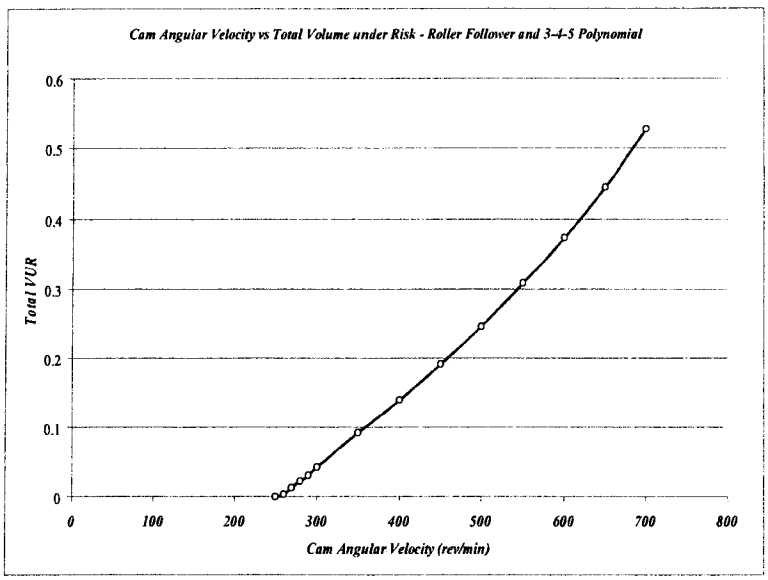


Figure 5.8 Effect of $\omega$ on volume under risk

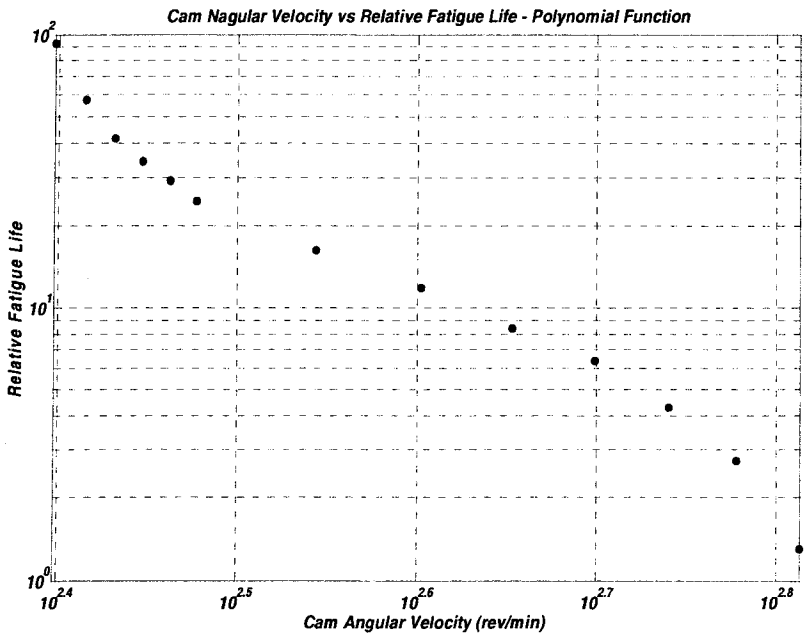


Figure 5.9 Effect of angular velocity on fatigue life – polynomial displacement function

### 5.1.1.2 Cam Angular Velocity Effect on Fatigue Life:

The effect of the camshaft angular velocity '$\omega$'on the fatigue life is investigated. Figure 5.7 shows that when the camshaft angular velocity increases, a stiffer spring will be required to keep the follower in contact with the cam all the time. This is due to the increase in inertia force that increases with increasing angular velocity. The increase in the inertia force and spring force will increase the Von Mises stress distribution and the 'volume under risk' as shown in figure 5.8. Therefore, the increase in the Von Mises Stress distribution and the volume under risk will reduce the cam fatigue life as shown in Figure 5.9.

### 5.1.1.3 Total Lift $h$ Effect on Fatigue Life:

Figure 5.10 shows the effect of changing the follower total lift $h$ on the cam fatigue life. It can be seen that as the total lift increases the fatigue life decreases. Since there is a direct relationship between the follower total lift and the follower acceleration therefore, increasing the total lift will increase the follower acceleration. The increase in the follower acceleration increases the inertia forces. This requires a stiffer spring to keep the follower in contact with the cam. Besides it, increasing the total lift will increase the deflection of the spring that leads to an increase in the spring force. Hence the combined effect of the stiffer spring and the force of inertia increase the stress levels in the cam. That, in turns, increases the volume under risk and affects the cam fatigue life negatively.

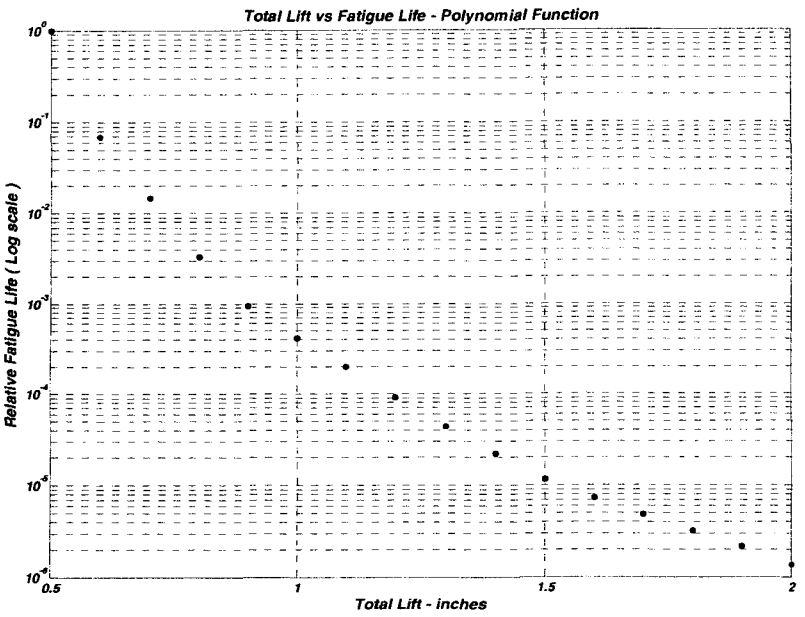


Figure 5.10 Effect of total lift h on cam fatigue life – polynomial displacement function

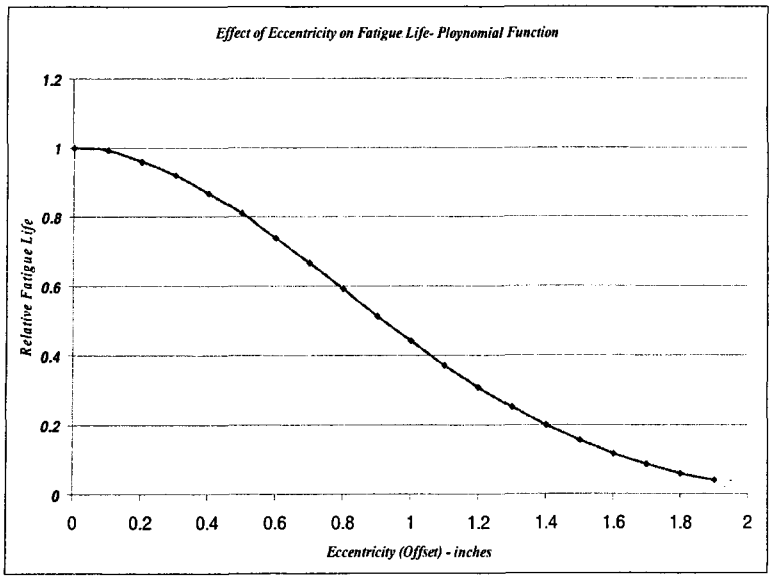


Figure 5.11 Effect of eccentricity on fatigue life

#### 5.1.1.4 Follower Eccentricity Effect on Fatigue Life:

The effect of the follower eccentricity on the fatigue life has also been investigated. From figure 5.11, it is clear that when the eccentricity is applied, the cam fatigue life has been decreased. So the eccentricity or the offset has an adverse effect on the cam fatigue life and it shouldn't introduce in design process unless it is necessary for other purposes like reducing the pressure angle.

#### 5.1.1.5 Second Dwell Angle Duration Effect on Cam Fatigue Life:

The effect of the second dwell duration on the fatigue life is investigated as well. Four cases are investigated in this study where the second dwell angles were 30 degrees, 45 degrees, 60 degrees and 90 degrees. It is found that the Hertzian stresses in the second dwell portion in the cam are much higher than that in the rise or fall portions and therefore, the volume under risk will be much higher in the second dwell portion in the cam than that in the rise or fall cam portions. Also reducing the cam second dwell duration and increasing the rise and fall portions duration will reduce the follower acceleration in the rise and fall portion and then will reduce the follower inertia force. Therefore, the reduction in the inertia forces in the rise and fall portions in the cam will reduce the Hertzian stresses and the volume under risk in these portions. Also decreasing the second dwell duration will decrease the volume under risk contributed due to the second dwell angle duration. All of these factors lead to the improvement in the cam fatigue life. Figure 5.12 shows that using small total dwell angle duration improves the fatigue life substantially were cam fatigue life was a maximum when the second dwell angle duration was 30 degrees.

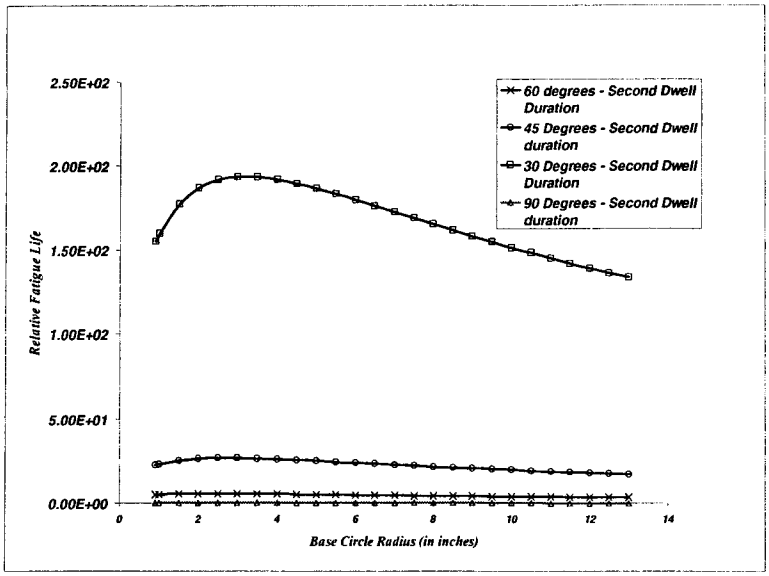


Figure 5.12 The effect of second dwell angle on fatigue life

### 5.1.1.6 Follower Radius of Curvature Effect on Fatigue Life:

The changing in follower radius of curvature is investigated in this study. As it would be expected the Hertzian stresses at the contact zone between the follower and the cam decreased with increasing the radius of curvature. As the roller – follower radius of curvature increased the degree of conformity between the cam and the roller follower will increase. This increase in conformity will increase the contact area between the cam and the follower. Increasing the contact area will decrease the load per unit area in the contact zone. This increase in contact area will reduce the Hertzian stresses and the volume under risk. Therefore, the decrease in the Hertzian stresses and the volume under risk will improve the cam fatigue life as it shown in figure 5.13.

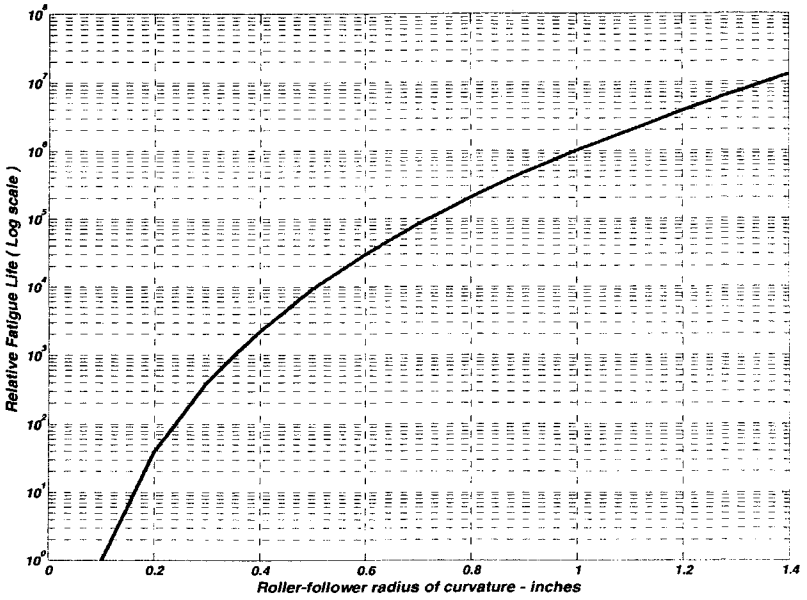


Figure 5.13 Cam relative fatigue life at different radii of curvature

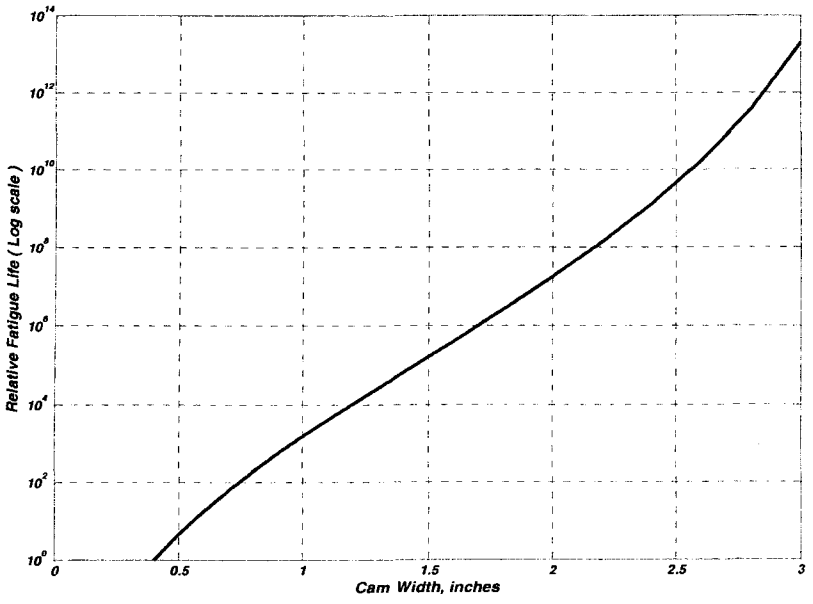


Figure 5.14 The effect of cam width on fatigue life

### 5.1.1.7 Cam Width Effect on Fatigue Life:

The contact area between the follower and the cam in the contact zone is a rectangular area and increasing the cam width will increase the contact area. This increase in contact area will reduce the load per unit area and the Hertzian stresses and volume under risk will decrease in the contact area. Therefore, this drop in Hertzian stresses and volume under risk will improve the cam fatigue life as it shown in figure 5.14.

### 5.1.2 Cycloidal Displacement Function Results:

Fatigue life has been investigated and calculated for the cycloidal function in the same way that fatigue life was investigated for the 3 – 4 – 5 polynomial function and under the same conditions using the IH mathematical formulation for different base circle radii. Also the effect of angular velocity $\omega$, total lift h (rise or fall), eccentricity and second dwell duration parameters on the volume under risk, stresses and cam fatigue life have been investigated at that optimum size. The results are provided in the appendix section.

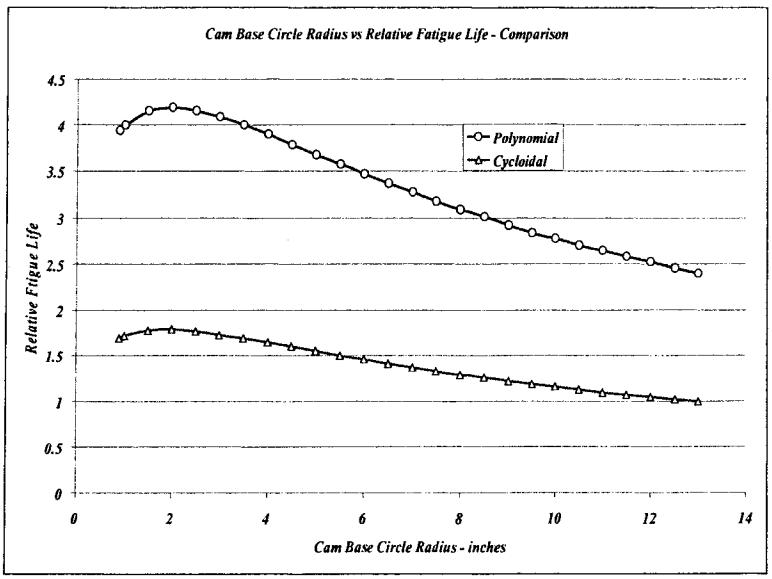


Figure 5.15 A comparison between the 3 – 4 – 5 polynomial fatigue life and cycloidal fatigue life

Figure 5.15 provides a comparison between cycloidal fatigue life and 3 – 4 – 5 polynomial fatigue life. From figure 5.15, we conclude that 3 – 4 – 5 polynomial displacement function provides a longer fatigue life than the cycloidal displacement function.

**5.2 Cam Flat – Face Follower Systems Results:**

In this part of the study, the results of the cam flat – face follower mechanism for the 3 – 4 – 5 polynomial and cycloidal displacement functions will be presented and discussed in the following subsections. The study for the flat – face follower has been conducted under the same conditions of the roller follower system where the cam angular velocity was 700 rev/min, the total lift (rise or fall) $h$ was 1.5 inches, the follower mass was 0.5 lb and the follower and cam material were steel 4140. In addition to the previous conditions, the tangential stresses due to friction has been included and two friction coefficients has been investigated were $\mu = 0.3$ and $\mu = 0.35$.

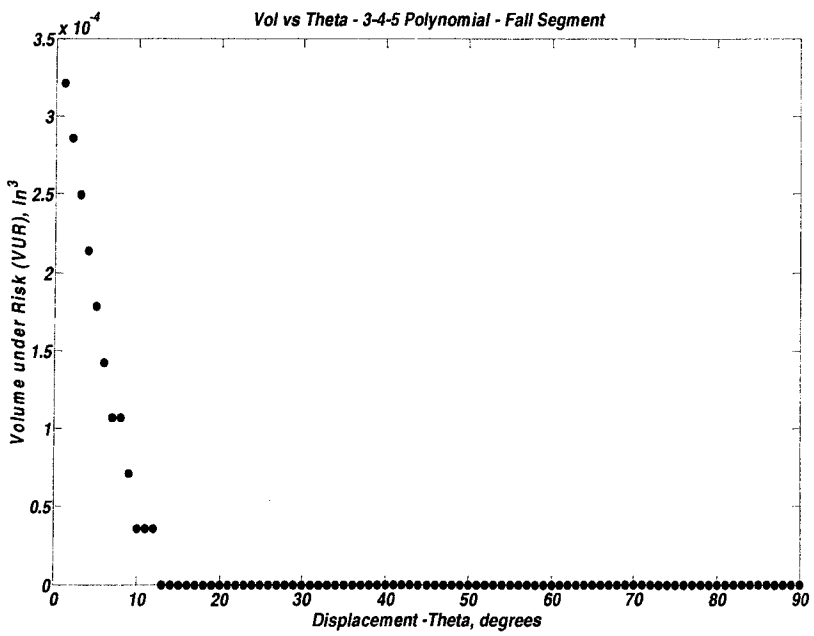


Figure 5.16 Volume under risk in the fall segment – flat face follower & $\mu = 0.35$

### 5.2.1 Polynomial (3 – 4 – 5) Displacement Function Results:

The stress distribution in the contact zone in the cam flat – face follower also has been determined and simulated using the program codes that been written in Matlab. The volume under risk was calculated and simulated where the Von Mises stress distribution in this volume is higher than the endurance limit. Figure 5.16 shows the volume under risk in the fall segment in cam flat – face follower system. It is found that the volume under risk in flat – face follower system is less than that in the roller follower system under the same conditions. This is due to the effect of the flat – follower where the radius of curvature of the flat – follower is infinity which makes the contact area between the cam and the follower larger than that in the roller follower. This large contact area reduces the stress distribution in the cam and then reduces the volume under risk. Figure 5.17 shows the total volume under risk in the rise, fall and second dwell segments in the cam. It is found that the volume under risk increased in small values with the increase in the cam base circle radius when the cam radius of curvature was negative in some regions. The volume under risk kept increasing with the cam base circle radius until it reached a maximum point. After that a lower drop in the volume under risk was observed. A sharp drop in the volume under risk occurred at 2.2 inches. Further increase in the radius resulted in an additional drop in the volume under risk however; it was much lower than the one observed at 2.3 inches. The prime reason of the significant drop was the positive values of the radius of curvature throughout the cam.

After that the stress weighted average depth has been calculated and determined, and then Ioannides – Harris mathematical fatigue life model was applied to calculate the fatigue life and the Nikas model was applied to calculate the relative fatigue life. Relative fatigue life has been investigated and calculated for the 3 – 4 – 5 polynomial function at different base

circle radii. Also other cam parameters such as the follower radius of curvature, angular velocity $\omega$, total lift $h$, (rise or fall), second dwell angles duration, and cam width.

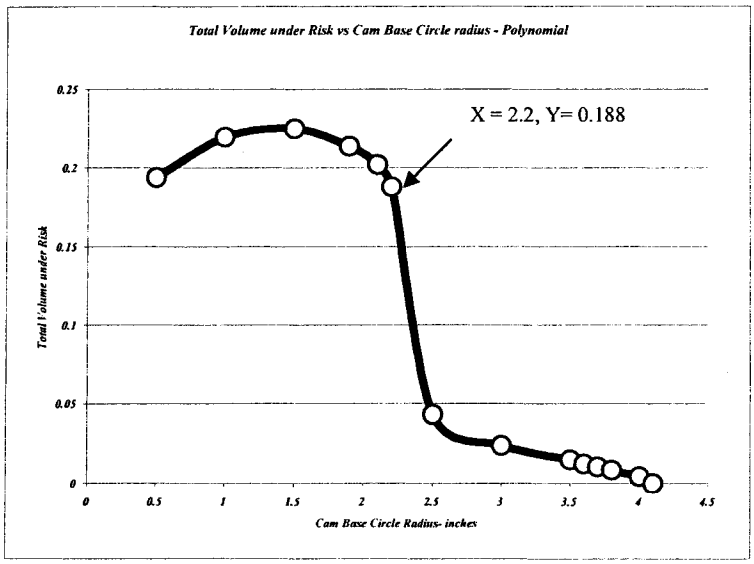


Figure 5.17 Total volume under risk in the rise, fall and second dwell cam segments – flat face follower and $\mu = 0.35$

### 5.2.1.1 Cam Base Circle Radius:

Starting at a very small cam base circle radius, the cam fatigue life improves with increasing the cam base circle radius. Cam fatigue life keeps improving with increasing the cam base circle radius till the life become infinity. From figure 5.18 it is shown that in the beginning, the cam fatigue life improves in small values where the cam radius of curvature is negative at some parts on the cam. But once the cam radius of curvature becomes positive everywhere in the cam, the cam fatigue life starts improving rapidly till it becomes infinity. Figure 5.18 shows clearly the major effect of the radius of curvature in cam fatigue life. It is

found that for the cam fatigue life to become infinity doesn't require a large cam. Under the previous mentioned conditions, the cam fatigue life became infinity when the cam base circle radius was below 4 inches.

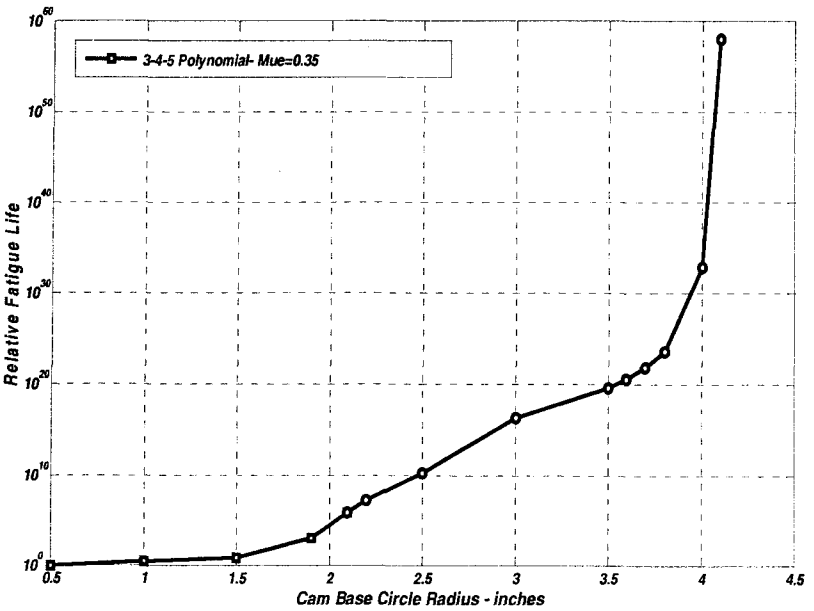


Figure 5.18 Effect of cam base circle radius on fatigue life - $\mu = 0.35$

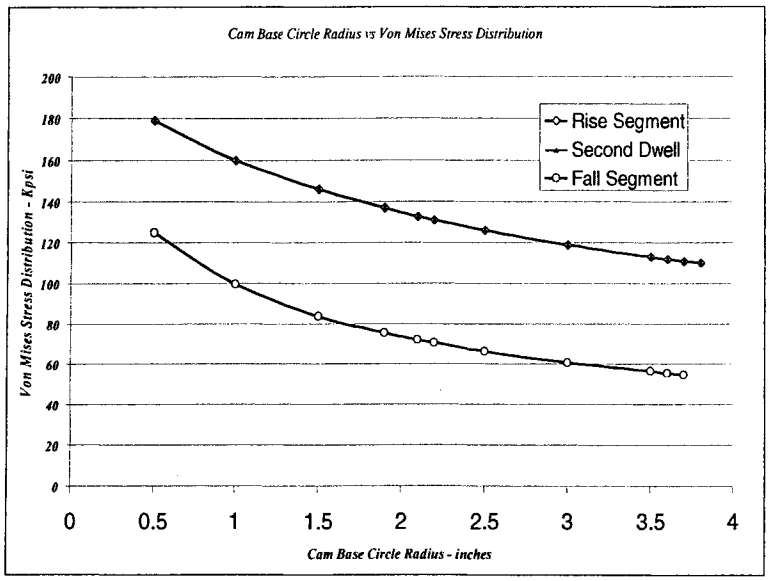


Figure 5.19 Effect of cam base circle radius on Von Mises stress distribution - $\mu = 0.35$

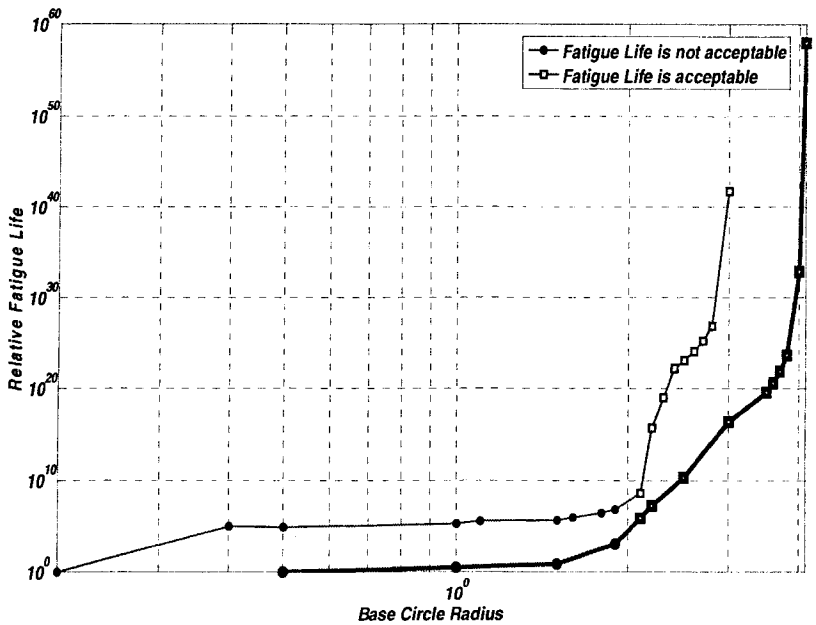


Figure 5.20 Cam flat face fatigue life comparison between $\mu = 0.3$ and $\mu = 0.35$

Figure 5.19 shows the drop in the Von Mises stress distribution – in the rise, fall and second dwell duration segments – with increasing the cam base circle radius. The Von Mises stress distribution didn't drop rapidly as it happened in the roller follower case. This is due to the effect of the flat follower radius of curvature on the contact area and hence on the stresses.

Undercutting will occur when the cam radius of curvature is negative on the cam because the flat follower can't follow a concave cam [1]. Therefore, the cam can't be made in the red area in figure 5.18 where the cam radius of curvature at that region is negative. From the above discussion, it is obvious the major effect of the flat follower on the stress distribution in the cam and the cam fatigue life. It is found that the cam fatigue life, Von Mises stress distribution and volume under risk in the cam flat – face follower mechanism behave differently than that in the cam roller – follower mechanism.

Cam fatigue life has been investigated for two different friction coefficient factors which are 0.3 and 0.35. Figure 5.20 shows a comparison between the cam fatigue life at these two different coefficient factors. From this figure it is obvious that the cam fatigue life with 0.3 friction coefficient factor will be higher than that at 0.35 friction coefficient factor (the solid curve represent the cam fatigue life at 0.35 friction coefficient factor).

After investigating the cam fatigue life at different cam base circle radii, the effect of other parameters on the volume under risk, Von Mises stress distribution and fatigue life in cams have been investigated. The parameters that have been investigated are angular velocity $\omega$, total lift h (rise or fall), second dwell duration and cam width.

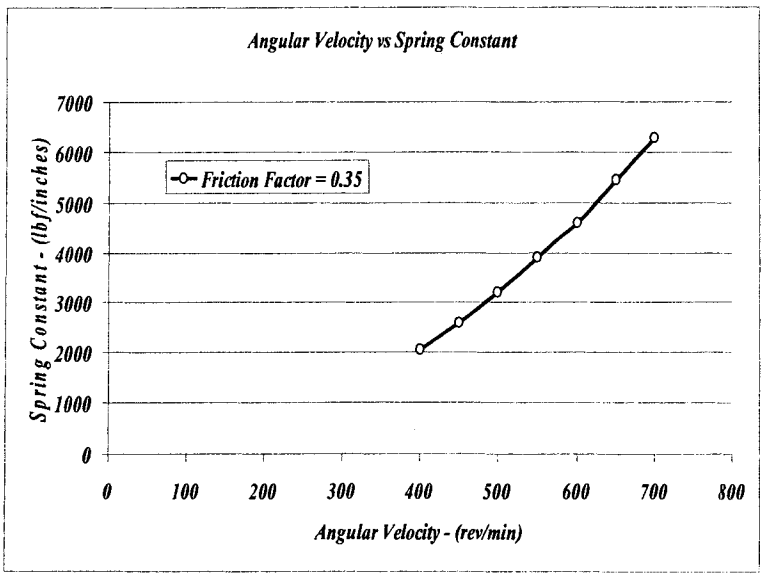


Figure 5.21 Spring constant required for keeping the follower in contact with the cam

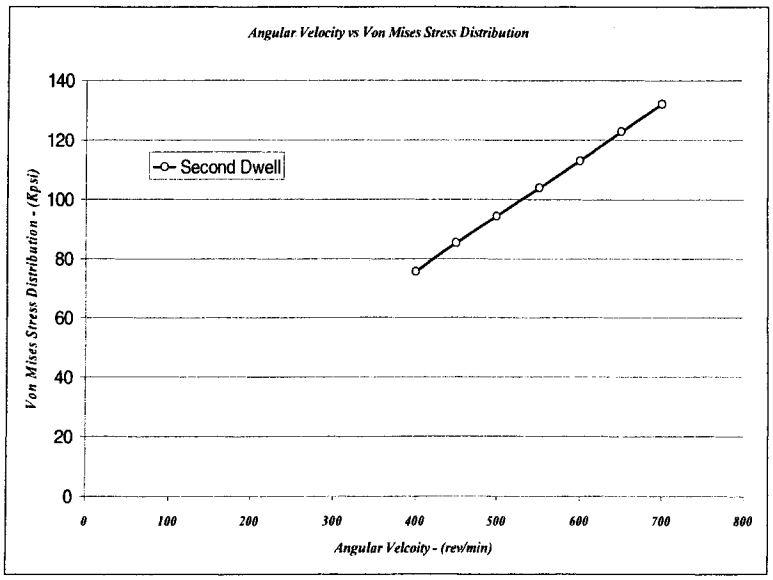


Figure 5.22 Effect of angular velocity on Von Mises stress distribution in second dwell duration – Polynomial displacement function and $\mu = 0.35$

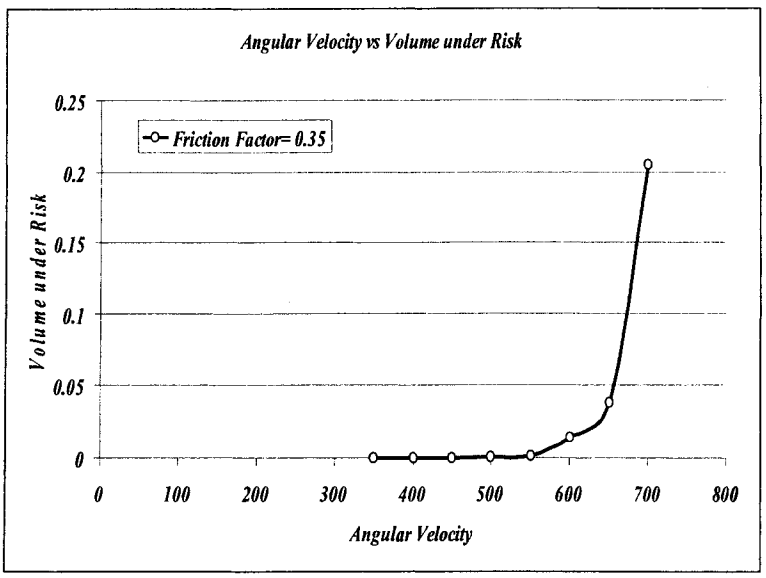


Figure 5.23 Effect of $\omega$ on volume under risk – polynomial displacement function and $\mu = 0.35$

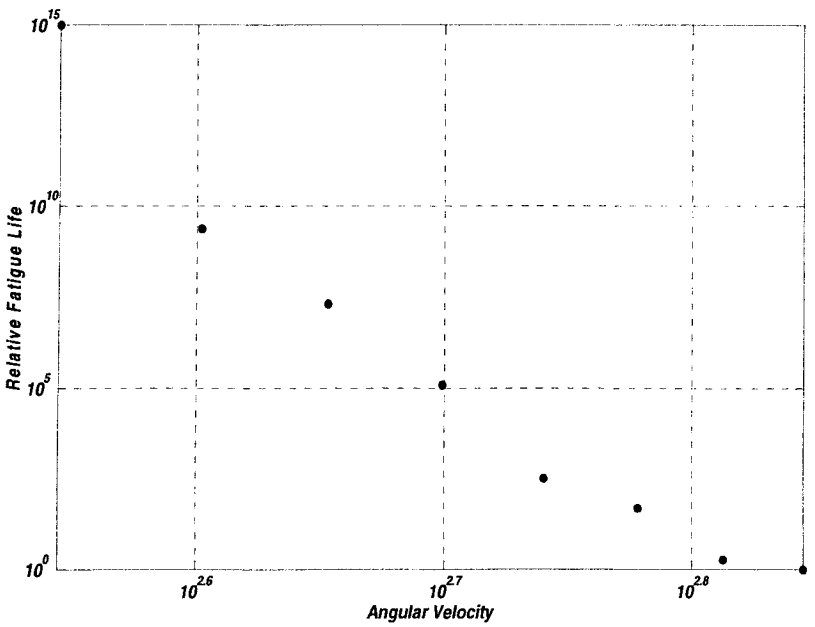


Figure 5.24 Effect of Angular Velocity on Fatigue Life – Polynomial displacement function and $\mu = 0.35$

#### 5.2.1.2 Cam Angular Velocity Effect on Fatigue Life:

The effect of the camshaft angular velocity '$\omega$'on the fatigue life is investigated and as it was expected that increasing the angular velocity resulted in an increase in the spring stiffness that required to keep the follower in contact with the cam all the time as shown in figure 5.21 This increase in the spring stiffness resulted in an increase in the Von Mises stress distribution and the volume under risk as shown in figures 5.22 and 5.23 respectively. Therefore, the increases in the Von Mises stress distribution and the volume under risk will reduce the cam fatigue life as shown in figure 5.24.

#### 5.2.1.3 Total Lift $h$ Effect on Fatigue Life:

As it was expected, it is found that increasing the total lift lead to a decrease in the cam fatigue life. Since there is a direct relationship between the follower total lift and the follower acceleration therefore, increasing the total lift will increase the follower acceleration. The increase in the follower acceleration increases the inertia forces. This increase in the inertia forces requires a stiffer spring to keep the follower in contact with the cam all the time. Also increasing the total lift will increase the deflection of the spring that leads to an increase in the spring force. Hence the combined effect of the stiffer spring and the force of inertia increase the stress levels in the cam. That, in turns, increases the volume under risk and affects the cam fatigue life negatively.

#### 5.2.1.4 Second Dwell Duration and Cam Width:

The effect of the second dwell duration on the fatigue life is investigated as well. Four cases are investigated in this study where the second dwell angles were 30 degrees, 45 degrees, 60 degrees and 90 degrees. It is found that the second dwell duration in flat face

follower has the same effect on volume under risk, Von Mises stresses and fatigue life as that in roller follower.

### 5.2.2 Cycloidal Displacement Function Results:

Fatigue life has been investigated and calculated for the cycloidal function in the same way that fatigue life was investigated for the 3 – 4 – 5 polynomial function and under the same conditions using the IH mathematical formulation for different base circle radii. Also the effect of angular velocity $\omega$, total lift h (rise or fall), eccentricity and second dwell duration parameters on the volume under risk, stresses and cam fatigue life have been investigated at that optimum size. The results are provided in the appendix section.

Figure 5.25 provides a comparison between cycloidal fatigue life and 3 – 4 – 5 polynomial fatigue life. From figure 5.25, we conclude that 3 – 4 – 5 polynomial displacement function provides a longer fatigue life than the cycloidal displacement function.

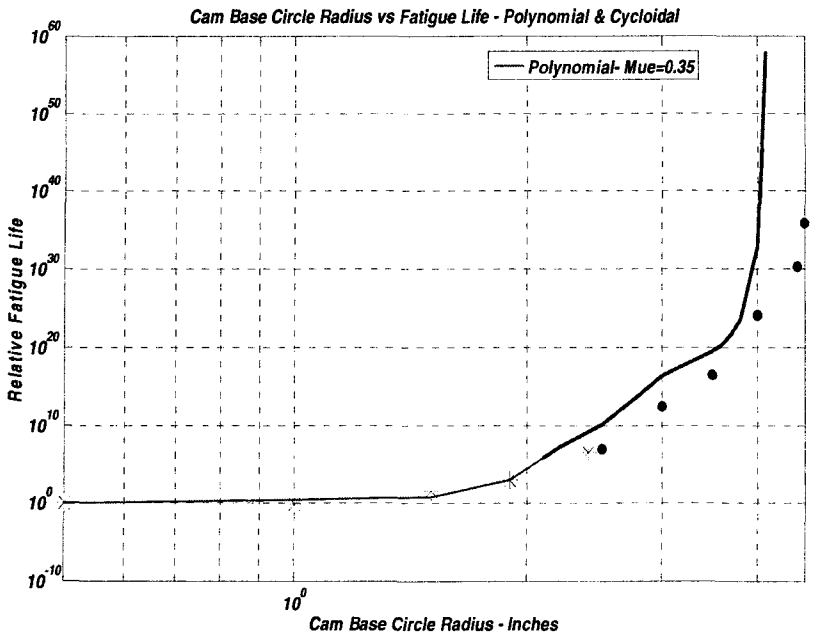


Figure 5.25 A comparison between the 3 – 4 – 5 polynomial fatigue life and cycloidal fatigue – flat face follower

# CHAPTER 6. Conclusions and Future Work

In this thesis, a logical procedure has been developed for the theoretical prediction of cam fatigue life with two main objectives. The first objective was to predict the cam fatigue life for two different types of cam follower systems; namely the translating roller follower and the translating flat – faced follower systems. The second objective was to estimate the cam optimum fatigue life on the bases of the cam base circle radius and other cam parameters. To achieve these two goals a strategy and methodology has been proposed for that purpose. Program codes have been written in Matlab to calculate the loads applied on the system, calculate and simulate the Von Mises stress distribution in the contact area and finally calculate the volume under risk in the cam where the stresses at that volume are higher than the endurance limit. After that, Ioannides and Harris mathematical model for the prediction of fatigue life in ball bearings has been adopted and the cam fatigue life has been investigated.

From the simulation studies performed using the codes written in Matlab, we can draw the following conclusions:

- The 3 – 4 – 5 polynomial displacement function has a longer fatigue life than the cycloidal displacement function. This is due to the fact that the cycloidal function has relatively large magnitudes of peak acceleration and peak velocity compared to the 3 – 4 – 5 polynomial function or other displacement functions. High peak acceleration and peak velocity are the only drawbacks of the cycloidal function.

- For the translating cam roller follower systems, starting at the minimum acceptable cam base circle radius, cam fatigue life improves with increasing cam base circle radius until the optimum cam size has been reached where the fatigue life is a maximum. After that, any further increase in the cam base circle radius resulted in a decrease in the cam fatigue life.
- Camshaft angular velocity plays a major rule in cam fatigue life. As the camshaft angular velocity increases, cam fatigue life drops dramatically. This is due to the fact that angular velocity has an effect on the acceleration that leads to an increase in the inertia forces. It's recommended not to use high angular velocities when using polynomials or cycloidal functions.
- The total lift h (rise or fall) has an effect on the cam fatigue life. Higher values of h will lead to an increase in the inertia forces. Also higher values of h will cause the spring to be compressed to higher levels which leads to higher spring forces. The higher spring force combined with higher inertia force will produce higher loads on the cam. This will increase the stress distribution and reduce the cam fatigue life. Small total lift values are recommended.
- Introducing eccentricity in cam design is not recommended. Eccentricity has an adverse effect on fatigue life. Introducing eccentricity in cam design will degrade the cam fatigue life no matter how small the eccentricity. So it's not recommended to use eccentricity unless providing eccentricity is necessary to reduce cam pressure angle.
- The major part of the material volume under risk in double dwell cams comes from the second dwell portion. The total second dwell duration has a great effect on fatigue life. Cams with smaller total second dwell angle will have a higher fatigue life than the same cam size with a higher total second dwell angle.

- For the translating flat – face follower cam systems, starting at the minimum acceptable cam base circle radius, cam fatigue life improves with increasing the cam base circle radius until the infinite fatigue life was reached. Reaching the infinite fatigue life in translating flat – face follower systems doesn't require a large cam with a large cam base circle radius. Comparing the fatigue life in roller follower with that in the flat face follower under the same conditions, it is found that the fatigue life in flat – face follower could become infinity at a specific cam base circle radius while fatigue life in the roller follower couldn't reach infinite limit no matter how much the cam base circle increased. In the contrary, increasing the cam base circle radius in roller – follower after reaching the optimum life has an adverse effect on cam life.
- From fatigue life behavior for the translating roller follower and translating flat – faced follower systems, it is found that fatigue life behavior differs from one system to another depending on the type of the follower.
- In the translating flat – faced follower system, it is found that the cam radius of curvature plays the major rule that controls the behavior of the cam fatigue life. It is found that at the moment when the cam radius of curvature becomes positive at every point on the cam surface, the cam fatigue life improves significantly.

**6.1 Future Work:**

Although much has been accomplished in this study, there is a great deal that remains to be done. Future research directions will be focused on the following aspects:

1. Extend the fatigue life investigations for other materials that don't exhibit an endurance limit like Aluminum.
2. Investigate fatigue life for other cam follower systems
3. Introduce the effect of the forces due to vibration in the system
4. Determine the proportional constant experimentally and compare the results with the simulation.
5. Experimental investigation should be done to verify the theoretical results found in this work.

# APPENDIX A Follower Displacement Functions and Curves

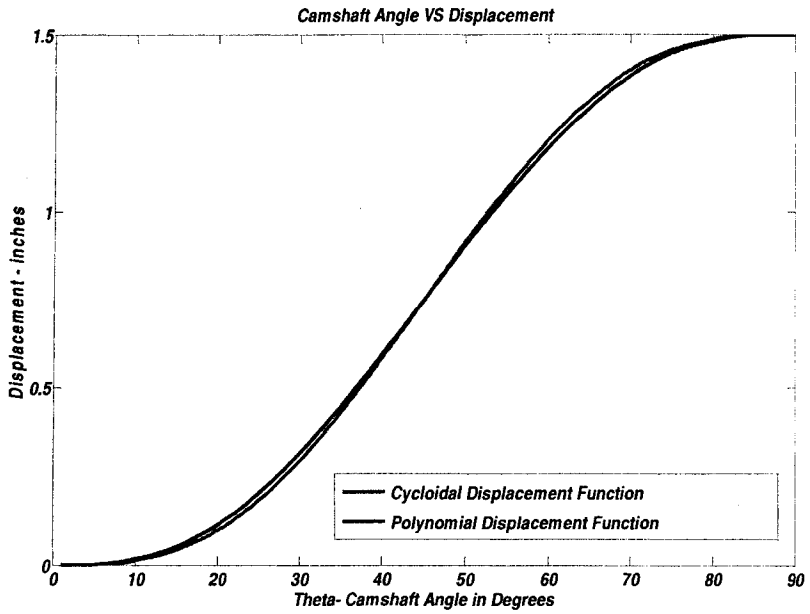


Figure A.1 Comparison of 3 – 4 – 5 Polynomial and cycloidal displacement functions – rise segment on cam

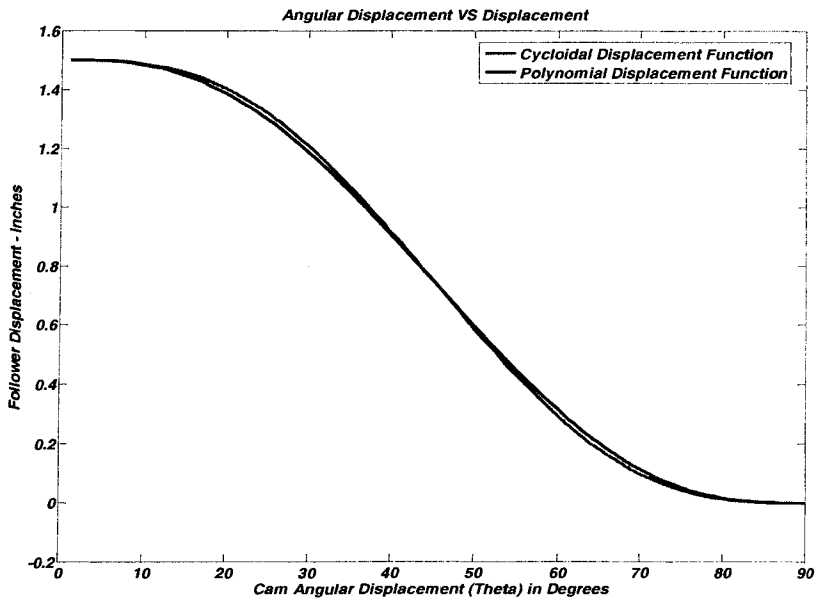


Figure A.2 Comparison of 3 – 4 – 5 Polynomial and cycloidal displacement functions – fall segment on cam

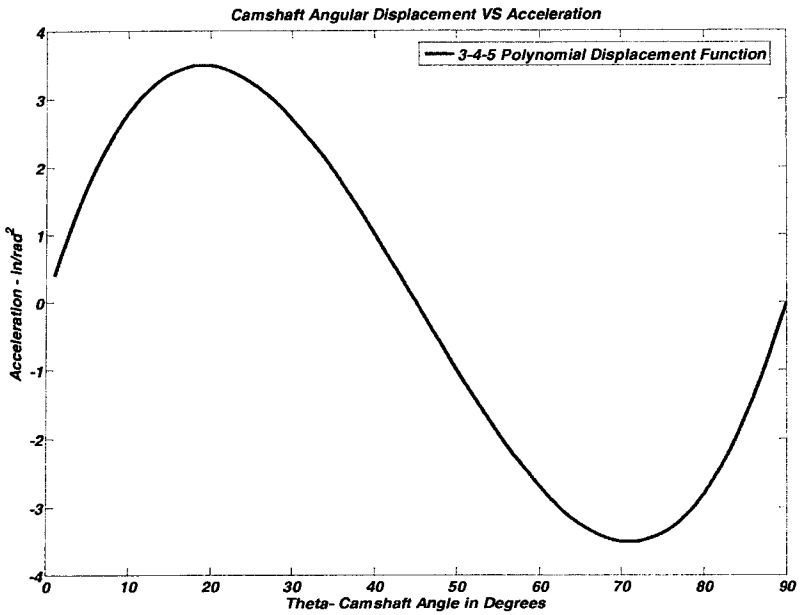


Figure A.3 3 – 4 – 5 polynomial acceleration function on cam rise segment

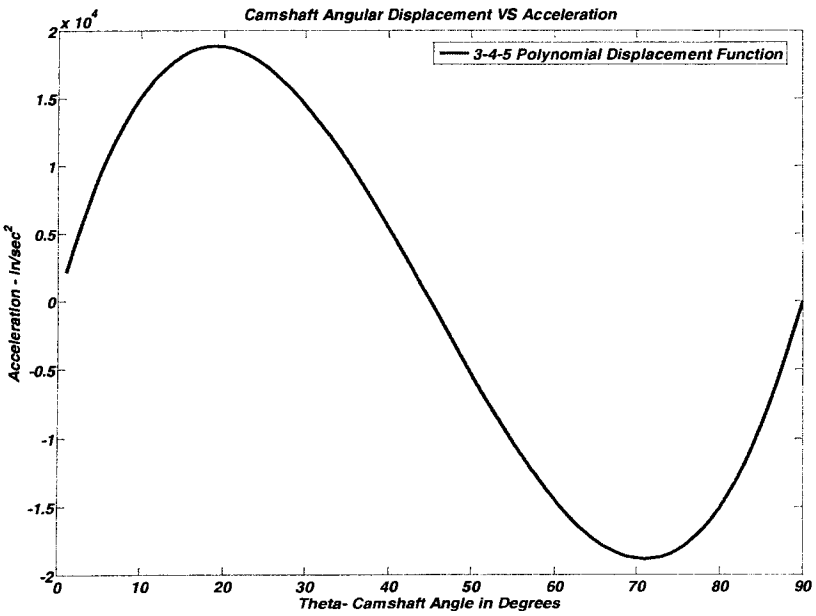


Figure A.4 3 – 4 – 5 polynomial acceleration function on cam rise segment

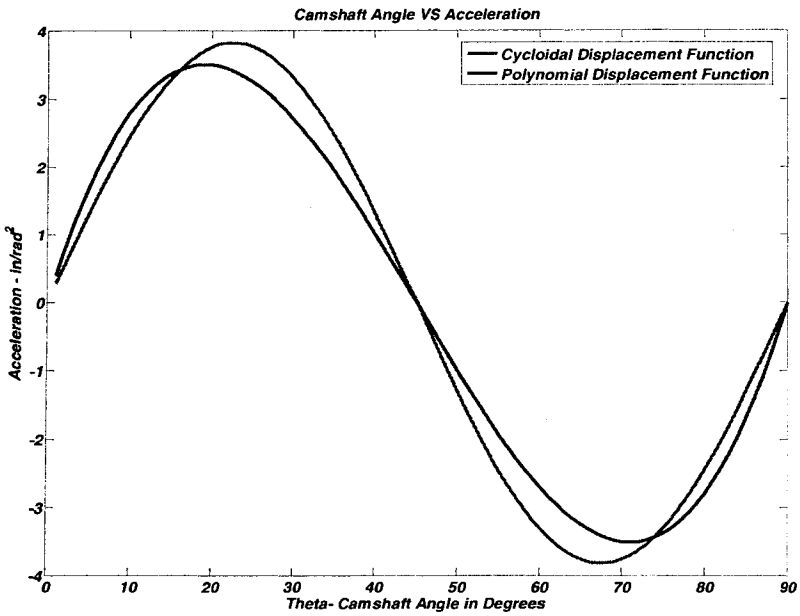


Figure A.5 Comparison of 3 – 4 – 5 polynomial and cycloidal acceleration functions on cam rise segment

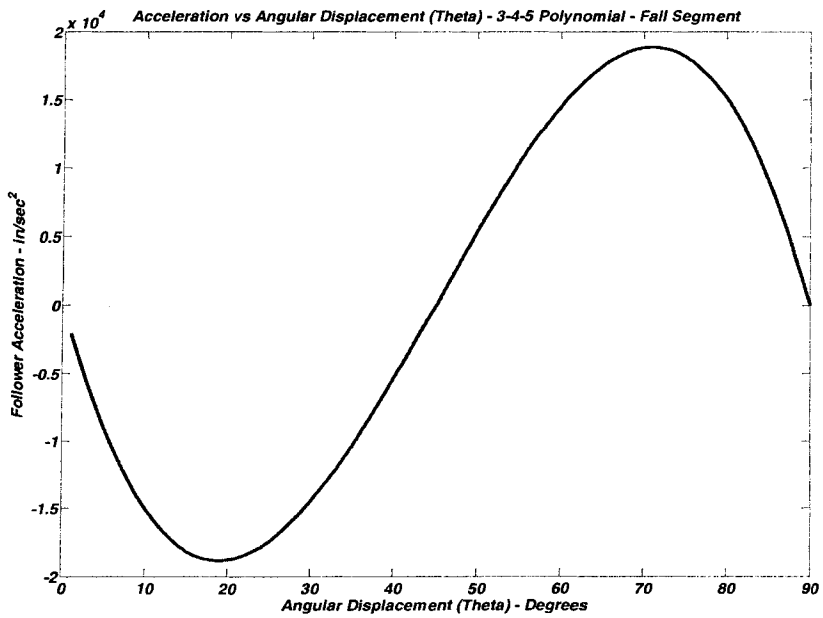


Figure A.6 3 – 4 – 5 polynomial acceleration function on cam fall segment

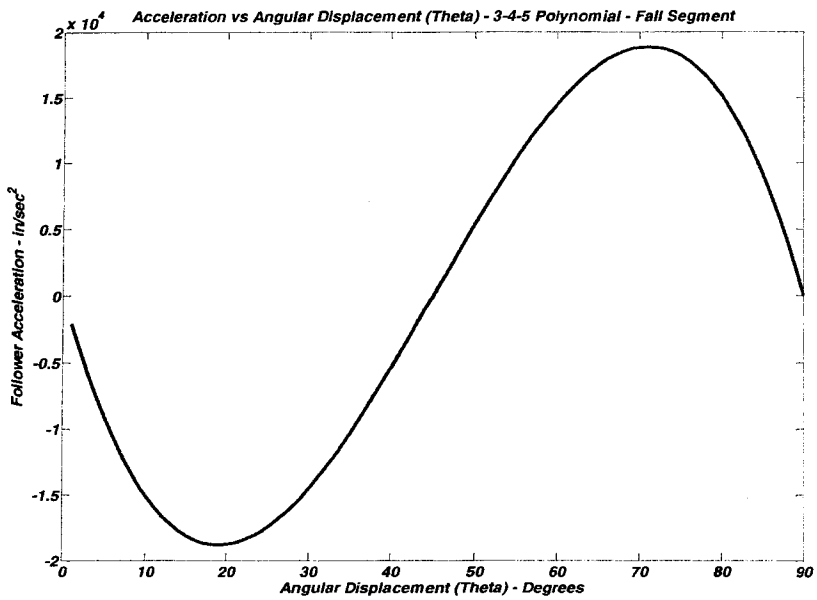


Figure A.7 3 – 4 – 5 polynomial acceleration function on cam fall segment

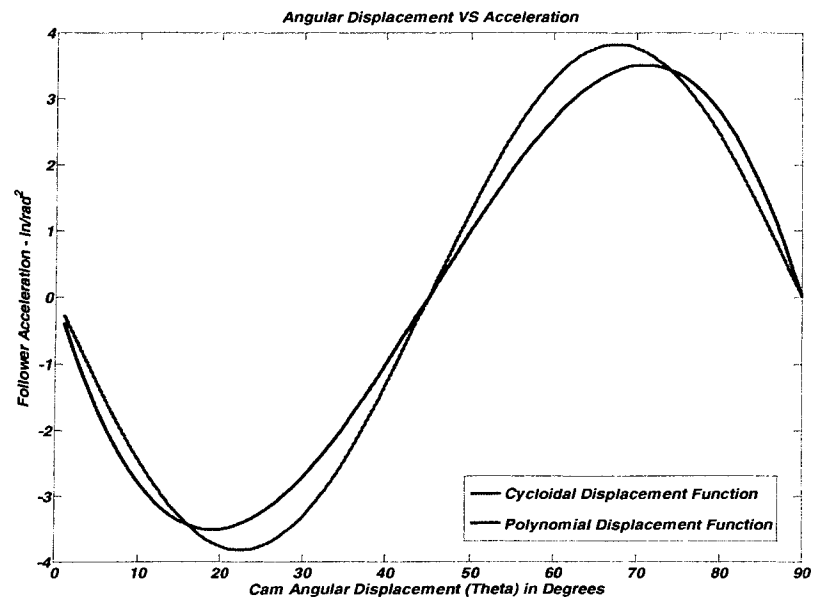


Figure A.8 Comparison of 3 – 4 – 5 Polynomial and cycloidal acceleration ($in/rad^2$) functions on cam fall segment

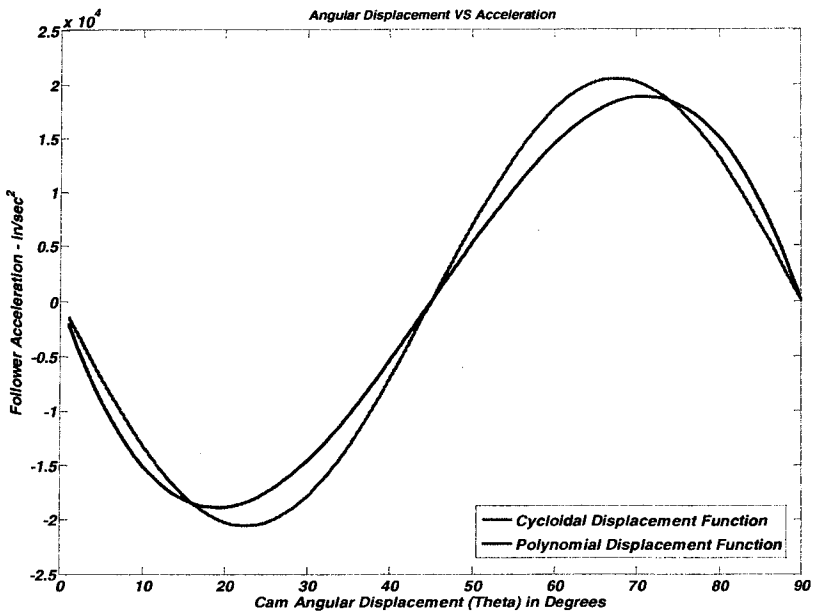


Figure A.9 Comparison of 3 – 4 – 5 Polynomial and cycloidal acceleration ( $in/\sec^2$ ) functions on cam fall segment

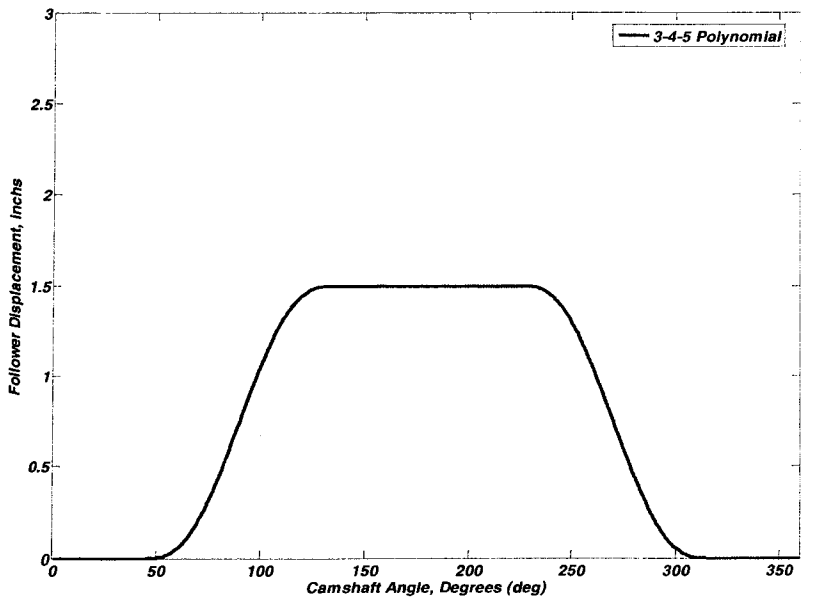


Figure A.10 Follower displacement program; 3 – 4 – 5 polynomial displacement function

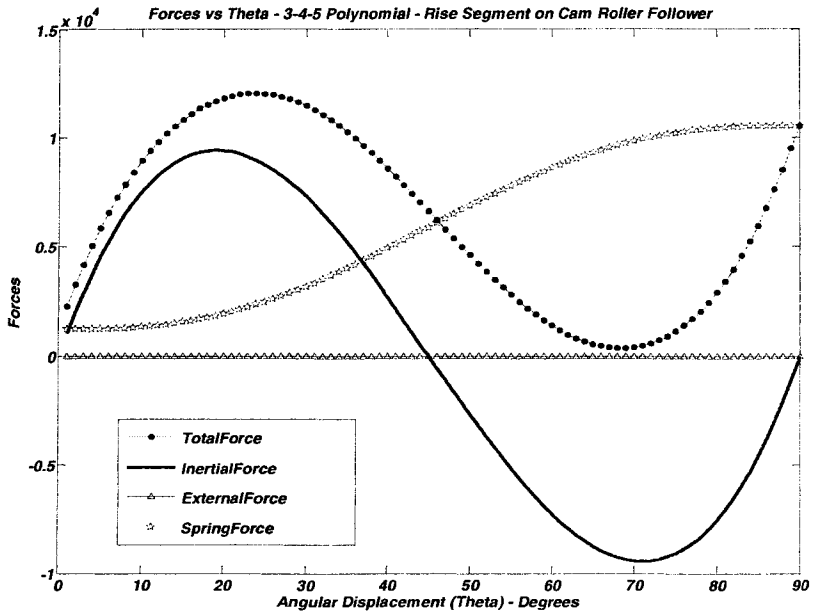


Figure A.11 Forces on the rise segment on cam roller follower

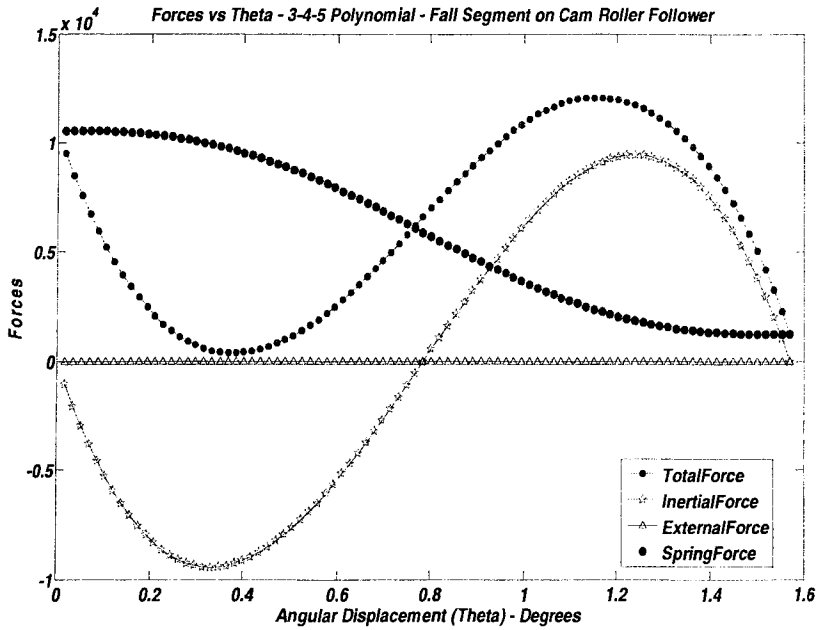


Figure A.12 Forces on the fall segment on cam roller follower

# APPENDIX B Cam Roller – Follower Results

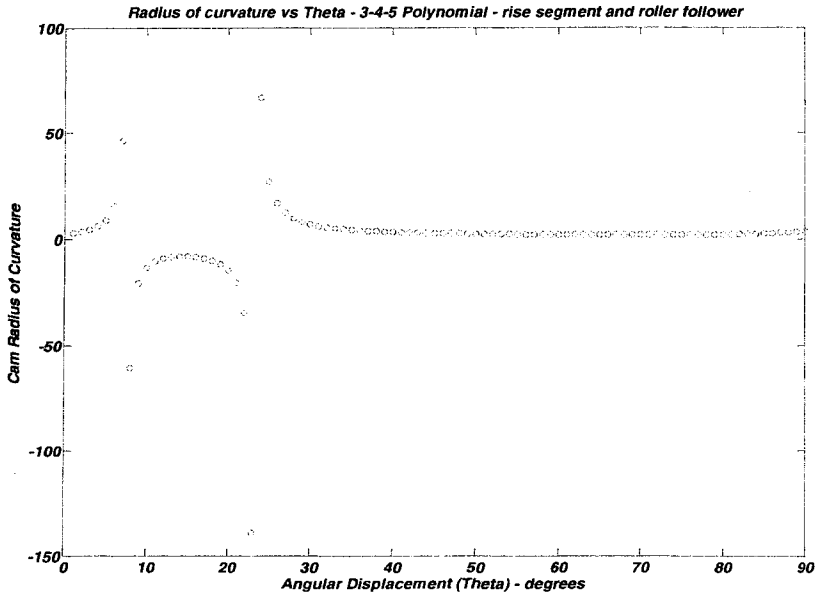


Figure B.1 Cam radius of curvature on cam rise segment for polynomial displacement function

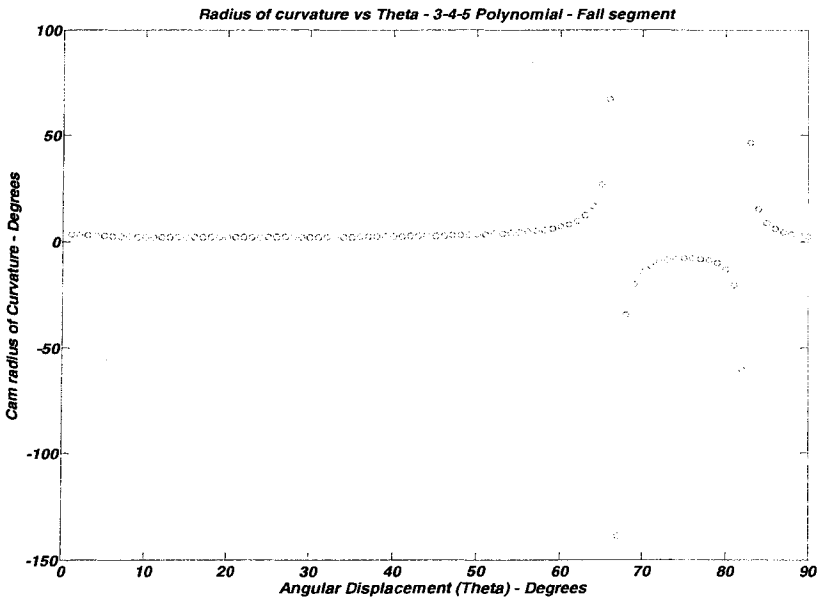


Figure B.2 Cam radius of curvature on cam fall segment for polynomial displacement function

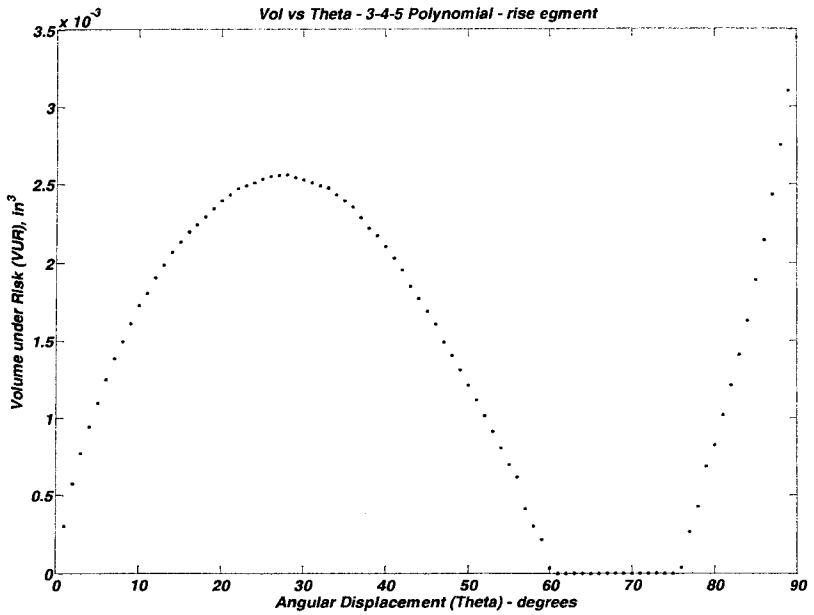


Figure B.3 Volume under risk on cam rise segment for cam roller follower system

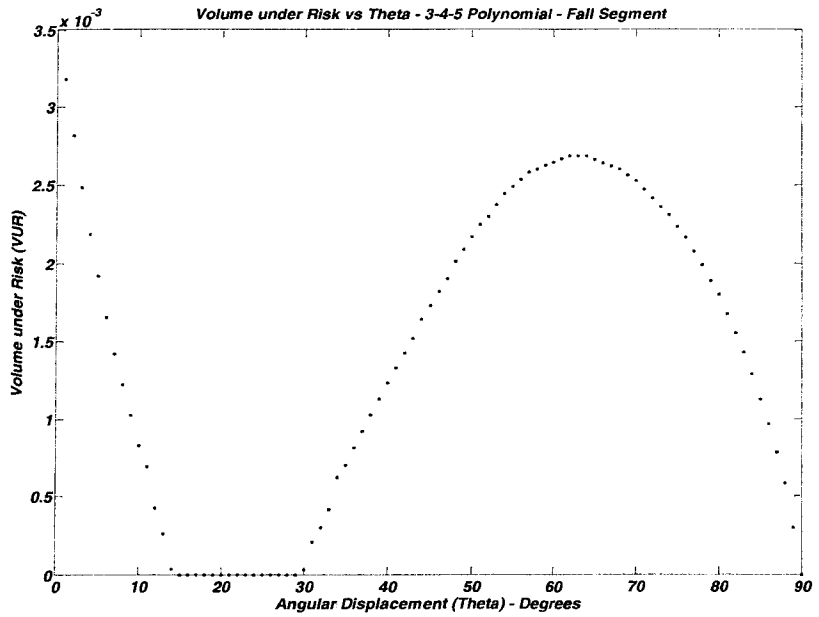


Figure B.4 Volume under risk on cam fall segment for cam roller follower system

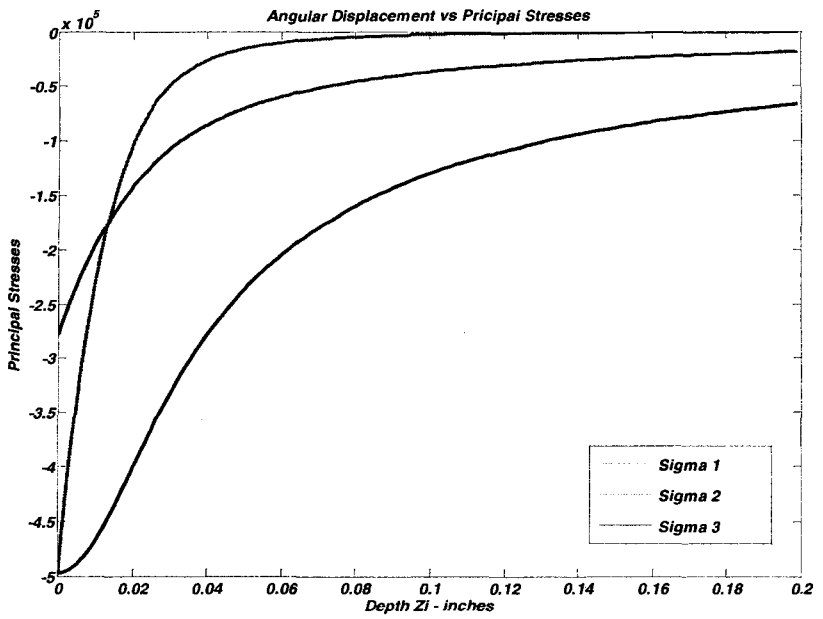


Figure B.5 Principle stresses on cam rise segment for cam roller follower system

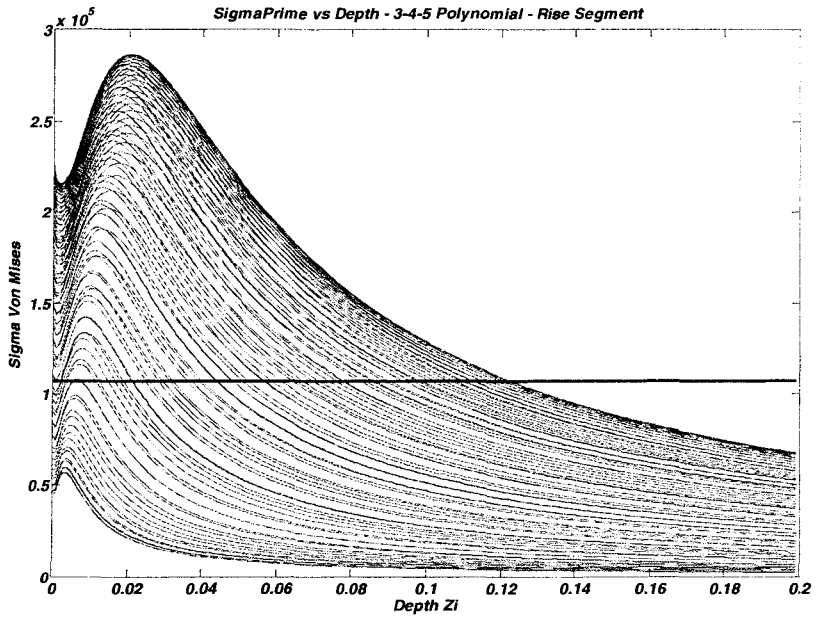


Figure B.6 Von Mises stress distribution on cam rise segment for cam roller follower system


Figure B.7 Pressure angle on cam rise segment for cam roller follower system

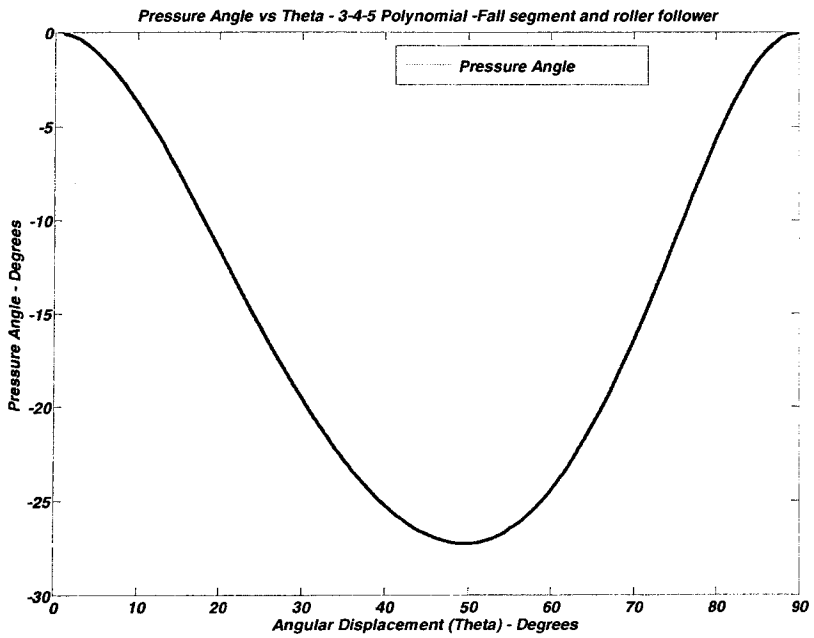


Figure B.8 Pressure angle on cam fall segment for cam roller follower system

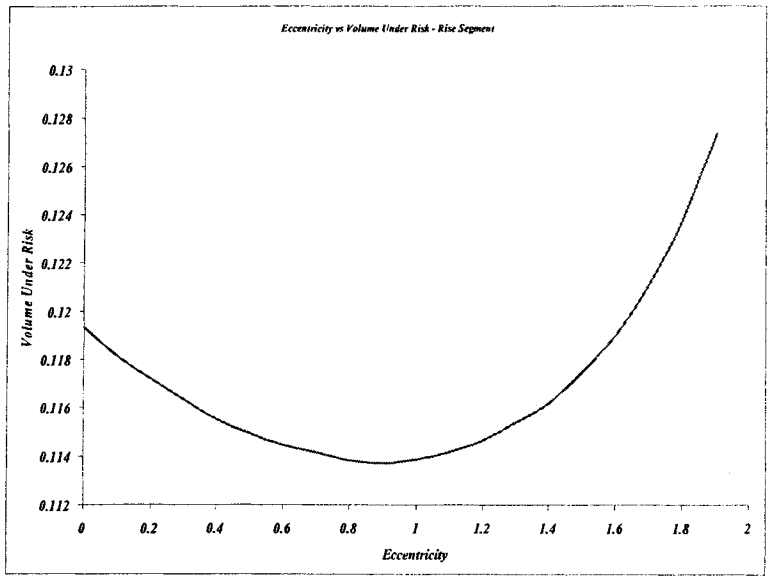


Figure B.9 Effect of eccentricity on volume under risk on cam rise segment for polynomial function

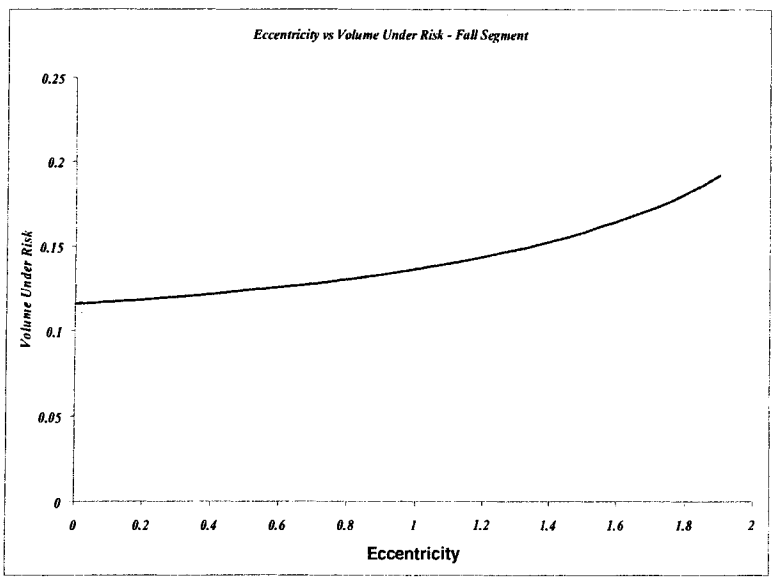


Figure B.10 Effect of eccentricity on volume under risk on cam fall segment for polynomial function

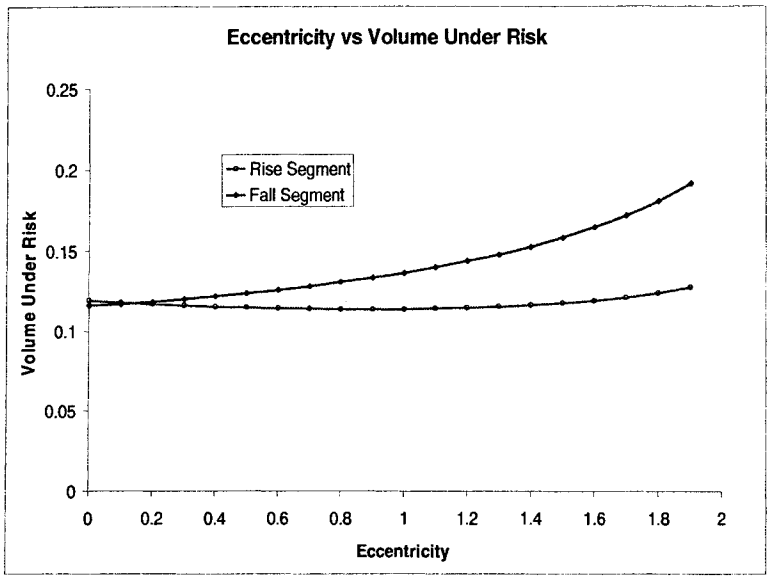


Figure B.11 Comparing the effect of eccentricity on volume under risk for rise and fall segments on cam – polynomial function

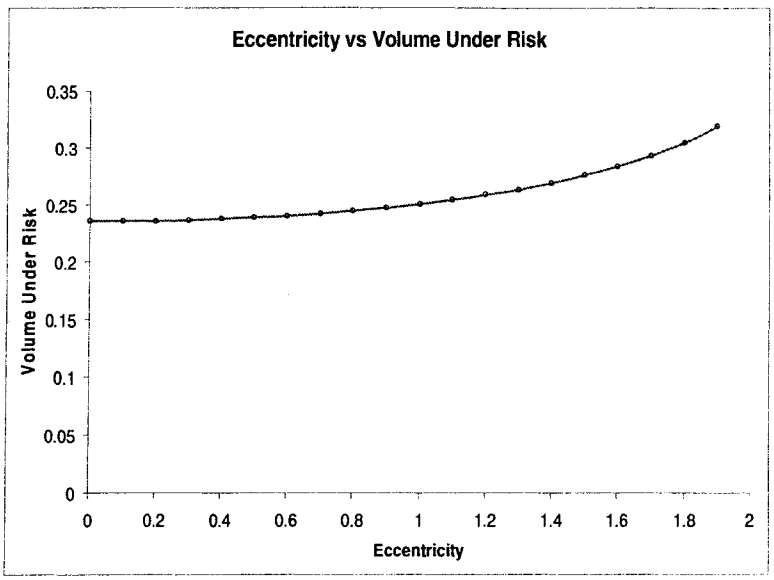


Figure B.12 Effect of eccentricity on total volume under risk for polynomial function

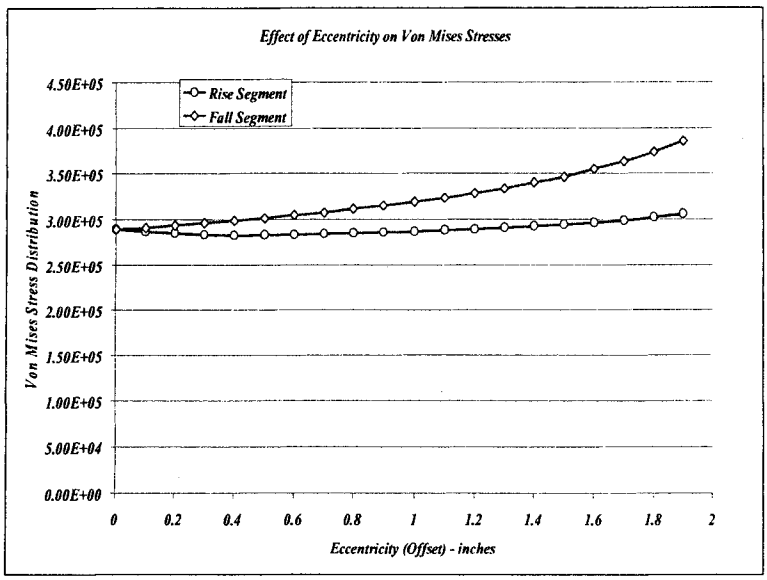


Figure B.13 Effect of eccentricity on Von Mises stress distribution for rise and fall segments on cam for polynomial function

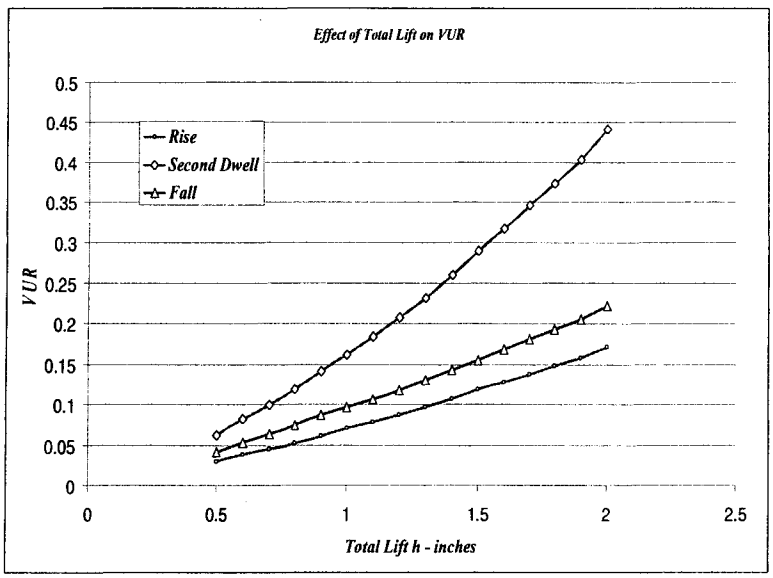


Figure B.14 Effect of total lift on volume under risk for polynomial function

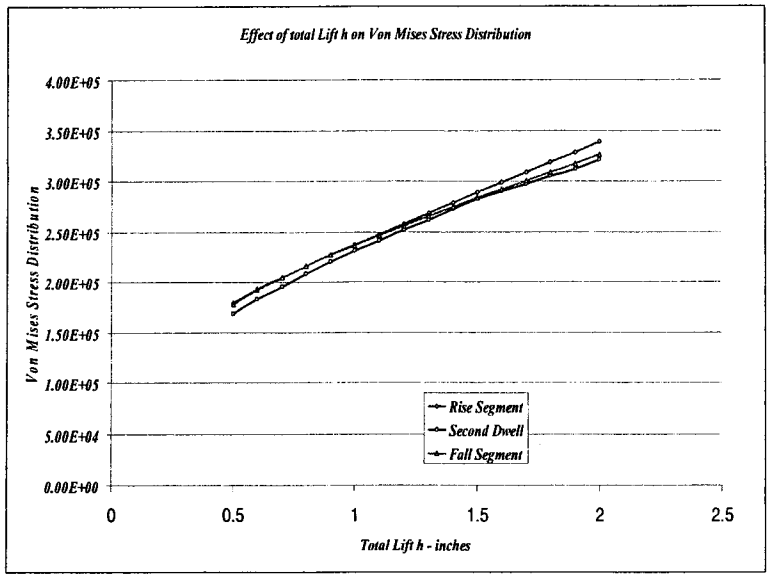


Figure B.15 Effect of total lift on Von Mises stress distribution for polynomial function

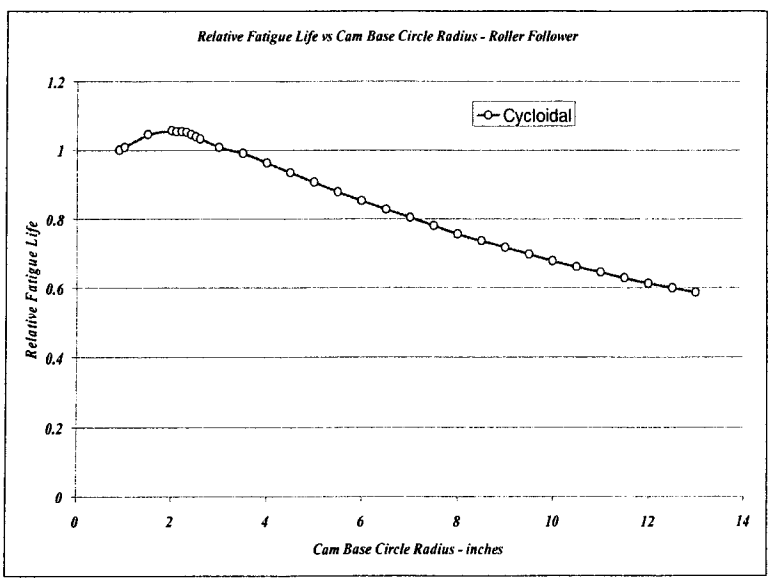


Figure B.16 Relative fatigue life at different cam base circle radii for roller follower and cycloidal function

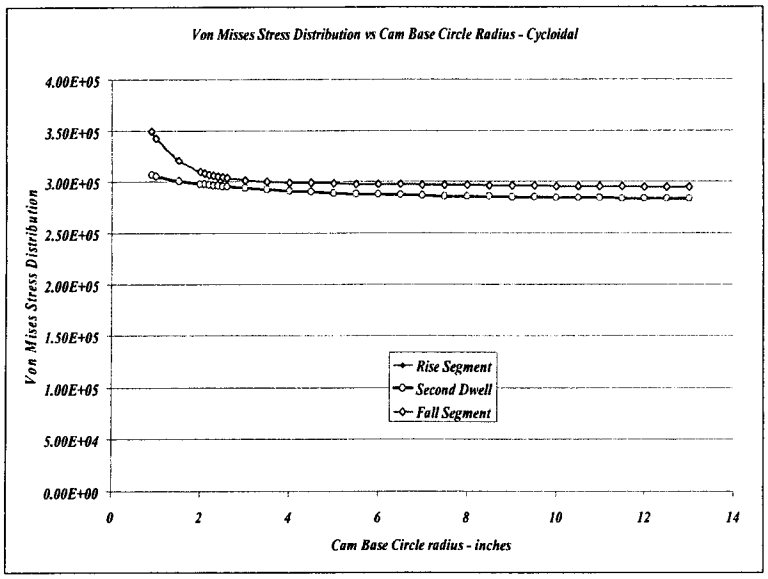


Figure B.17 Von Mises stresses at different cam base circle radii for rise, second dwell and fall cam segments - roller follower and cycloidal function

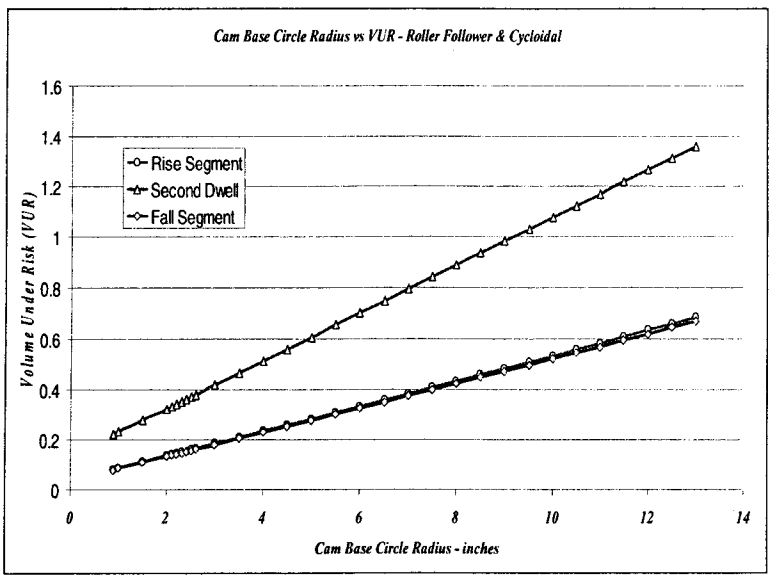


Figure B.18 Volume under risk at different cam base circle radii for rise, second dwell and fall cam segments - roller follower and cycloidal function

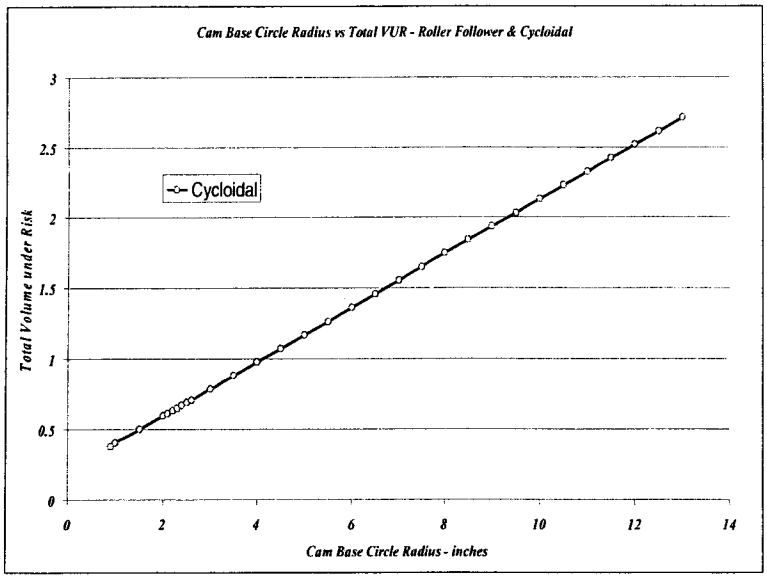


Figure B.19 Total volume under risk at different cam base circle radii for roller follower and cycloidal function

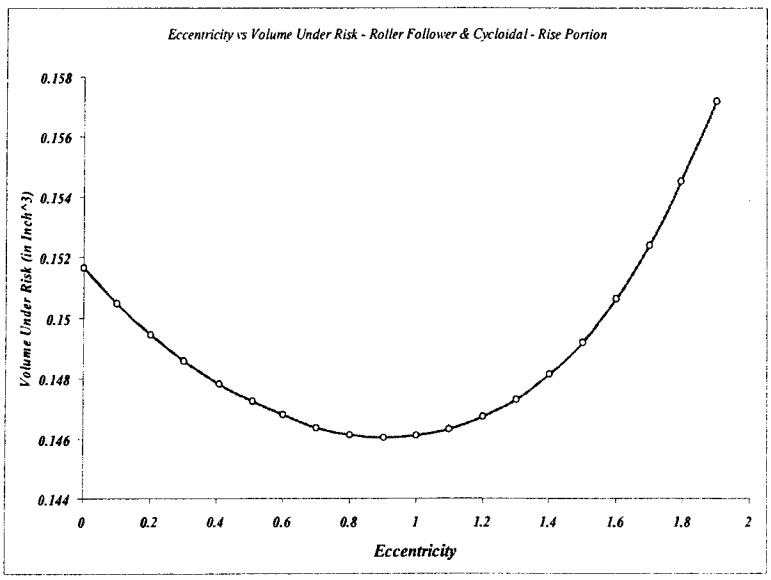


Figure B.20 Effect of eccentricity on volume under risk on cam rise segment for cycloidal function

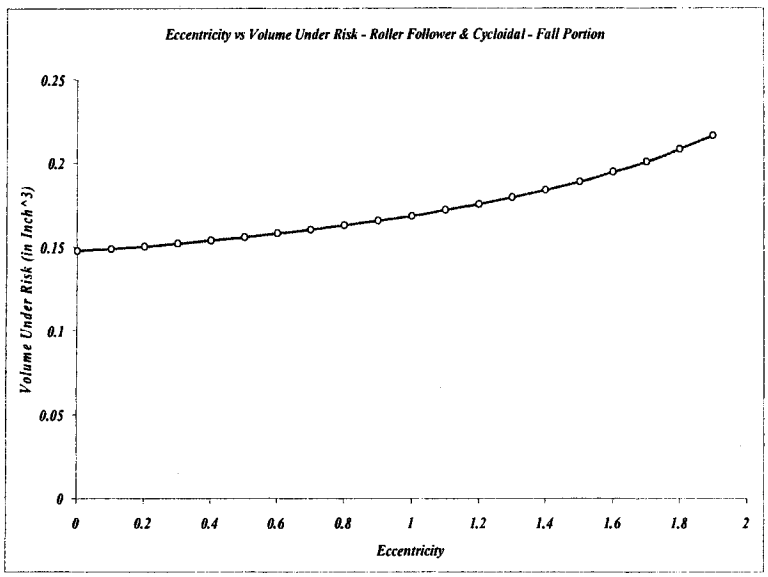


Figure B.21 Effect of eccentricity on volume under risk on cam fall segment for cycloidal function

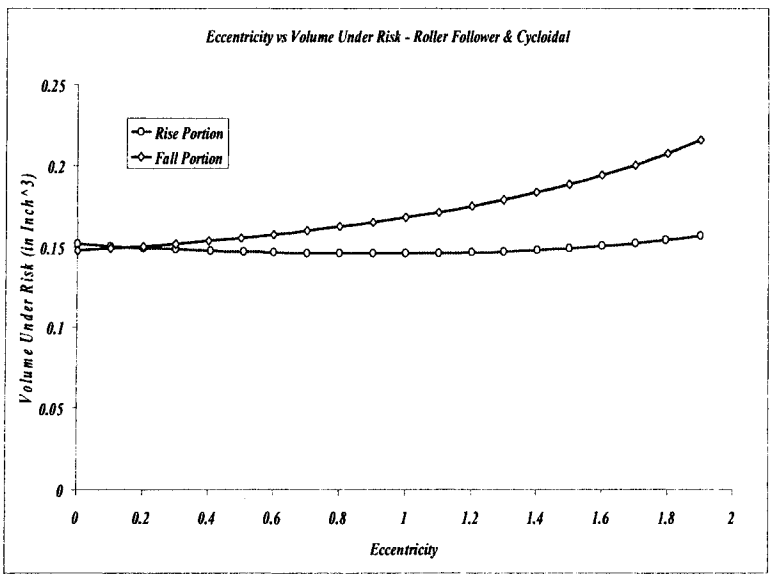


Figure B.22 Comparing the effect of eccentricity on volume under risk for rise and fall segments on cam – cycloidal function

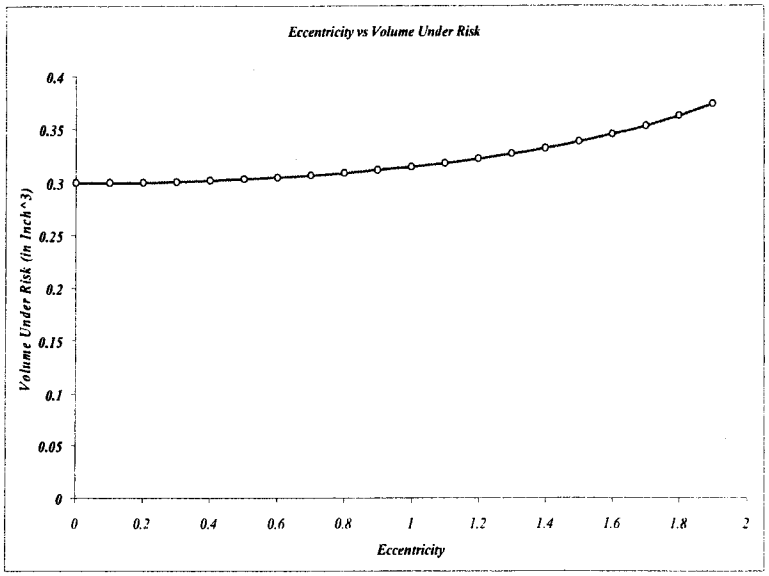


Figure B.23 Effect of eccentricity on total volume under risk for cycloidal function

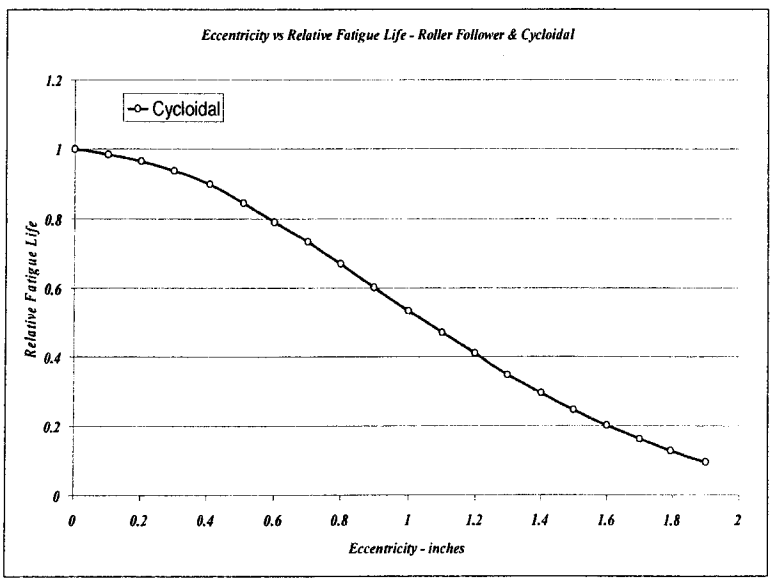


Figure B.24 Effect of eccentricity on fatigue life for cycloidal function

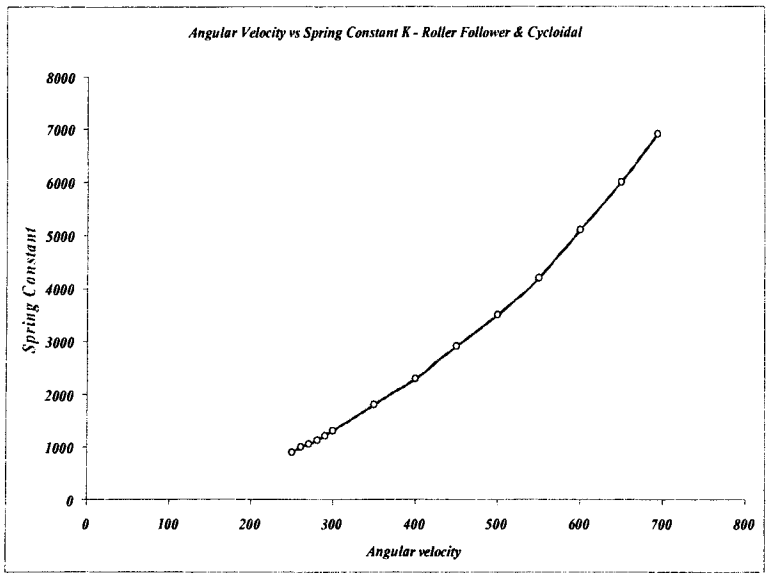


Figure B.25 Spring constant required to keep the follower in contact with the cam

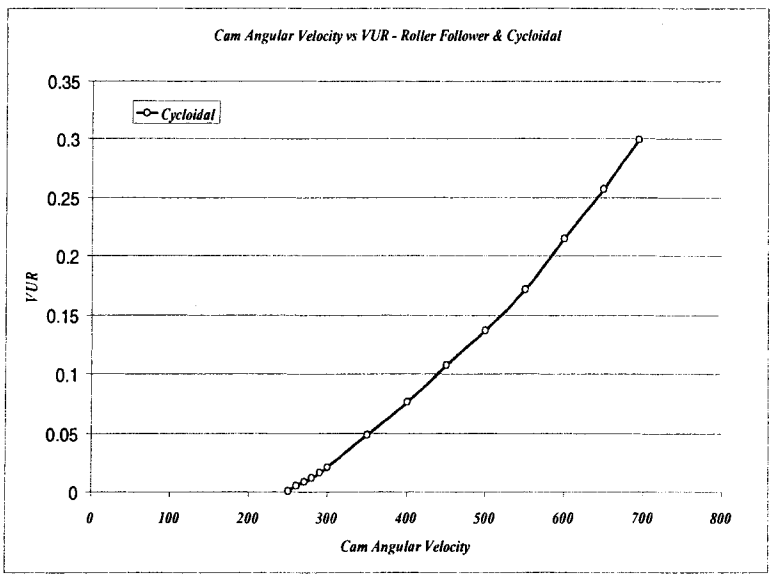


Figure B.26 Effect of $\omega$ on volume under risk

# APPENDIX C Cam Flat – Face Follower Results

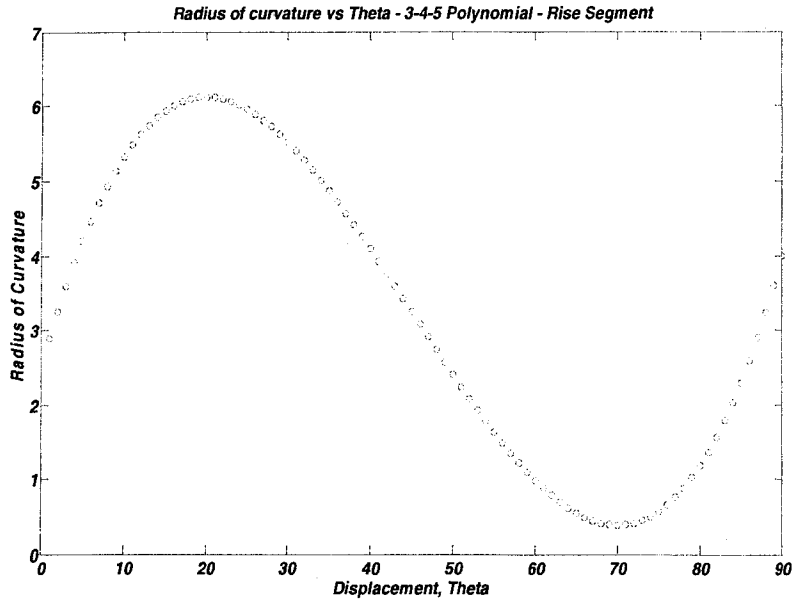


Figure C.1 Cam radius of curvature for flat – face follower on cam rise segment

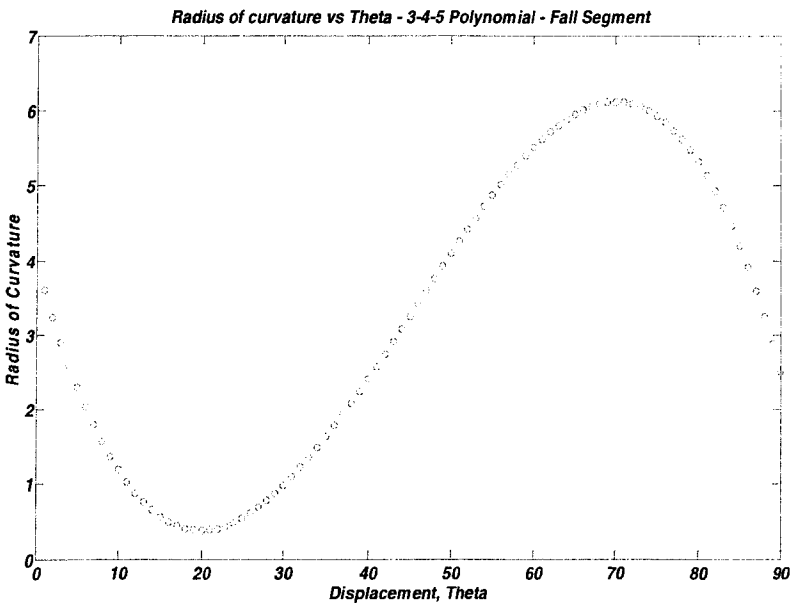


Figure C.2 Cam radius of curvature for flat – face follower on cam fall segment

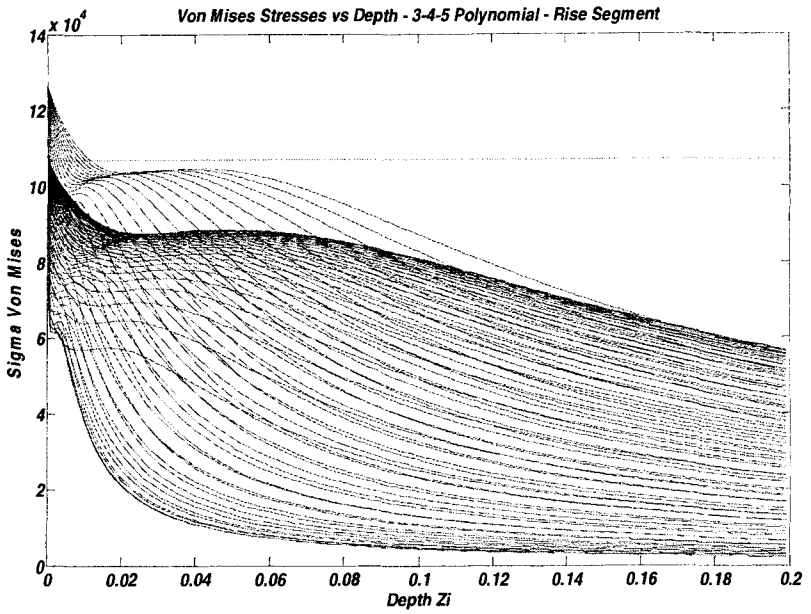


Figure C.3 Von Mises stress distribution in the flat – face follower on cam rise portion for $R_b = 2.5 inches$

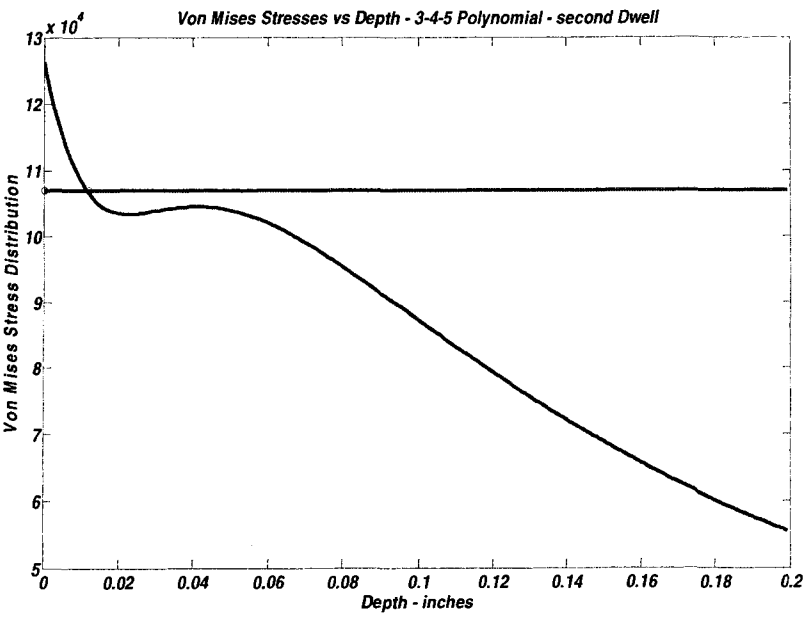


Figure C.4 Von Mises stress distribution in the flat – face follower on cam second dwell portion

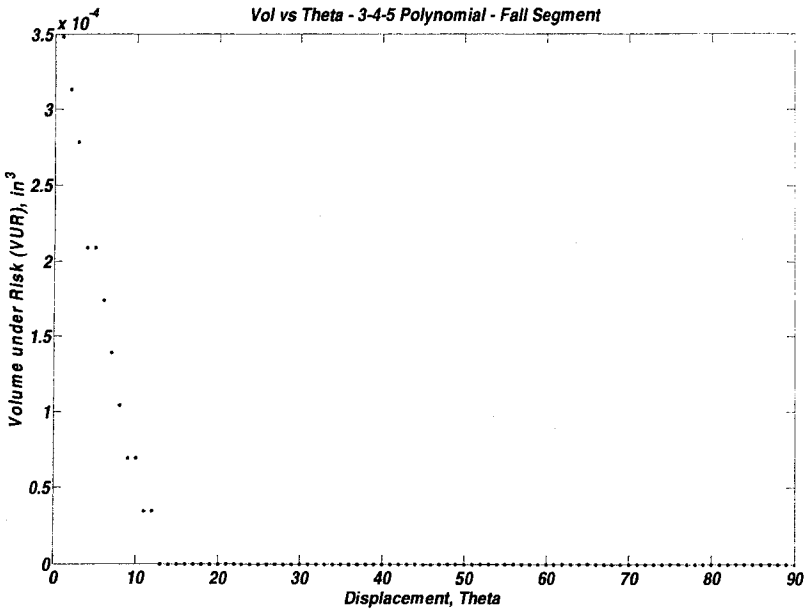


Figure C.5 Volume under risk on cam fall segment for cam flat – face follower system – polynomial (3 – 4 – 5), $R_b = 2.4$ inches and $\mu = 0.35$

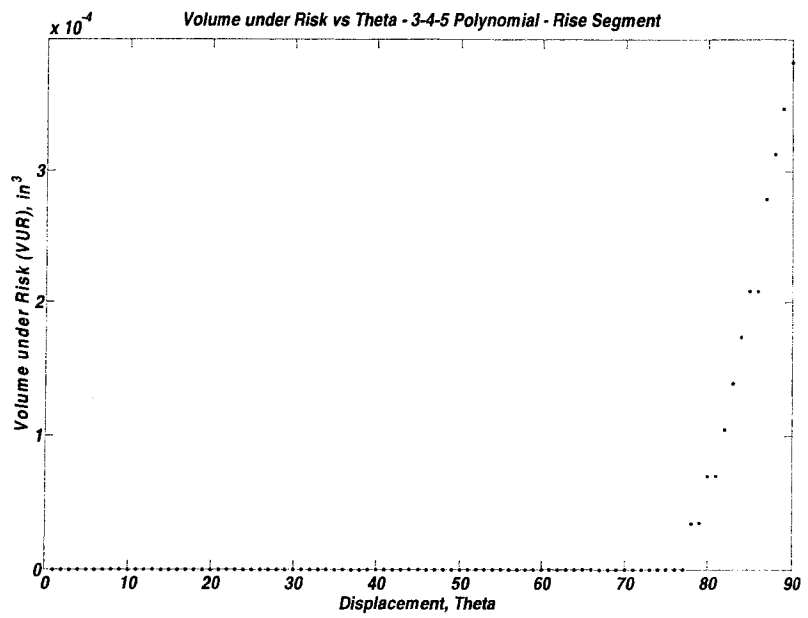


Figure C.6 Volume under risk on cam fall segment for cam flat – face follower system – polynomial (3 – 4 – 5), $R_b = 2.4$ inches and $\mu = 0.35$

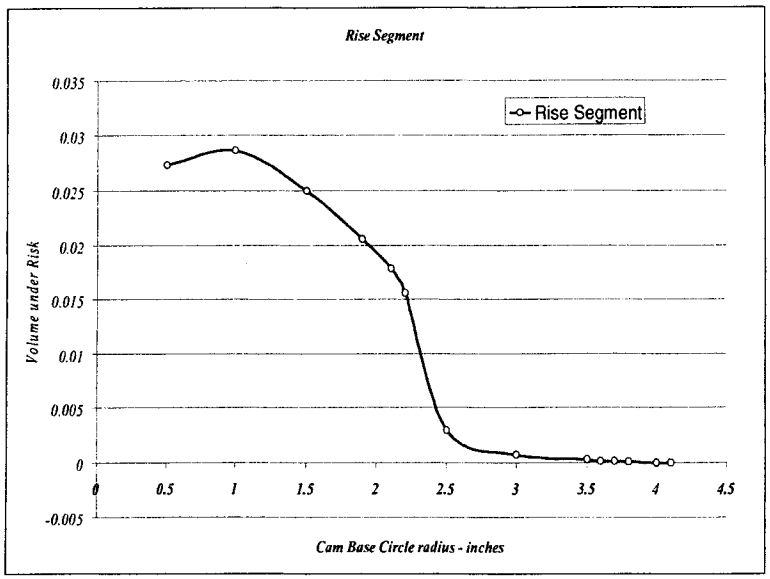


Figure C.7 Volume under risk at different cam base circle radii on flat face follower – rise segment and $\mu$=0.35

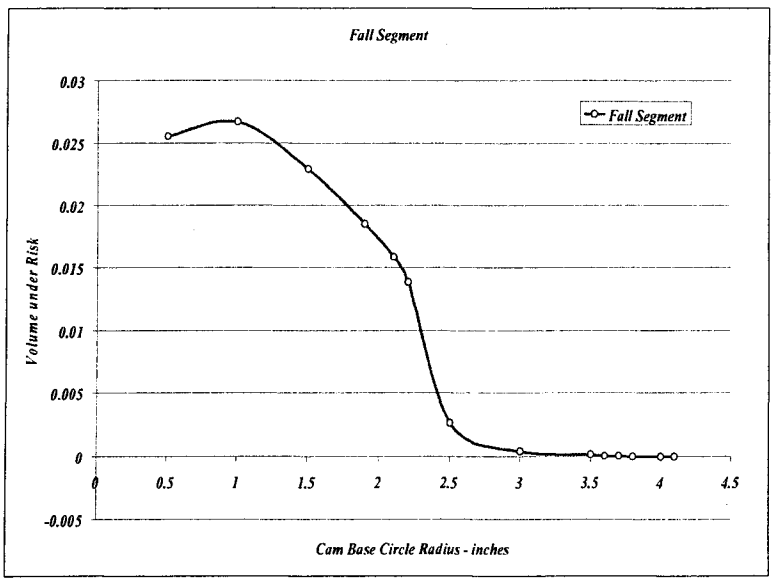


Figure C.8 Volume under risk at different cam base circle radii on flat face follower – fall segment and $\mu$=0.35

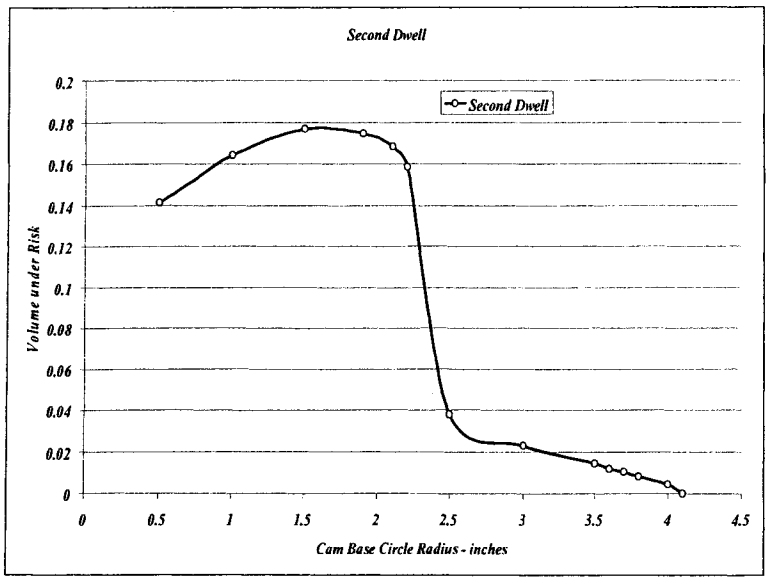


Figure C.9 Volume under risk at different cam base circle radii on flat face follower – second dwell segment and $\mu$ =0.35

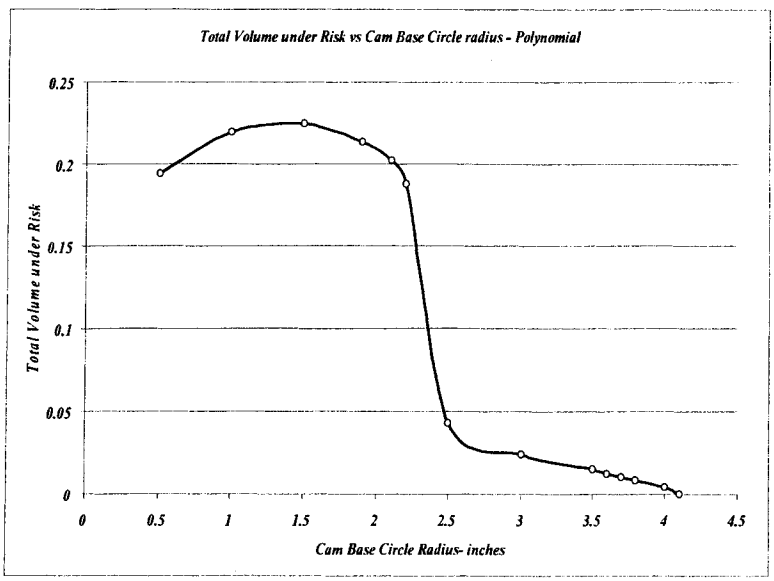


Figure C.10 Total volume under risk at different cam base circle radii on flat face follower and $\mu$ =0.35

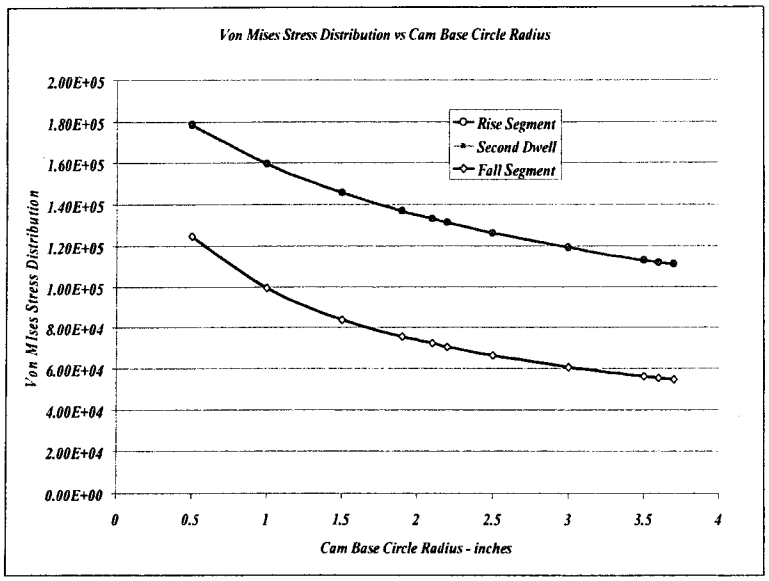


Figure C.11 Von Mises Stress Distribution for rise, second dwell and fall cam segments and $\mu$=0.35

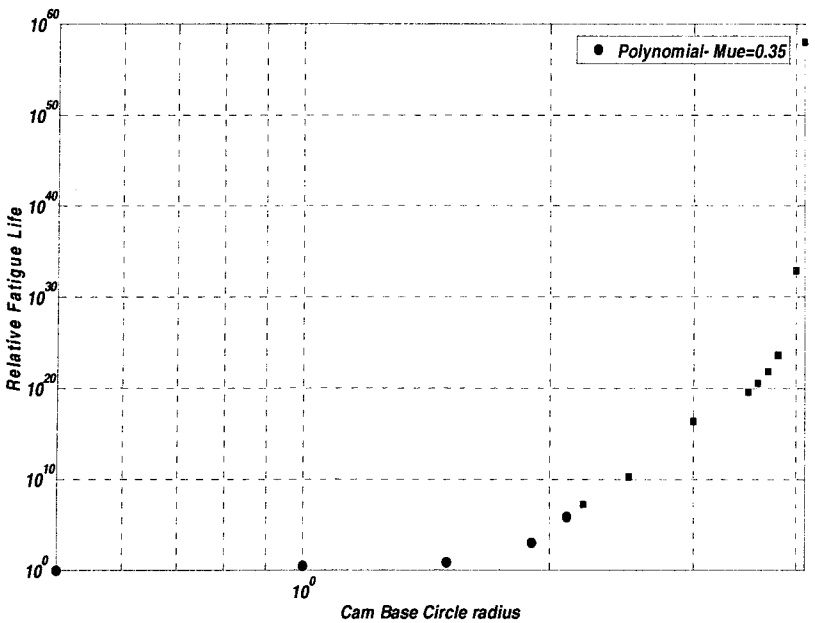


Figure C.12 Relative fatigue life at different cam base circle radii – $\mu$=0.35 and polynomial

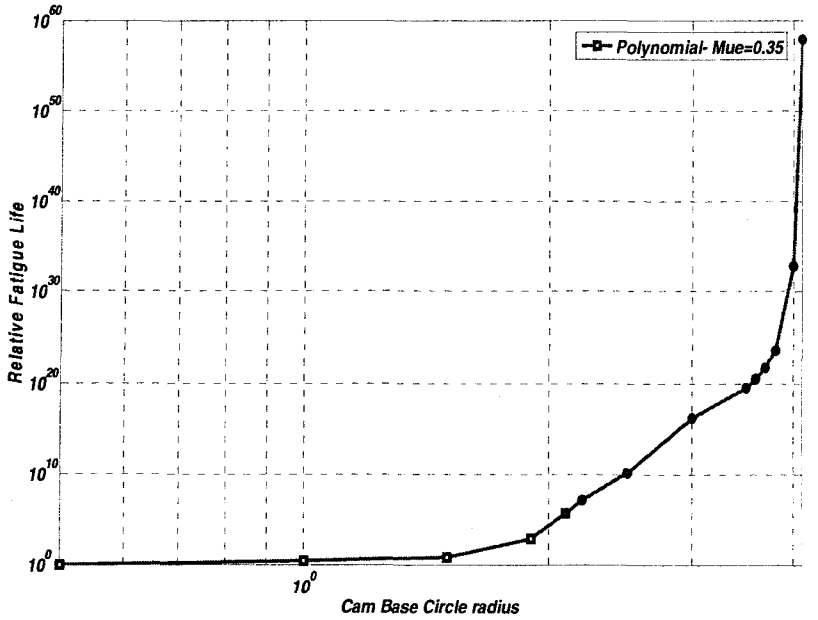


Figure C.13 Relative fatigue life at different cam base circle radii – $\mu$ =0.35 and polynomial

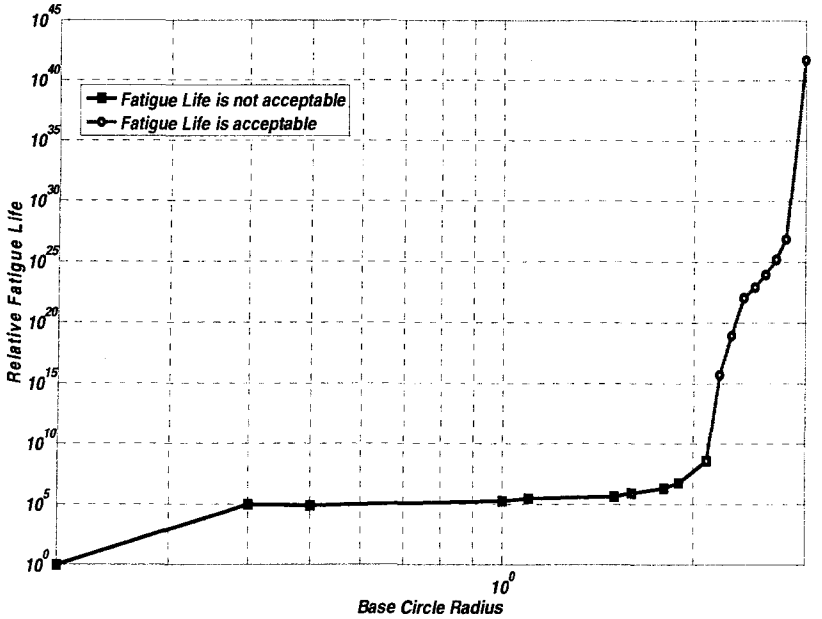


Figure C.14 Relative fatigue life at different cam base circle radii – $\mu$ =0.3 and polynomial

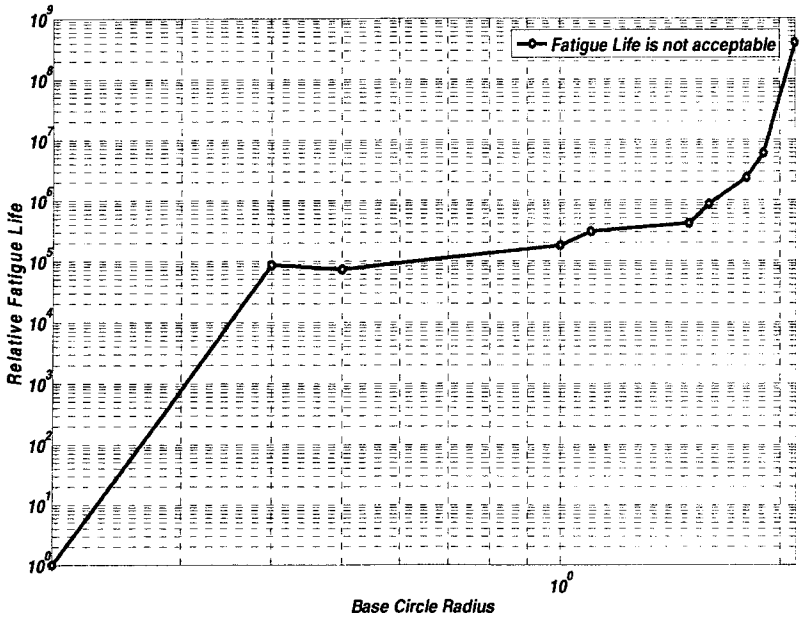


Figure C.15 Not acceptable relative fatigue life at different cam base circle radii – $\mu$ =0.3 and polynomial

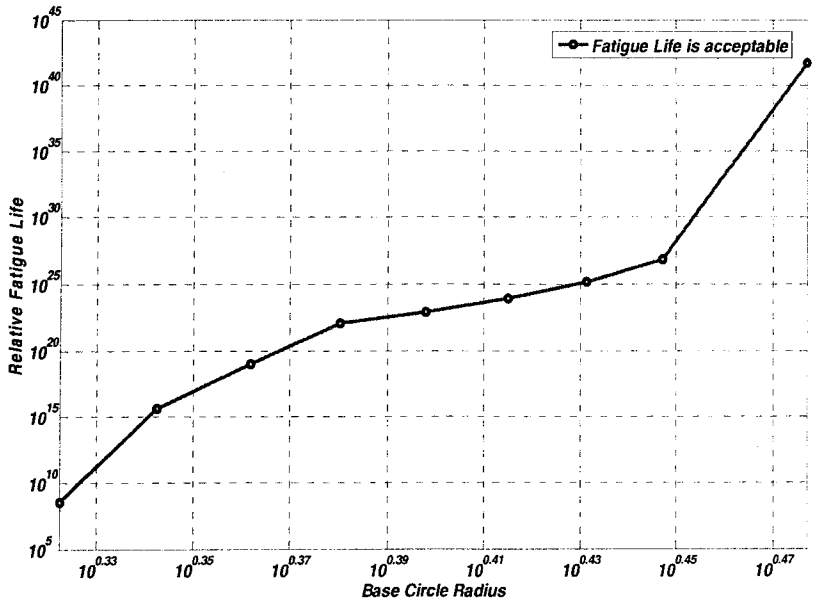


Figure C.16 Acceptable relative fatigue life at different cam base circle radii - $\mu$ =0.3 and polynomial

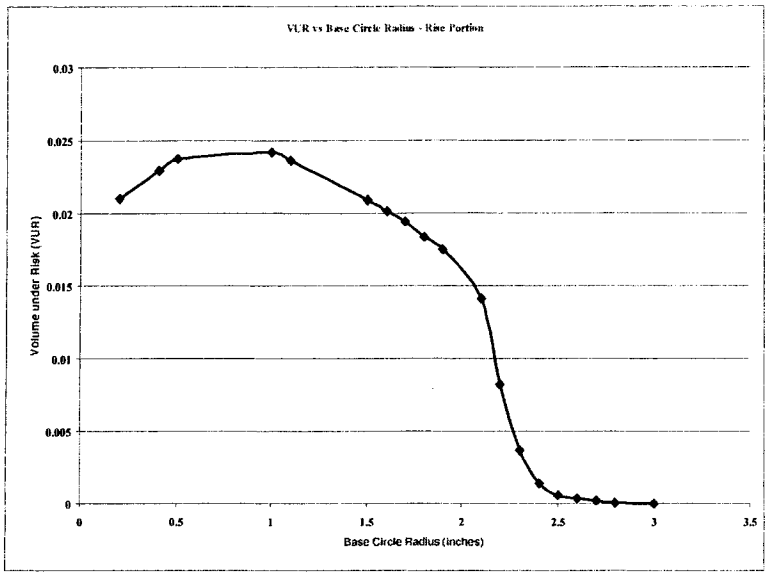


Figure C.17 Volume under risk at different cam base circle radii on flat face follower – rise segment and $\mu$=0.3

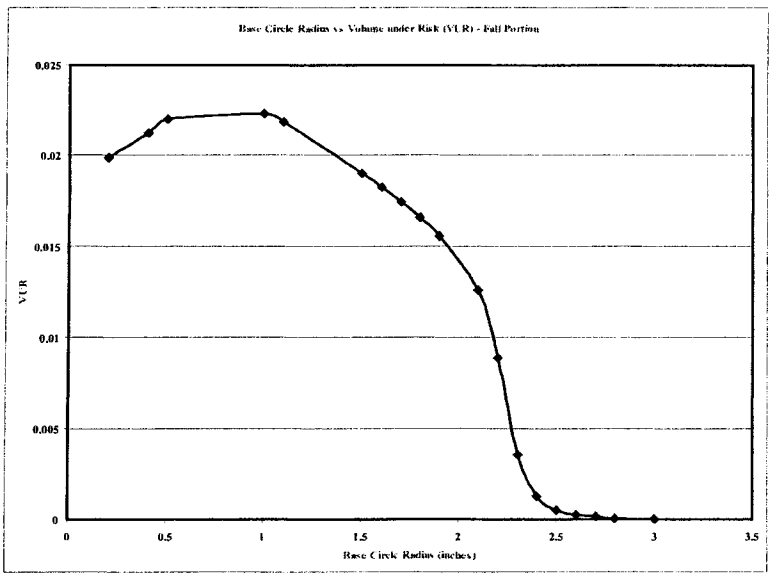


Figure C.18 Volume under risk at different cam base circle radii on flat face follower – fall segment and $\mu$=0.3

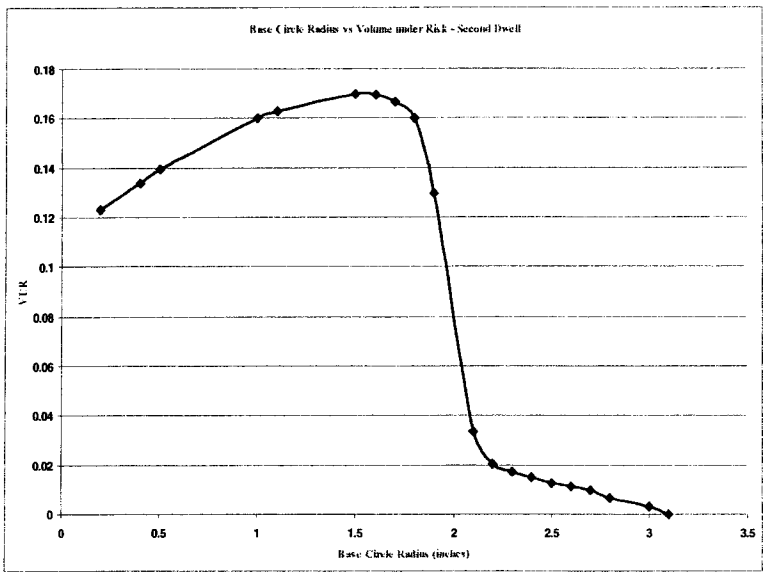


Figure C.19 Volume under risk at different cam base circle radii on flat face follower – second dwell segment and $\mu$ =0.3

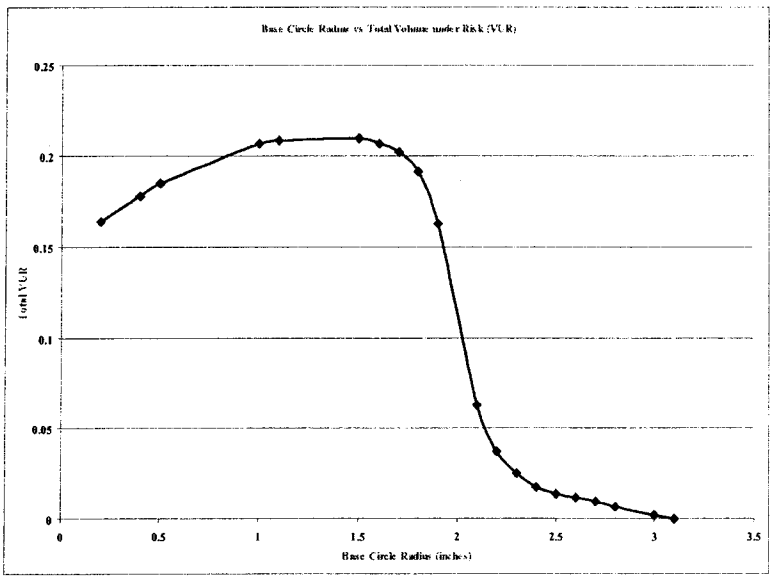


Figure C.20 Total volume under risk at different cam base circle radii on flat face follower –Polynomial and $\mu$ =0.3

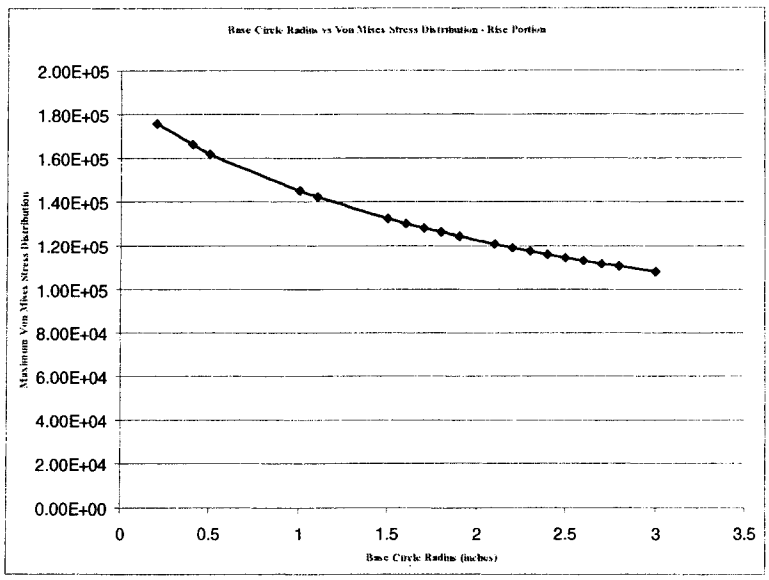


Figure C.21 Von Mises stress distribution at different cam base circle radii on flat face follower – rise segment, polynomial and $\mu$ =0.3

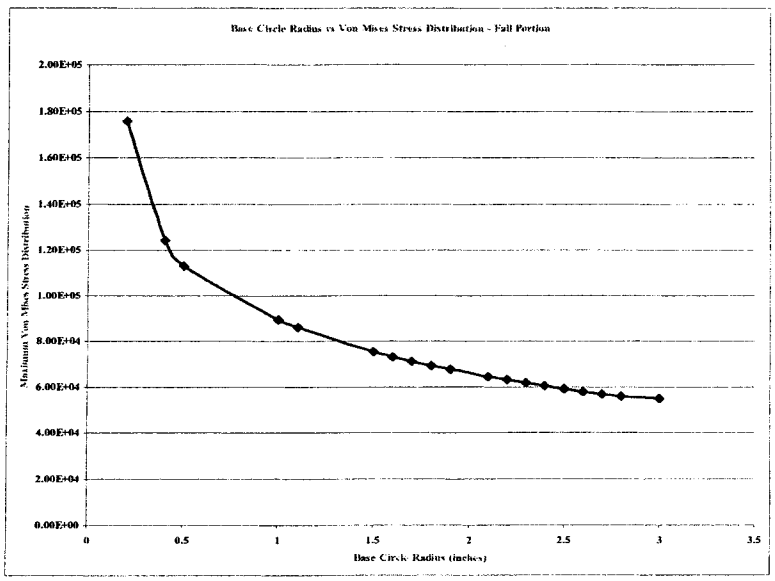


Figure C.22 Von Mises stress distribution at different cam base circle radii on flat face follower – fall segment, polynomial and $\mu$ =0.3

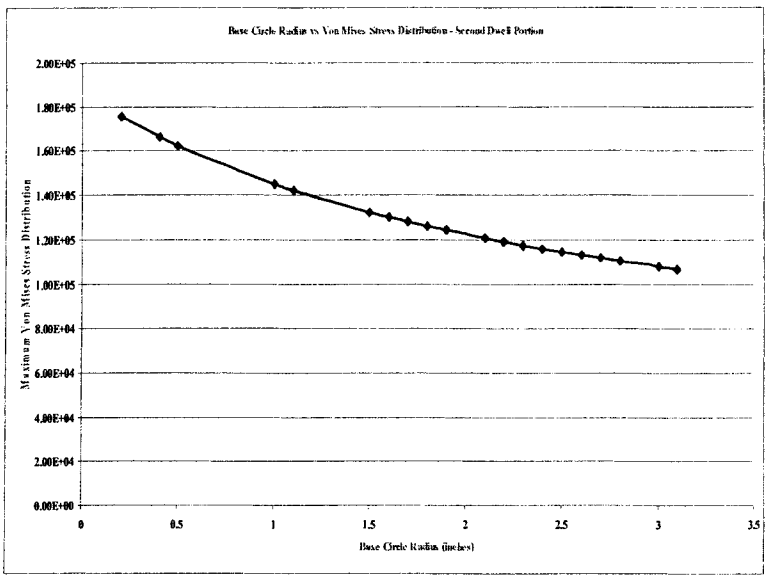


Figure C.23 Von Mises stress distribution at different cam base circle radii on flat face follower – second dwell segment, polynomial and $\mu$=0.3

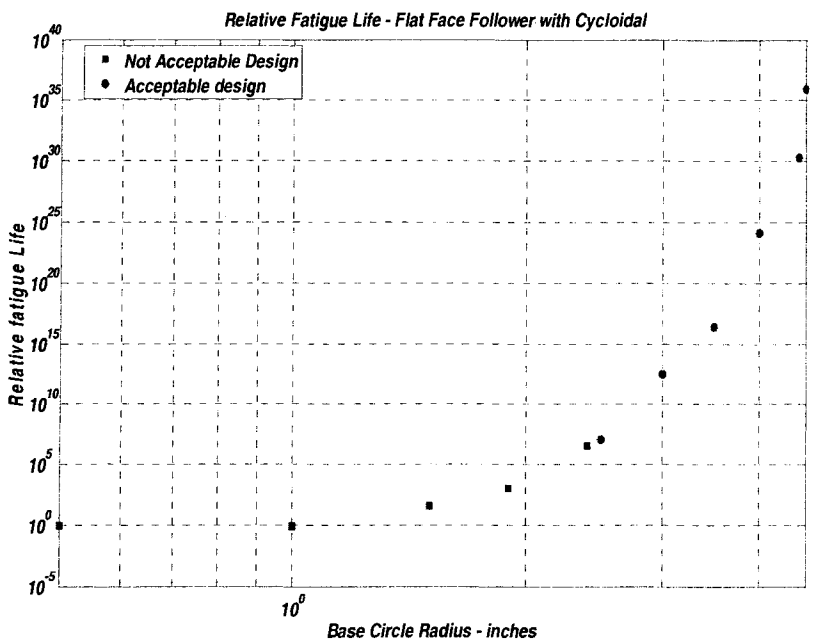


Figure C.24 Relative fatigue life at different cam base circle radii – $\mu$=0.35 and cycloidal

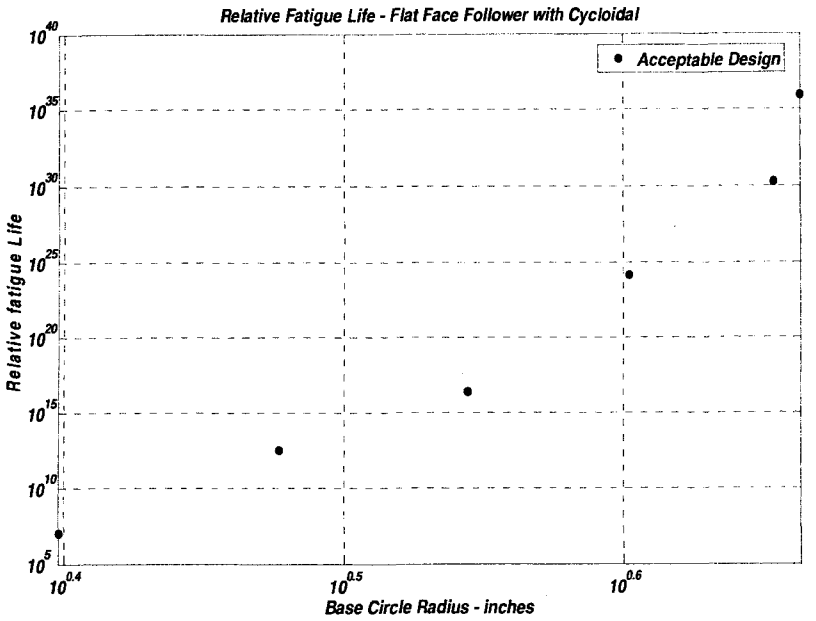


Figure C.25 Acceptable relative fatigue life at different cam base circle radii – $\mu$ =0.35 and cycloidal

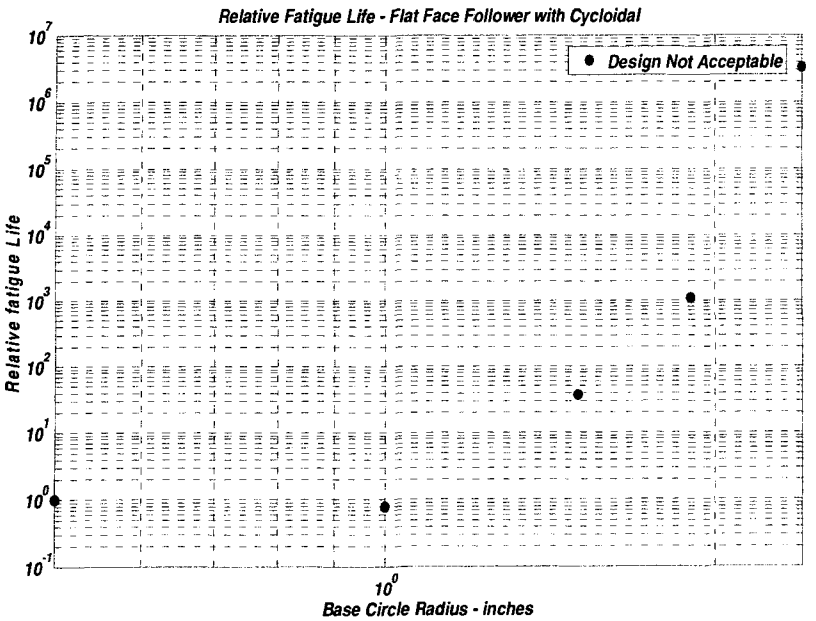


Figure C.26 Not acceptable relative fatigue life at different cam base circle radii – $\mu$ =0.35 and cycloidal

# REFERENCES

[1] Norton, R. L., "Cam Design and Manufacturing Handbook," Industrial Press Inc, New York 2002.

[2] Naylor, H., "Cams and Friction drives", Paper 15, p. 237, Conference on lubrication and Wear. Proc Inst mech. Engrs, 1967 – 1968

[3] British Technical Council of The Motor & Petroleum Industries, Cams and Tappets: A survey of information, December 1972

[4] Tribology Handbook 1973, Cams and Tappets, performance and materials section A23.

[5] Barwell, F. T. and Roylance, B. J., "Tribological Consideration in the Design and Operation of Cams – A Review of The Situation", Conference on Cams and Cam Mechanisms, The Institution of Mechanical Engineers p. 99 – 105, 1978

[6] Norton, R. L., Machine Design An Integrated Approach, 2$^{ND}$ Edition, pp. 471 – 486, Prentice – Hall, New Jersey 2000

[7] Reed, R. P., Smith, J. H. and Christ, B. W. "The Economic Effects of Fracture in the United States: Part I, Special Pub. 647 – 1, U.S. Dept. of Commerce, National Bureau of Standards, Washington, D. C., 1983

[8] Dowling, N. E., "Mechanical Behavior of materials" Prentice – Hall: Englewood Cliffs. N. J., pp. 340, 1993

[9] Hertz, H. "Gesammelte Werke", Leipzig, Germany, Vol. 1, 1895, English translation in Miscellaneous Papers, 1896.

[10] Smith, J.O. and Liu, C.K., "Stresses Due to Tangential and Normal Loads on an Elastic Solid with Application to Some Contact Stress Problems", Journal of Applied Mechanics Trans., ASME, 75: pp. 157 – 166, 1953

[11] Morton, W. B. and Close, L. J. "Notes on Hertz's Theory of the Contact of Elastic Bodies", Philosophical Magazine, series 6, Vol. 43, pp. 320, 1922

[12] Coker, E. G. and Ahmed, M. S., "Contact Pressure and Stresses," The Institution of Mechanical Engineers, Vol. 1, London, England, pp. 365, July 1921

[13] Thomas, H. R. and Heorsch, V. A.," Stresses Due to the Pressure of one Elastic Solids on Another," Bulletin of Engineering Experiment Station No. 212. University of Illinois, 1930

[14] Lundberg, G., "Elastische Beruehrung Zweier Halbraeume," Forschung auf dem Gebiete des Ingenieurwesens, Ausgabe A, Vol. 10, September – October, 1939, pp. 201 – 211

[15] Mindlin, R. D., "Compliance of Elastic Bodies in Contact," Journal of Applied Mechanics, Trans. ASME, Vol. 71, 1949, pp. 259 – 268

[16] Poritsky, H., "Stresses and Deflections of Cylindrical Bodies in Contact With Application to Contact of Gears and Locomotive Wheels," Journal of Applied Mechanics, Trans. ASME, Vol. 72, 1950, pp. 191 – 201

[17] M'ewen, E., "Stresses in Elastic Cylinders in Contact along A generatrix," Philosophical Magazine, Vol. 40, 1949, pp. 454 – 459, Cambridge

[18] Griffith, A. A., "The Phenomenon of rupture and flow in solids", Phil. Trans. A221, 163 – 198, 1921

[19] Sneddon, I. N., "The distribution of stress in the neighborhood of a crack in an elastic solid", Proc. Roy. Soc., Lon, A187, 229 – 260, 1946.

[20] Westergaard, H. M. "Bearing Pressures and Cracks", Journal of Applied Mechanics, 6, A49 – 53, 1939.

[21] Irwin, G. R., "Fracturing of metals", Proc ASM Symposium, Chicago 1947, 147 – 166, Cleveland, ASM (1948)

[22] Orowan, E., "Fundamentals of Brittle Behavior in Metals". In Fatigue and Fracture of Metals, Edited by W. M. Murray, p. 139 – 167, 1952.

[23] Irwin, G. R., "Analysis of Stresses and Strains Near The End of A Crack Traversing A Plate", Trans. ASME Journal of Applied Mechanics, 24, 361 – 364, 1957

[24] Albert, W. A. J. "Über treibseile am Harz" Archive für Mineralogie Geognosie Bergbau und Hüttenkunde, vol. 10, pp215-34, 1838

[25] Hoppe, O., "Alberts Versuche und Erfindungen", Stal u. Eisen, Vol. 16, p. 437, 1896

[26] Rankine, W. J. M., "On The causes of The Unexpected Breakage of The Journals of Railway Axels, and on The Means of Preventing Such Accidents by Observing The Law of Continuity in Their Construction". Proc. Instn. Civ. Engnrs. Vol. 2, p. 105, 1843.

[27] Hodgkinson, E. A., and others "Report of the Commissioners appointed to enquire into the application of iron to railway structures", H. M. Stationery Office. Command Paper No. 1123, 1849

[28] Wohler, A. "Versuche zur Ermittlung der auf die Eisenbahnwagenachsen Einwirkenden Krafte und der Widerstandsfahigkeit der Achsen". Z. f. Bauwesen. p. 583, 1860, Also Z. f. Bau p. 233, 1863, p. 67, 1866, p. 73, 1870. Abs. Engineering, p. 199, 1871

[29] Fairbairn, W. "Experiments to Determine The Effect of Impact, Vibratory Action, and Long Continued Changes of Load on Wrought – Iron Girders", Phil. Trans. Roy. Soc. Vol. 154, p. 311, 1864

[30] Bauschinger, J., "Ueber die Veranderungen der Elastizitatsgrenze und der Festigkeit des Eisens und Stahls Durch Strecken, Quetschen, Erwarmen Abkuhlen und Durch Oftmals Wiederholte Belastung", Mitt: Mech – Tech Lab. Munchen XIII, 1886.

[31] Ewing, J. A. "On Hysteresis in The Relation of Strain to Stress", Rep. Brit. Ass, p. 502, 1889.

[32] Ewing, J. A. and Rosenhain, W. "Experiments in Micro – Metallurgy – Effect of Strain", Proc. Roy. Soc Vol. 67, p. 85, 1899

[33] Ewing, J. A. and Humfrey, J. C. W. "The Fracture of Metals under Repeated Alternations of Stress", Phil. Trans. Roy. Soc. Vol. 200, p. 241, 1903.

[34] Gilchrist, J. "On Wohler's Laws", The Engineer. Vol. 90, p. 203, 1900

[35] Guillet, A. "Intervention de L'amortissement dans L'essai des Fers", Rev. Metall. Memoires, p. 885, 1909

[36] Bairstow, L. "The Elastic Limits of Iron and Steel under Cyclical Variations of Stress", Phil. Trans. Roy. Soc. Vol. 210, p. 35, 1910

[37] Le Chatelier, H., "Sur l'essai des metaux par amortissement des mouvements vibratoires", Rev. Metall. Memoires, p. 887, 1909

[38] Gough, H. J., "The Fatigue of Metals", Benn, London, 1926

[39] Moore, H. F. and Kommers, J. B., "The Fatigue of Metals", McGraw – Hill, New York, 1927

[40] Battelle Memorial Institute, "Prevention of the Failure of Metals under Repeated Stress", John Wiley & Sons, New York, 1941

[41] H. J. Grover, S. A. Gordon and L. R. Jackson, "Fatigue of Metals and Structures", Battele Memorial Institute, 1960

[42] Fermont, Ch. "La Fatigue des Metaux et les Nouvelles Methodes D'essais", Genie Civil., 22nd and 29th October; 19th and 26th November, 1910

[43] Bannantine, J. A., Comer, J. J and James, L. H.,"Fundamentals of Metal Fatigue Analysis", Prentice Hall, Englewood Cliffs, New Jersey, 1990.

[44] Graf, O., "Die Dauerfesigkeit der Werkstoffe und der Konstruktions – elemente", Julius Springer, Berlin, 1929

[45] Mailander, R. "Dauerbruche und Dauerfestigkeit", Krupp. Mh. Vol. 13, p. 56, 1932

[46] Ludwik, P., "Ermudung", International Association for Testing Materials, Zurich Congress, September 1931

[47] Locarti, L., "La Faica dei Materiali Metallici", Hoepli, Milan, 1950

[48] Ros, M. and Eichinger, A., "Die Bruchgefahr Fester Korper Bei Wiederholter Beanspruchung Ermudung Metalle", Eidgenossische Materialprufungsanstalt an der E. T. H. Zurich, No. 173, 1950.

[49] Lundberg, G., and Palmgren, A., "Dynamic Capacity of Rolling Bearings", Acta Polytechnica, Mechanical Engineering series, Royal Swedish Academy of Engineering Sciences, Vol. 1, No. 3, 7, 1947

[50] Lundberg, G., and Palmgren, A., "Dynamic Capacity of Rolling Bearings", Acta Polytechnica, Mechanical Engineering series, Royal Swedish Academy of Engineering Sciences, Vol. 2, No.4, 96, 1952

[51] Harris, T.A., "Lundberg – Palmgren Fatigue Theory: Considerations of Failure Stress and Stressed Volume", Journal of Tribology, Vol. 121, January 1999

[52] Harris, T.A and McCool, J. "On The Accuracy of Rolling Bearing Fatigue Life Prediction" ASME Journal of Tribology, Vol. 118, pp. 297 – 310, 1996

[53] Harris, T. and Barnsby, R. "Tribological Performance Prediction of Aircraft Gas Turbine Mainshaft Ball Bearings", Proceedings of the 1997 World Tribology Congress, London, Sept. 8 – 12

[54] Ioannides, E. and Harris, T. A. "A New Fatigue Life Model for Rolling Bearings," Journal of Tribology, Vol. 107, pp. 367 – 378, July 1985.

[55] Angeles, J and Lopez – Cajun, C. S., "Optimization of Cam Mechanisms". Kluwer Academic Publishers, 1991, p. 6

[56] Muller, J., "The History of Cams and Cam Mechanism", Proc. 7th World Congress on The Theory of Machines and Mechanisms, Seville, p. 1649 – 1652, 1987

[57] Koumans, P. W., " The Calculation of The Maximum Pressure Angle and The minimum Radius of Curvature of A Cam Using Special Graphs", Conference on Cams and Cam Mechanisms, The Institution of Mechanical Engineers p. 116 – 122, 1978.

[58] Chicurel, R., "Cam Size Minimization by Offsetting," ASME Paper No. 62-WA-22, pp. 25-30, 1962.

[59] Suchora, D. H., Werner, B. C. and Paine, W. A., "Pressure Angle Characteristics of Radial Cams with Offset Reciprocating Roller Followers", Machine Elements and Machine dynamics, ASME, p. 103 – 114, 1994

[60] Chan, Y. W. and Sim, S. K., "Optimum Cam Design", International Journal of Computer Applications in Technology, Vol. 9, No. 1, p. 34 – 47, 1996.

[61] Neklutin, C. N., "Designing Cams for Controlled Inertia and Vibration", Machine Design, pp. 143 – 160, June 1952.

[62] Erdman, Arthur G. and Sandor, George N., "Mechanism Design Analysis and Synthesis – Volume I", 3rd edition, Prentice – Hall, New Jersey 1997.

[63] Hertz, H.R, J. Reine Angew. Math. (Crelle s J.), vol. 92, pp. 156 – 171 (1881).

[64] Nikas, George K., "Fatigue Life and Traction Modeling of Continuously Variable Transmissions", Journal of Tribology, Vol. 124, pp. 689 – 698, October 2002.

[65] http://composite.about.com/library/glossary/e/bldef-e1982.htm

[66] Shigley, JR. E., Mischke, C. R., and Budynas, R. G., "Mechanical Engineering Design", 7th edition, McGraw Hill, New York 2003.